Pattern Diversity Characterization of Reconfigurable Antenna Arrays for Next Generation Wireless Systems

A Thesis

Submitted to the Faculty

of

Drexel University

by

George Dimanson Sworo

in partial fulfillment of the

requirements for the degree

of

Doctor of Philosophy in

Feb 2015

Dedications

To my family: My beautiful wife Christine for her enduring love and patience; my sons Jahaziel and Hezekiah for giving me purpose in this life; my mother Grace without whose relentless love and support, I wouldn't have gotten this far in life; To all my sisters for being there for me. To my Dad for coming back into my life. To Sally France without whose untold support and prayer I wouldn't be where I am today. I am eternally grateful to you. To the Yugga family, whose resilience, and tenacity inspires me everyday. I will always be grateful for your constant love. Thank you all so much. God is so gracious to me!

Acknowledgments

I am deeply grateful to my Advisors Dr. Moshe Kam, and Dr. Kapil Dandekar for their guidance, insight and wisdom.

I would like to thank the Gwin family, especially my brother from another mother Christopher Gwin for being the big brother I never had. I am also very grateful to Frank Stiefel and his family for their true friendship; and to the countless friends whose acquaintances I have had the pleasure of meeting through my Haddonfield connection. Special thanks to the Hymerlings for their boundless generosity.

To Joe Sun, Megan Doherty, and the family at APO UPENN, Thanks for nurturing and providing me with the best advice and environment to succeed at UPENN. To NSBE UPENN and Cora Ingrum, thank you for your academic mentorship.

To Peggy Hanefors for helping me find my feet at UPENN and for being a good friend. To my big brother in Christ and good friend, William Okech, thank you so much for always reminding me of who I am.

Special thanks to Longun Jimmy, Yengi Desmond, Maring Kennedy, and Allam Margret for their camaraderie and inspiration through a collective dream to serve our beloved nation of South Sudan and Africa at large. Lets keep on dreaming! Not forgetting Helen Kulabako and Windle Trust International for giving us a chance when no one did.

Many thanks to my lab mates at Data Fusion and Drexel Wireless Systems Labs.

Time and space would not permit me to thank the countless people that I have been lucky enough to call friends during these formative years of my life. From the refugee camps to the United World Colleges to the University of Pennsylvania and Drexel University, you know who you are, I sincerely thank you from the bottom of my heart for being a part of this exciting journey of my life. Lets keep changing the world for the better.

Table of Contents

List of Tables

List of Figures

Abstract

Pattern Diversity Characterization of Reconfigurable Antenna Arrays for Next Generation Wireless Systems

George Dimanson Sworo

Advisors: Kapil R. Dandekar, Ph.D. and Moshe Kam, Ph.D.

The use of multi-antenna technology in wireless radio communications has attracted tremendous attention due to its potential to increase data rates without requiring additional bandwidth and transmission power. This has been driven by the burgeoning demand for high data rates and the need for instantaneous and ubiquitous access to information. It is therefore no surprise that current and future generation wireless standards such as LTE and WiMAX have adopted the use of adaptive multi-antenna systems also known as adaptive Multiple Input and Multiple Output (MIMO) as their de facto transmission technology.

In this thesis work, we focus on the design of a smart wireless antenna system, and the study of relevant techniques that enable us to reap the benefits of their deployment in small wireless devices with MIMO capability. Specifically, we employ a new class of adaptive antenna systems known as Reconfigurable Antenna Systems (RAS) for portable devices. These antennas are capable of dynamically changing their electrical and radiation characteristics to suit the conditions of the wireless channel. The changing radiation patterns lead to pattern diversity gains that improve system performance. This is in contrast to conventional non-reconfigurable arrays which depend on signal processing techniques such as antenna grouping and beamforming to achieve performance gains. However, despite the demonstrable system-level performance benefits of RAS in adaptive MIMO, few of these antennas have been adopted and integrated in state-of-the-art wireless standards. Their usage has been partly

inhibited by the prohibitive costs of implementation and operation in a real wireless infrastructure.

As part of this thesis research effort we attempt to integrate these new antennas into a cost-effective real wireless MIMO testbed for use in current generation technologies. The solution integration is carried-out through the use of readily available software-defined radio frameworks. We first design, analyze and characterize the pattern diversity in RAS antenna arrays that resonate at frequencies suitable for 4G applications. We then study the benefits of pattern diversity obtained from RAS arrays over conventional space diversity approaches such as antenna grouping and beamforming. This dissertation also presents low-complexity adaptive physical layer models and algorithms to exploit the benefits of RAS array integration in MIMO wireless systems. We implement these algorithms in software-defined radio frameworks, experimentally test, and benchmark them against other established approaches in literature. And finally, integrate and test these RAS array design prototypes as part of the MIMO wireless system that leverages a state-of-the-art wireless base station and mobile terminals.

CHAPTER 1: INTRODUCTION

In wireless radio communications, multivariate channel factors can cause signal strength attenuation and degradation, which can adversely affect the quality of communications. These channel impairments are a result of signal transmissions over a wireless channel - a logical radio link or medium that connects a data source and a data sink - that is used to convey the information signal. A defining characteristic of the wireless channel is the variation of the channel strength or state over time and over frequency [1].

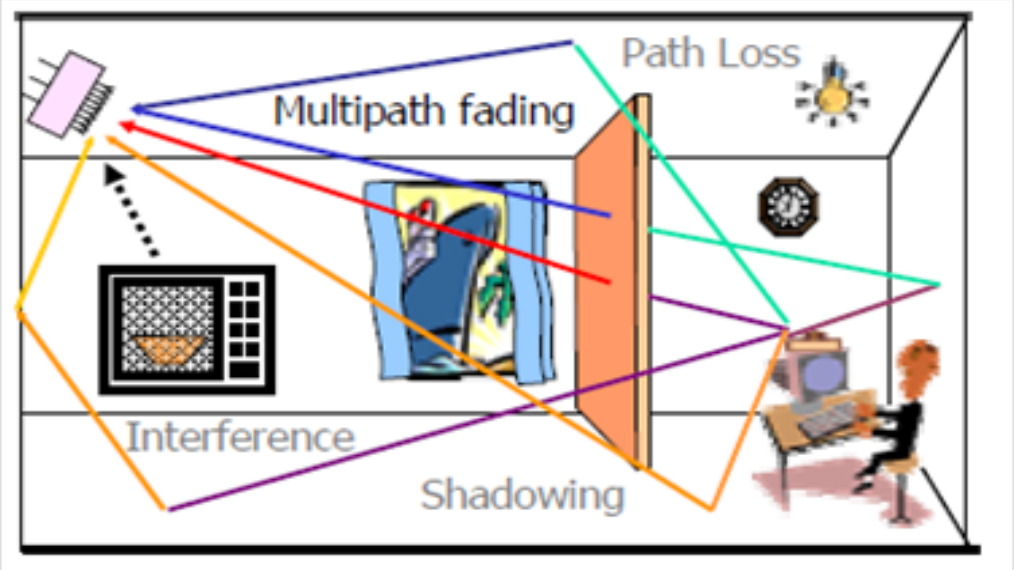

Figure 1.1: Transmission over a Wireless Channel (Adapted from [2]).

Fig. 1.1 depicts the propagation of a signal over a wireless channel between the transmitter (located at the top left) to the receiver (at the bottom right). It illustrates the possible paths traversed by a signal in a typical indoor channel environ-

ment. These paths are influenced by various channel impairment sources such as a microwave, which introduces interference; walls, which introduce shadowing; reflective or obstructive surfaces that causes multipath fading [3].

1.1 Motivation and Problem Statement

The performance of a system in a wireless environments that experiences fading due to multipath propagation is often affected by the spatial distribution of the multipaths. These multipaths are multiple wavefronts that can cause random variations in the signal strength. This effect leads to a channel phenomenon called spatial selectivity. Traditionally, spatial selectivity causes the signal power to fluctuate rapidly over time and distance and can lead to multipath fading. This multipath fading– a pitfall of wireless transmission– can be turned into a benefit by using multi-antenna systems. Multi-antenna systems also known as MIMO can effectively take advantage of these random fading, to increase data rates and link reliability (reduced fading) [4] without requiring additional bandwidth or increased transmit power. These systems leverage the spatial characteristics of the multipath channel to achieve spatial diversity or gain by placing seperate antennas in the dense multipath environment. The multiple antennas can then be used to simultaneously transmit independent data streams over the channel to increase data rate. MIMO spreads the same total transmit power over the antennas to achieve array gain that improves the spectral efficiency (thus, more bits per second per hertz of bandwidth) [5] – [7]. The spatial diversity can also be achieved by combining the signals from separate antennas to maximize the resultant signal amplitude.

However, when the channel consists of few multipaths, the measured signals at the different antennas of the multi-antenna system can become spatially correlated. Spatial correlation–a correlation between the signal's spatial direction and the av-

erage received signal gain –degrades the performance of multi-antenna systems and limits the number of antennas that can be used for a given MIMO link. For this reason, MIMO antenna arrays must be designed to reduce spatial correlation to yield the additional degrees of diversity and improve system performance [155]. Moreover, the design and analysis of multi-antenna arrays is coupled to the physical layer capabilities of the MIMO system. This dependency is due to the fact that the physical layer depends on signal processing algorithms that operate on the multivariate propagation channel characteristics that determines the performance of the MIMO arrays. Specifically, spatial correlation is a function of both spatial characteristics such as angular spread, the number of scatterers, and antenna array parameters including the antenna geometry, element spacing and pattern, polarization, and mutual coupling [153]. These variables in-turn affects the performance of the physical layer signal processing techniques.

1.1.1 Brief Overview

Various research efforts in [5], and [7]–[10] have established that adaptive antenna wireless systems increase spectral efficiency and provide flexible data rates in multipath fading channels. These systems employ MIMO technology and use multiple antennas at both the transmitter and the receiver to improve signal reception and transmission rates. This is why MIMO technology have become an integral part of the fourth-generation (4G) wireless communication standards such as WiMAX, Long-Term Evolution (LTE) and beyond.

Typical MIMO systems employ multiple antenna elements at both the transmitter and the receiver. These elements can either be co-located and coupled via a controller as part of an array or are physically separated from each other. The use of arrays have been demonstrated to improve signal transmission range and reliability, how-

ever, arrays require large spacing and complex signal processing; these constraints render them impractical to deploy in portable wireless devices such as routers or access points. This limitation motivated research efforts in the design of a compact alternative antenna solution for small devices: a single antenna structure that can act as a multiple element array.

This dissertation focuses on a new class of adaptive antenna array systems known as Reconfigurable Antenna Systems. These reconfigurable antenna technology has been shown to offer performance gains in MIMO systems by increasing channel capacity [10] and Signal-to-Noise Ratio (SNR) [9] at the Receiver. RAS antennas offer the following benefits:

- These antennas are capable of dynamically changing their radiation patterns and enable MIMO systems to adapt to physical link conditions.
- RAS provide space and cost benefits in incorporating multiple elements in a single physical device [11], and by reducing the number of RF chains [112], [13].
- These antennas have been used to improve advanced interference management techniques like interference alignment [14].

Fig. 1.2 illustrates the fundamental differences between a standard MIMO system, a MIMO system equipped with Adaptive Antenna Arrays (AAA) and with reconfigurable antennas. Fig. 1.2(a) depicts a standard MIMO system that uses spatial multiplexing technology where different data is sent on the same time-frequency resource from different antennas so that spectrum efficiency is multiplied without expending more frequency resource. Fig. 1.2(b) compares and contrasts a MIMO system that uses antenna grouping algorithms for signal processing with one that employs reconfigurable antennas. In the first case (left of Fig. 1.2(b)) , antennas are grouped into sub-arrays and a hybrid of beamforming and spatial multiplexing

techniques is used for signal processing. Beamforming leverages the fact that every physical antenna within the sub-array transmits the same signal and performs a weighted processing on each antenna element in the sub-array to steer the transmit beam to the target receiver. The spatial multiplexing aspect is then realized from the use of multiple sub-arrays to send independent data streams. The second scenario (right of Fig. 1.2(b)) leverages the pattern diversity of the reconfigurable antennas to affect how the transmitter or receiver perceives the wireless channel. The transceiver pair is provided with a range of channel paths to select or adapt in order to enhance performance.

In addition to adapting antenna arrays or radiation patterns of its transceivers to the channel conditions, such a MIMO systems can also leverage physical layer link adaptation techniques to improve transmission rate and bit error rates. Link adaptation simply refers to a set of techniques where modulation, coding, and other signal transmission parameters are changed on the fly to better adjust to the changing channel conditions. The literature on link adaptation or Adaptive Modulation and Coding (AMC) is vast. However, the representative approaches found in [15]–[19] have demonstrated that adaptive modulation and coding systems exhibit great performance enhancements compared to systems that do not exploit the quality of the radio channel.

1.2 Problem

Although reconfigurable antennas have been in development for the last 30 years, few are in use. From the system perspective, the benefits and costs of implementation of reconfigurable antennas are unclear from a system perspective. “System and operating environment complexity makes it difficult to identify a particular antenna functionality that will automatically result in greater throughput, higher link relia-

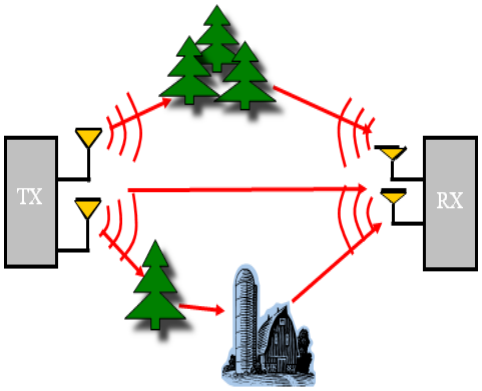

(a) Standard MIMO

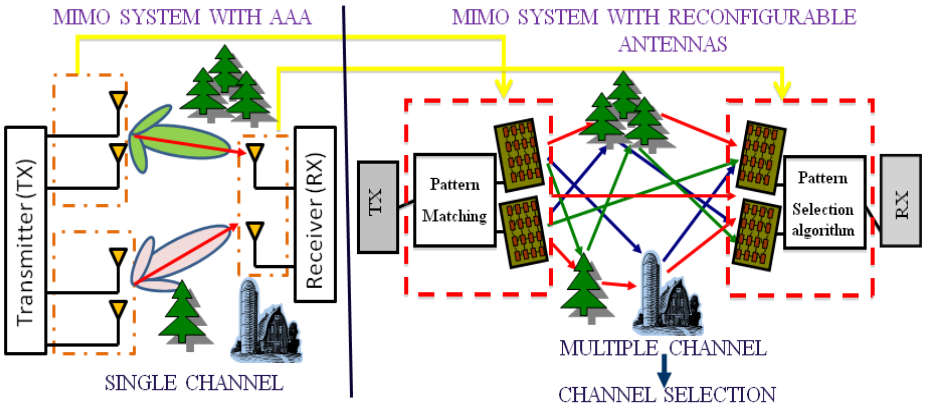

(b) MIMO System with Adaptive Antenna Array and Reconfigurable Antennas

Figure 1.2: Standard MIMO System versus a MIMO System with Reconfigurable Antennas (Adapted from [8]).

bility, or lower bit error rates [20].” Also, the concept of reconfigurability was initially designed for frequency switched antenna systems but has also been slowly adopted for pattern reconfigurability – although the concept has not yet been fully accepted.

To date, a lot of the research effort in MIMO antenna arrays have either separately focused on developing techniques that uses conventional antennas as adaptive arrays [21] – [23], or building compact reconfigurable antenna arrays for adaptive MIMO as an alternative to conventional arrays [20] – [26]. A few quantitative studies have also considered the system-level performance benefits of antenna reconfigurabil-

ity [9], [10] and [112]. These works are however limited to simulation studies rather than practical implementations in a real-time MIMO system. Their approaches also decouples the design of the reconfigurable antenna arrays from that of the physical layer signal processing. And in so doing fail to take full advantage of multi-antenna systems when applied in spatially correlated channel environments. As already established, spatial correlation degrades the performance of multi-antenna systems by limiting the number of antennas that can be used for a given MIMO link. Also, the dependence of spatial correlation on both spatial characteristics of the channel and antenna array parameters such as antenna geometry and pattern, requires a different design approach.

In this thesis work we attempt to bridge the gap between the concept and theory of reconfigurable antenna array systems and their practical integration in a wireless communication system. We integrate working prototypes of pattern-reconfigurable antenna arrays in a 4G wireless framework and implement relevant physical layer algorithms that leverage their capabilities. Our design technique couples the design of the reconfigurable antenna arrays with the physical layer signal processing algorithms to improve system performance. Specifically, a system-level implementation of a MIMO physical layer model that leverage the capabilities of reconfigurable antennas is carried out in concert with various signal processing and link adaptation algorithms. The algorithms are designed and developed with computational efficiency in mind in order to optimize the performance benefits of these antenna arrays.

Among the myriad of MIMO signal processing techniques, approaches that take advantage of spatial multiplexing, spatial diversity, Beamforming or spatial filtering, were implemented and benchmarked against other works in literature. Notably, the approaches in [21], [23], and [104] which employ spatial multiplexing and transmit beamforming, antenna grouped algorithms are implemented. The work in [21] pro-

poses a multimode antenna selection algorithm that dynamically adjusts both the number of substreams and the mapping of substreams to antennas, for a fixed data rate, to the channel conditions. It also discusses a dual-mode selection algorithm that switches between spatial multiplexing and beamforming. It also derives several expressions that characterize the various criteria for selecting the number of substreams and the optimal mapping of substreams to transmit antennas. In [23], an adaptive algorithm that selects between beamforming, multimode antenna selection and spatial multiplexing is presented. This model extends the work in [21] to demonstrate capacity gains derived from adaptively switching between MIMO schemes. The work in [104] introduces several mode selections criteria and a low complexity criterion which is derived from a low complexity antenna grouping algorithm.

However, all these works employ conventional antenna arrays and limited attempts have been made to implement pattern reconfigurable antenna arrays. The proposed model in this dissertation leverages the pattern diversity derived from using reconfigurable antenna arrays to improve system performance in lieu of conventional antenna arrays approaches.

1.3 Contributions

The main implication of our work is the demonstration of the benefits of pattern reconfigurable antenna arrays to motivate their integration in portable MIMO wireless systems – systems that are too small to employ conventional antenna arrays due to space/design limitations. This integration is possible due to the fact that a single reconfigurable antenna structure is used to act as a multiple element array in lieu of several physical antenna elements. Other contributions of this dissertation are summarized below:

1. Provide a pattern diversity characterization of reconfigurable antenna arrays

that resonate in the frequency band between 2.5 – 3GHz for application in next generation wireless systems.

- Demonstrate and benchmark the benefits of pattern diversity derived from reconfigurable antennas through an exhaustive study of the spatial parameters and characteristics that affects MIMO array wireless transmissions. Specifically, the effects of spatial correlation on the performance of reconfigurable antenna systems against that of conventional arrays derived from techniques such as antenna grouping; this is motivated by the dependence of spatial correlation on both spatial characteristics such as angular spread, the number of scatterers, and antenna array parameters including the antenna geometry, element spacing and pattern, polarization, and mutual coupling
- Analyze the performance of these pattern reconfigurable antennas as an integral part of a WiMAX/LTE system through field testing and benchmark their performance against that of conventional commercial antenna arrays. Part of this work is published in [27]

2. Implement an adaptive system-level physical layer model for MIMO array system that leverage the capabilities of reconfigurable antennas and wireless transmission architectures such as OFDM, spatial multiplexing and precoding.

- Experimentally benchmark the proposed model against some simulation-based quantitative models that use antenna grouping in lieu of RAS
- Propose a low complexity adaptive algorithm for joint antenna state or configuration selection and link adaptation based on post processing SNR (ppSNR) as a performance metric and is published in [118] and [29].

3. Integrate pattern reconfigurable antennas into a 4G wireless system, specifically WiMAX/LTE platform.

    - Benchmark the performance of reconfigurable antennas with conventional commercial antennas for WiMAX/LTE applications. Part of this work appears in [27] and [30]

1.4 Organization

This thesis is organized as follows: Chapter 2 discusses the motivation for adaptive multi-antenna communication systems and introduces adaptive antenna array systems known as reconfigurable antenna arrays for MIMO communications.

Chapter 3 provides an overview of MIMO communication architectures and transmission techniques used in concert with MIMO signal processing. The concept of BLAST transmission for multi-antennas processing is first introduced, followed by a discussion of the relevant detection/decoding algorithms used in a MIMO system employing V-BLAST.

Chapter 4 presents the principle of MIMO-OFDM transmission for wireless transmissions in frequency selective wireless channels as the system model for next generation technologies.

Chapter 5 introduces the design of a pattern reconfigurable antenna arrays for applications that operate in the frequency band between 2.5–2.7 GHz. The antenna specifications and design methodology are described, followed by a presentation of some experimental results.

Chapter 6 proposes a joint antenna state selection and link adaptation algorithm that leverages the capabilities of reconfigurable antennas and adaptive modulation to increase throughput in MIMO-OFDM systems. Field experimentation results for the implementation of a 2x2 MIMO-OFDM system in a Software Defined Radio (SDR)

framework are presented. Chapter 7 presents a system-level implementation of several MIMO approaches in the SDR framework presented in Chapter 6. Chapter 8 presents a platform for integrating pattern reconfigurable antennas in next generation systems.

Chapter 9 provides a summary of this thesis work and contributions, including the future work.

CHAPTER 2: ADAPTIVE MULTI-ANTENNA COMMUNICATIONS SYSTEMS

In theory, the performance of wireless communication systems can be improved by using multiple antennas for signal transmission and reception. Ideally, the propagation channels between each transceiver antenna pair are statistically independent and identically distributed (i.i.d); this enables the generation of multiple independent channels with identical characteristics by precoding, which, can be used for either transmitting multiple data streams or increasing the reliability. Realistically, however, the channels between different antennas are often correlated and therefore the potential multi-antenna gains may not be obtainable [31], [32]. Spatial correlation - a correlation between the signal's spatial direction and the average received signal gain - degrades the performance of multi-antenna systems and limits the number of antennas that can compactly be squeezed on a device. This is because it decreases the number of independent channels that can be created by precoding [33], [156]. However, rich multipath propagation decreases the spatial correlation by spreading the signal such that multipath components are received from many different spatial directions [155]. This is the reason why recent research in this field has focused on the development of adaptive antenna systems that exploit multipath propagation to mitigate the effects of wireless channel fading or fluctuations. In this chapter we introduce a new class of adaptive antenna systems and the techniques commonly used to leverage their capabilities in multi-antenna communication.

2.1 Adaptive Antenna Array Systems

The term "Adaptive Antenna" was first used to describe a self-phasing antenna system which reradiates a signal in the direction from which it was received [36]. The adaptive aspect stems from the fact that it performs without any prior knowledge of the direction in which it is to transmit. Generally, an Adaptive Antenna System (AAS) can focus it's transmit energy to the direction of the receiver and, while receiving, it can focus the energy to the direction of the transmitter. The technique used for this purpose is known as Beamforming or Beamsteering or Beamshaping; it works by adjusting the width and the angle of the antenna radiation pattern or beam. AAS systems often employ adaptive arrays – a number of antenna elements coupled together via a controller – to exploit the spatial dimension in signal processing to improve system operating parameters: such as capacity, quality, coverage and cost. They make use of these adaptive arrays to allow the antenna to steer the beam to any direction of interest while simultaneously nulling interference [37]. The direction of the signal beams is estimated using the direction-of-arrival (DOA) estimation methods [38]. Fig. 2.1 illustrates the use of an adaptive antenna array for beamforming in a mobile network.

2.1.1 Reconfigurable Antenna Systems (RAS)

Reconfigurable Antenna Systems [39]–[45] are a new class of adaptive antenna systems that dynamically tune their electrical or radiation characteristics in response to multivariate wireless channel fluctuations. These antennas are capable of dynamically changing their radiation patterns, polarization states, and frequency of operation to accommodate the operating requirements [8]. Recently, different solutions employing various techniques for reconfiguring the radiation characteristic have been proposed. These techniques fall under one of these categories:

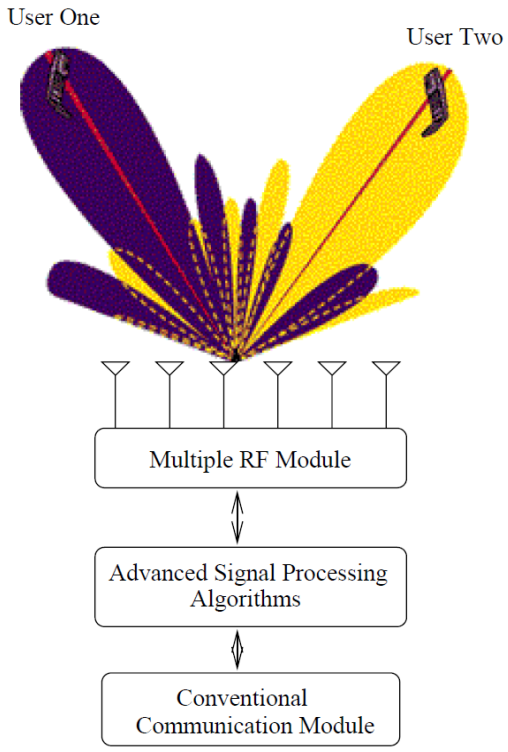

Figure 2.1: Using Adaptive Antenna Array for Beamsteering (Adapted from [38]).

(i) Pattern Diversity: exploits the difference in radiation pattern between two or more co-located antennas (array) to decorrelate the sub-channels of the link [116]. "This technique helps to achieve independent fading by transmitting/receiving on different signal paths at each antenna. In the ideal case each array element has a radiation pattern that points in a direction different from all the others in order to capture signals that are uncorrelated from those collected at the other elements [8]."

(ii) Spatial Diversity: uses multiple antennas that are physically separated in space and exploits the phase delay between the antennas to decorrelate the fading signals [47]. This technique requires a minimum spacing between antenna elements depending on the environment and the width of the multipath angle of arrival.

This scheme allows multiple users to share a limited communication spectrum and avoid co-channel interference.

(iii) Polarization Diversity: uses antenna array with orthogonal polarizations. The benefit of this scheme is the ability to use antennas located in the same place, unlike spatial diversity. The work in [48] demonstrates the impact of polarization diversity on sub-channel decorrelation and channel capacity in MIMO systems.

Bried Review of Related Works in Reconfigurable Antennas

The literature of reconfigurable antennas is vast and still growing. Several works in [166]–[169] have proposed reconfigurable antennas that are reconfigurable in frequency. These works design and characterize radio frequency microelectromechanical (RF-MEMS)-based reconfigurable antennas that operates in multiple frequencies for various application. The reconfigurability between the modes is achieved by using RF MEM switch technology, which enables changing antenna length and electrical properties, thereby the resonance frequency. However, despite the excellent switching characteristics of the MEMS technology, the reliability and packaging of these switches is problematic and their power handling capability is limited.

For application in mobile communications, the works [159], [160], and [161], [43], and [45] have leveraged polarization, spatial, and pattern reconfigurable antennas to improve link reliability in wireless communications. While other research works in [170]-[171] have developed reconfigurable antennas for laboratory on chip applications in the medical field. Their antenna reconfiguration mechanism rely on electrowetting based on digital microfluidics to implement a frequency reconfigurable antenna.

The wireless laboratory at Drexel University has focused on designing, testing and fabricating pattern reconfigurable including

(i) Reconfigurable length dipole antenna [10]: This antenna consist of a dipole that

can be reconfigured in length using PIN diode switches. The switch configuration can be modified in a manner that is adaptive to changes to the environment. This antenna is normally developed as part of an array whose elements are a quarter of a wavelength apart. The configuration of switches then affects the mutual coupling between the array elements, and subsequently, the radiation pattern of each antenna element. This leads to different degrees of pattern diversity that can be used to improve link capacity ;

(ii) Reconfigurable radius circular patch antenna [39], [40]: it is based on a standard circular patch antenna design and enables a single antenna element to be used as a two element array by using multiple feed points. By exciting different electromagnetic modes and varying the size of the circular patch antenna as well as the feed location, different polarization and radiation patterns cane be generated at the far-field. These antennas exploit the techniques of pattern and polarization diversity to increase the diversity level of the system and the amount of received signal power ;

(iii) Reconfigurable length spiral antenna [41]: This antenna structure consists of a single arm Archimedean spiral whose arm length can be reconfigured using PIN diode switches. The length variation excites different radiation patterns at the same frequency of operation.;

(iv) Reconfigurable leaky wave antenna [42]: This is a composite right left handed (CRLH) microstrip structure that incorporates varactor diodes for fixed-frequency voltage-controlled operation. Beam scanning is achieved by modulating the capacitance of the structure by adjusting a bias voltage applied to the varactors. Each excitation bias voltage generates a different radiation pattern that can be used to improve diversity.

In this thesis, we use reconfigurable adaptive antenna arrays that leverage pattern diversity to improve system performance. Specifically, we design and characterize pattern reconfigurable microstrip arrays based on a reference design for 4G applications. We investigate the benefits offered by radiation pattern diversity in these reconfigurable antenna arrays. Our motivation for these antenna arrays stems from the findings of previous studies, which have shown that the capacity of conventional multi-element arrays (MEAs) is adversely affected by spatial correlation–as a result of both spatial channel characteristics and antenna array geometry and radiation patterns. However, the design flexibility of pattern reconfigurable antenna arrays enables us to exploit the antenna geometry and mutual coupling between radiating array elements to generate uncorrelated channels. This results in pattern diversity that can improve capacity and offer a unique opportunity for antenna system miniaturization for portable wireless devices.

CHAPTER 3: MIMO COMMUNICATION ARCHITECTURES AND TECHNIQUES

Even though the benefits of antenna arrays for MIMO communication have been demonstrated in [10], [41], [49] and several other efforts, the full advantages of these arrays are dependent on the use of MIMO processing and transmission techniques. This fact is especially crucial for adaptive antenna arrays like reconfigurable antenna arrays that rely on shift processing and implementation. The tremendous potential and impact of MIMO processing on capacity increase was reported in [6], [7], and [50]. However, in order to design efficient communication algorithms for MIMO systems and to understand the performance limits, it is also important to understand the nature of the channel. In this chapter we present an overview of MIMO signal processing architectures and the relevant transmission techniques used in concert with them.

3.1 MIMO Transmission Architectures

As briefly discussed in Chapter 1, numerous theoretical investigations have demonstrated that the multipath wireless channels can be exploited using MIMO systems to improve channel capacity. However, these capacity benefits can only be realized through the use of appropriate MIMO processing architectures [5] and [51]. These approaches are commonly known as BLAST (Bell Laboratories Layered Space-Time) architectures and have become the de facto reference architectures for high performance MIMO systems. The BLAST architecture utilizes multi-element transmit and receive arrays to provide high capacity wireless communications. In rich multipath environment that experiences Rayleigh scattering, the BLAST structure leads to the-

oretical rates which grow linearly with the number of antennas for a system that employs equal number of transmit and receive antennas. These rates have been shown to approach the Shannon capacity limit in [52]. Two types of BLAST architectures have been widely publicized: D-BLAST [5] and V-BLAST [51]. In this section we present a brief overview of the D-BLAST architecture and provide a more detailed treatise of V-BLAST. We utilize the V-BLAST processing structure for implementation of a realistic MIMO communication system presented in [118] as part of this thesis work.

3.1.1 D-BLAST Transmission

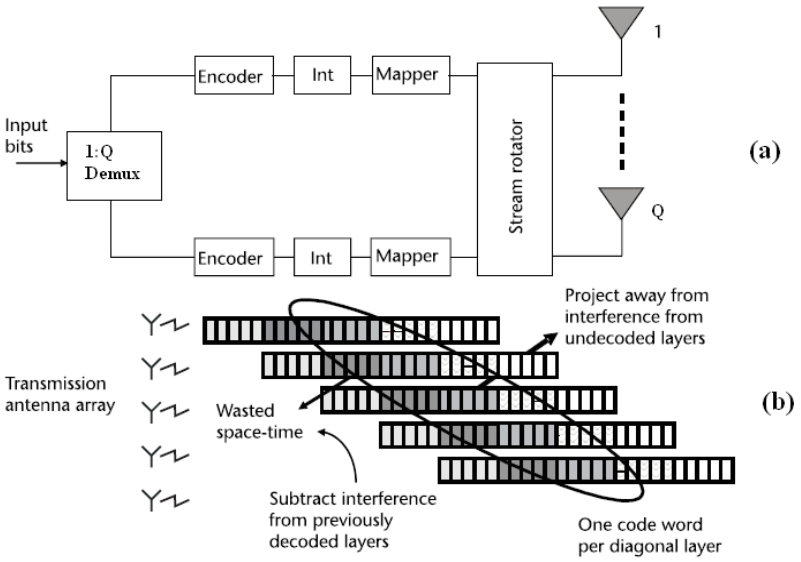

Figure 3.1: D-BLAST Transmission Technique/Diagonal Encoding (Adapted from [53]).

D-BLAST which stands for diagonal BLAST (D-BLAST), is a diagonally-layered space-time architecture proposed by Foshchini in [5]. In this architecture, the information bit stream from the source is first demultiplexed (at the Demux block) into

several Q substreams – one stream per transmit antenna. Each substream is separately encoded, interleaved and mapped to complex symbols (refer to Fig. 3.1 (a)). Before going to the antenna, the signal substream is rotated in a round-robin fashion so that the bit-substream and antenna association is periodically recycled [53]. The symbols of each substream are dispersed diagonally across antennas and time as illustrated in Fig. 3.1 (b).

Each block in Fig. 3.1 (b) represents a transmitted symbol. A layer consists of Q consecutive blocks with the same color. Each layer is represented with a different shade and runs diagonally through the antenna elements as time progresses. Rather than commit each data substream to a single antenna, the D-BLAST ensures that none of the layers misses out because of a poor transmission path. However, one draw back of this layered approach is that it introduces space time wastage where no transmission can take place. But because the symbols are spread across antennas, the scheme captures transmit diversity.

At the receiver, the decoding is performed layer-by-layer since each diagonal layer constitutes a complete code word. D-BLAST uses a detection strategy that combines interference cancellation and suppression. This is to yield a symbol vector that is free of interference from all signals that were simultaneously transmitted from the other antennas. As depicted in Fig. 3.1 (b), the entries below the first diagonal layer is empty or zeros; this is illustrated by the wasted space-time. "To decode the first diagonal layer, the receiver generates a soft-decision statistic for each entry in that diagonal. In doing so, the interference from the upper diagonals is suppressed by projecting the received signal onto the null space of the upper interfaces. The soft statistics are then used by the corresponding channel decoder to decode this diagonal. The decoder output is then fed back to cancel the first diagonal contribution in the interface while decoding the next diagonal [53]." The rest of the diagonal layers are

decoded in the same manner.

3.1.2 Vertical BLAST (V-BLAST) Transmission

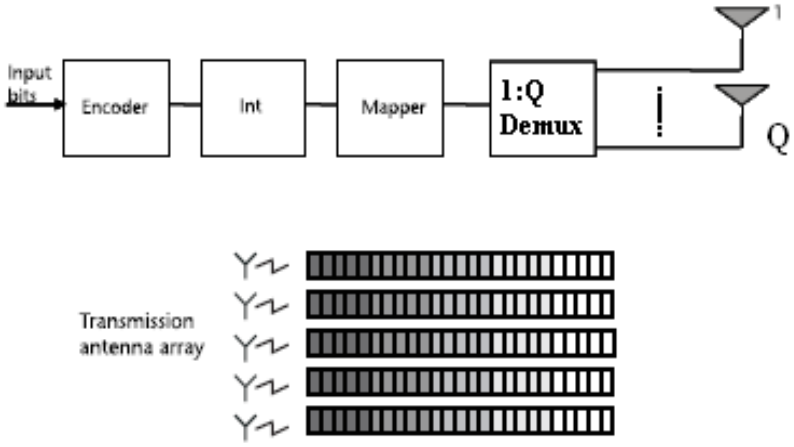

Figure 3.2: Vertical Encoding or V-BLAST System (Adapted from [53]).

The vertical BLAST is a variant of the diagonal approach and tries to reduce the computational complexity of the D-BLAST architecture by using simplified encoding [51]. As in D-BLAST, a single data stream is demultiplexed into Q substreams, however, in V-BLAST the bit stream is encoded, interleaved and mapped into symbols before being fed to the demultiplexer. VBLAST uses vertical encoding – each information symbol can be spread across all antennas and the layers are coupled; thus, there is no rotation of substreams as in D-BLAST. Diversity is improved since the transmission is spread over all transmit antennas and each substream is received by all receiving antennas.

The vertical encoding eliminates the space time wastage from the diagonal en-

coding in D-BLAST, but loses the transmit diversity because each stream goes over only one antenna. Fig. 3.2 illustrates the V-BLAST system. The transmitters are conventional QAM transmitters and operate cochannel at symbol rate 1/T symbols, with synchronized symbol timing. Receivers 1–P are also ordinary QAM receivers that operate cochannel (radio transmission occurs on the same frequency channel), each receiving the signals radiated from all Q transmit antennas.

At the decoder, V-BLAST implements a nonlinear detection technique based on Zero Forcing (ZF) combined with symbol cancellation to improve performance. Note, ZF is an equalization algorithm which applies the inverse of the frequency response of the channel to the received signal, to restore the signal after the channel. The key idea in the signal detection is to look at the signals from all the receive antennas simultaneously. This process is done by first extracting the strongest substream from the received signals, and then proceeding with the weaker signals; decoding the weaker signals is made easier since it is done after the strongest substream has been removed as a source of interference [53]. The process is known as Successive Interference Cancellation (SIC); and is similar to decision feedback equalization. The ordering of the substreams becomes important for the overall system performance when symbol cancellation is used. Ordering determines the post-detection SNR and the transmitted symbol with the smallest post-detection SNR ultimately dominate the error performance of the system. We will discuss V-BLAST detection or decoding process in more detail, shortly; but for simplicity we base our explanation on the generic MIMO system in Fig. 3.3.

A Generic MIMO Channel using V-BLAST Architecture

Consider a generic discrete-time MIMO system in Fig. 3.3 with Q antennas at the transmit side (TX) and P antennas receiver side (RX). The MIMO channel at a

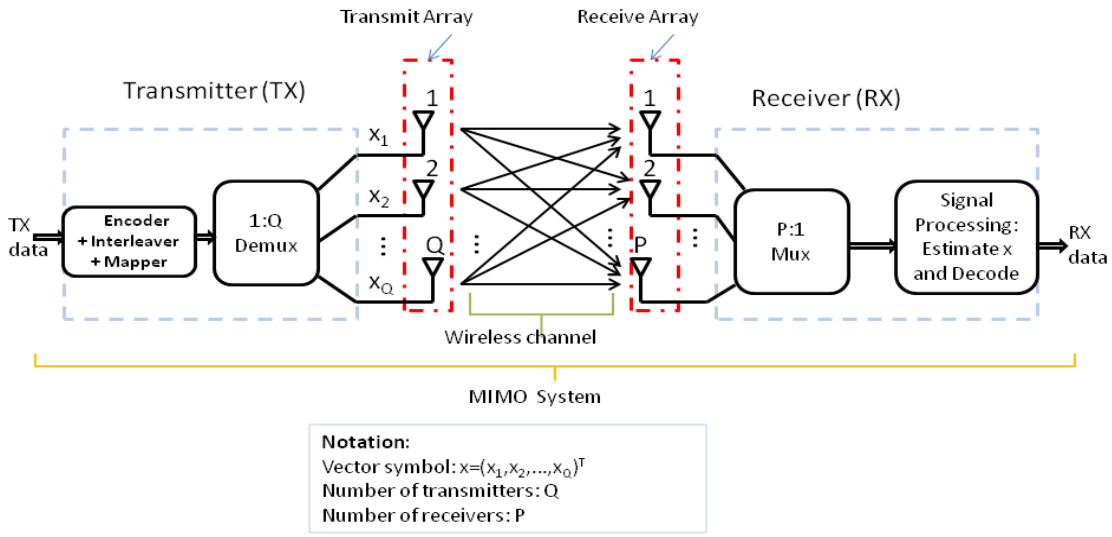

Figure 3.3: MIMO Transmission System using VBLAST

given instant is represented as a PxQ matrix **H**.

$$\mathbf{H} = \begin{bmatrix} H_{1,1} & H_{1,2} & \dots & H_{1,Q} \\ H_{2,1} & H_{2,2} & \dots & H_{2,Q} \\ \vdots & \vdots & \vdots & \vdots \\ H_{P,1} & H_{P,2} & \dots & H_{P,Q} \end{bmatrix}.$$

where $\mathbf{H}_{p,q}$ is the channel gain between the pth receive and qth transmit antenna pair. The qth column of **H** is the spatial signature of the qth transmit antenna across the receive antenna array. "The relative geometry of the Q spatial signatures determines the distinguishability of the signals launched from the transmit antennas at a receiver. This is important when independent data streams are launched from the transmit antennas, as in spatial multiplexing [54]."

For a frequency-flat fading – the delay spread in the channel is negligible compared to the inverse bandwidth – MIMO channel, the discrete-time signal relationship over

a symbol period is modeled by :

$$\mathbf{y} = \sqrt{\frac{E_x}{Q}}\mathbf{H}\mathbf{x} + \mathbf{z} \tag{3.1}$$

where $\mathbf{y}$ is the Px1 received signal vector, $\mathbf{x}$ is the Qx1 transmitted signal vector, $\mathbf{z}$ is the temporally Additive White Complex Gaussian Noise (AWGN) with $E[\mathbf{z}\mathbf{z}^H] = N_o\mathbf{I}_P$ and variance σ^2; $(.)^H$ denotes the hermitian transpose. E_x is the total average energy available at the transmitter over a symbol period after all losses due propagation and shadowing have been removed. It is assumed that the covariance matrix of $\mathbf{x}$, $\mathbf{R}_{xx} = E[\mathbf{x}\mathbf{x}^H]$ and satisfies $Tr(\mathbf{R}_{xx}) = Q$. The ratio $\rho = E_x/N_o$ is SNR per receive antenna. Furthermore, channel block fading – the channel time variation is negligible over L consecutive symbol periods (determined by the coherence time) [55]. Also, the transmitters are conventional QAM transmitters and operate cochannel at symbol rate 1/T symbols, with synchronized symbol timing. Receivers 1–P are also ordinary QAM receivers that operate cochannel, each receiving the signals radiated from all Q transmit antennas.

Implementing V-BLAST Detection: Zero-Forcing decoder

Suppose $\mathbf{x} = (x_1, x_2, ..., x_Q)^T$ denote the vector of transmit symbols. Then, the corresponding received P-vector $\mathbf{y}$ is given by (3.1). Since the processing takes place at the receiver where, under assumption the channel matrix $\mathbf{H}$ is invertible, $\mathbf{H}$ is inverted and the transmitted MIMO vector $\mathbf{x}$ is estimated by the ZF decoder as

$$\mathbf{x}_{est} = \mathbf{H}^{-1}\mathbf{x} \tag{3.2}$$

Conceptually, the ZF principle is based on a conventional Adaptive Antenna Array technique known as linear combinatorial nulling [56]. In this technique, the detection

algorithm starts by considering each substream as the desired signal, and the remainder as the interferers. Nulling is performed by linearly weighting the received signals such that all interfering terms are canceled. For Zero-Forcing, nulling is performed by selecting $1xQ$ dimensional weight vectors $\mathbf{w}_i, i = 1, 2, ..., Q$, referred to as nulling vectors [56], such that it satisfies

$$\mathbf{w}_i^T(\mathbf{H})_q = \begin{cases} 0, & q \neq i \\ 1 & q = i \end{cases} \tag{3.3}$$

where $(\mathbf{H})_q$ is the q-th column of $\mathbf{H}$ and $q = 1, 2, ..., Q$, denoting the qth transmitter. The decision statistic for the $i - th$ substream is therefore $r_i = \mathbf{w}_i^T\mathbf{y}$.

For simplicity, let $\mathbf{w}_i$ be the ith row of a matrix $\mathbf{W}$, then it follows that

$$\mathbf{WH} = \mathbf{I}_P, \tag{3.4}$$

where $\mathbf{W}$ is a matrix that represents the linear processing in the receiver. So, by forcing the interferers to zero, each desired element of $\mathbf{x}$ can be estimated. If $\mathbf{H}$ is not square, $\mathbf{W}$ equals the *pseudo-inverse* of $\mathbf{H}$ (denoted by $\mathbf{H}^\dagger$) given by

$$\mathbf{W} = \mathbf{H}^\dagger = (\mathbf{H}^H\mathbf{H})^{-1}\mathbf{H}^H. \tag{3.5}$$

The *pseudo-inverse* exists when $Q \leq P$ and all elements of $\mathbf{H}$ are assumed to be *i.i.d.* For $Q > P$, $\mathbf{H}^H\mathbf{H}$ is singular and its inverse does not exist. When the *pseudo-inverse* exists, the estimates of $\mathbf{x}$ (given by $\mathbf{x}_{est}$) is derived as follows

$$\mathbf{x}_{est} = \mathbf{Wx} = \mathbf{H}^\dagger\mathbf{x}(\mathbf{H}^H\mathbf{H})^{-1}\mathbf{H}^H\mathbf{x}. \tag{3.6}$$

One disadvantage of using Zero-Forcing is that it suffers from noise enhancements – it will amplify the noise by a large factor and destroy the signal power– especially for channels with a high condition number ($\mathbf{H}^H\mathbf{H}$). For this reason, V-BLAST detection combines ZF nulling with symbol cancellation or Successive Interference Cancellation (SIC) – the interference from the already-detected components of $\mathbf{x}$ is subtracted out from the received signal vector; resulting in a modified received vector in which, fewer interferers are present [51].

When SIC is used, the order of detection of the substreams or the components of $\mathbf{x}$ becomes important for system performance. Applying SIC with optimal ordering ensures that the reliability of the symbol which is decoded first is guaranteed to have a lower error probability than the other symbols. This lowers the chances of making incorrect decisions with the other symbols, and therefore lowers the overall error rate of detection. For our discussion, let the ordered set

$$\zeta \equiv \zeta_1, \zeta_2, ..., \zeta_Q \tag{3.7}$$

represent a permutation of the integers $1, 2, ..., Q$ specifying the order in which components of the transmitted symbol vector $\mathbf{x}$ are extracted. The general detection process for the V-BLAST structure proceeds as follows:

Step 1: Using nulling vector $\mathbf{w}_{\zeta_1}$, form a linear combination of the components of $\mathbf{y}$ to yield a decision statistic r_{ζ_1}:

$$r_{\zeta_1} = \mathbf{w}_{\zeta_1}^T \mathbf{y} \tag{3.8}$$

Step 2: Slice r_{ζ_1} to obtain $\hat{x}_{\zeta_1}$:

$$\hat{x}_{\zeta_1} = sgn(r_{\zeta_1}) \tag{3.9}$$

where $sgn(.)$ denotes the quantization (slicing) operation appropriate to the constellation in use.

Step 3: Assuming that $\hat{x}_{\zeta_1} = x_{\zeta_1}$, cancel x_{ζ_1} from the received vector $\mathbf{y}$; resulting in modified received vector y_2:

$$y_2 = \mathbf{y} - \hat{x}_{\zeta_1}(\mathbf{H})_{\zeta_1} \tag{3.10}$$

where $(\mathbf{H})_{\zeta_1}$ denotes the ζ_1th column of $\mathbf{H}$. Steps 1 to 3 are then performed for components $\zeta_2, ..., \zeta_Q$ by operating in turn on the progression of modified received vectors $\mathbf{y}_2, \mathbf{y}_3, ..., \mathbf{y}_Q$.

Note, the ζ_ith ZF nulling vector is defined as the unique minimum norm vector satisfying

$$\mathbf{w}_{\zeta_i}^T(\mathbf{H})_{\zeta_q} = \begin{cases} 0, & q \geq i \\ 1 & q = i \end{cases} \tag{3.11}$$

Thus, the ζ_ith ZF nulling vector, $\mathbf{w}_{\zeta_i}$, is orthogonal to the subspace spanned by the contributions to $\mathbf{y}_i$ due to those symbols not yet estimated and canceled. It can be shown that the unique vector in (3.11) is just the ζ_ith row of $\mathbf{H}_{\zeta_{i-1}}^{\pm}$, where the notation $\mathbf{H}_{\zeta_i}^{-}$ denotes the matrix obtained by zeroing columns $\zeta_1, \zeta_2, ..., \zeta_i$ of $\mathbf{H}$ and $^+$ denotes the *Moore-Penrose psuedoinverse* [57].

The full ZF V-BLAST algorithm detection algorithm is a recursive procedure, including determination of the optimal ordering and is given by **Algorithm 1** below [51]:

Algorithm 1 ZF V-BLAST Detection Algorithm

1: *initialization*:
2: $i \leftarrow 1$
3: $\mathbf{G}_1 = \mathbf{H}^+$
4: $\zeta_1 = \arg\max_q ||(\mathbf{G}_1)_q||^2$
5: *recursion*:
6: $\mathbf{w}_{\zeta_i} = (\mathbf{G}_1)_{\zeta_i}$
7: $r_{\zeta_i} = \mathbf{w}_{\zeta_i}^T \mathbf{y}_i$
8: $\hat{x}_{\zeta_i} = sgn(r_{\zeta_i})$
9: $\mathbf{y}_{i+1} = \mathbf{y}_i - \hat{x}_{\zeta_i}(\mathbf{H})_{\zeta_i}$
10: $\mathbf{G}_{i+1} = \mathbf{H}^{\pm}_{\zeta_i}$
11: $\zeta_{i+1} = \arg\max_{q \notin \{\zeta_1,\ldots,\zeta_i\}} ||(\mathbf{G}_{i+1})_q||^2$
12: $i \leftarrow i + 1$

3.2 MIMO Signal Processing Techniques

MIMO technology can be implemented using different signal processing techniques. These techniques have varying characteristics and are used for different scenarios. This section briefly introduces a handful of these multi-antenna technologies by analyzing various technical features and their application scenarios.

3.2.1 Spatial Multiplexing (SM)

In spatial multiplexing, multiple independent signals are transmitted over the same frequency at the same time. Thus, different data signals are sent on the same time-frequency resource from different antennas so that spectrum efficiency is multiplied without expending more frequency resource. Therefore, if the SM system consisting of Q transmit antennas and P receive antennas is used, then the maximum number of independent signals that can be transmitted is $min\{Q, P\}$. This is illustrated in Fig. 3.4(a). A spatial multiplexing system may be arranged in different ways: In the downlink channel, the P receive antennas may belong to the same user or may be used by P different users. Similarly, in the uplink, the transmit antennas

may either belong to the same user or different users. The availability of CSI, can help choose the best subset of transmit antennas in the case where all Q antennas are used by a single user or help select the best subset of users when the transmit antennas belong to different users.

Precoded Spatial Multiplexing (SM)

In point-to-point MIMO systems, precoded SM means that multiple data streams are emitted from the transmit antennas with independent and appropriate weightings such that the link throughput is maximized at the receiver output. In this usage, precoding refers to the process of prearranging the transmit signals in consideration of the channel state in such a way that the receiver can combine multiple antenna signals to detect the transmitted signal reliably [58]. This technique is illustrated in Fig. 3.4(b).

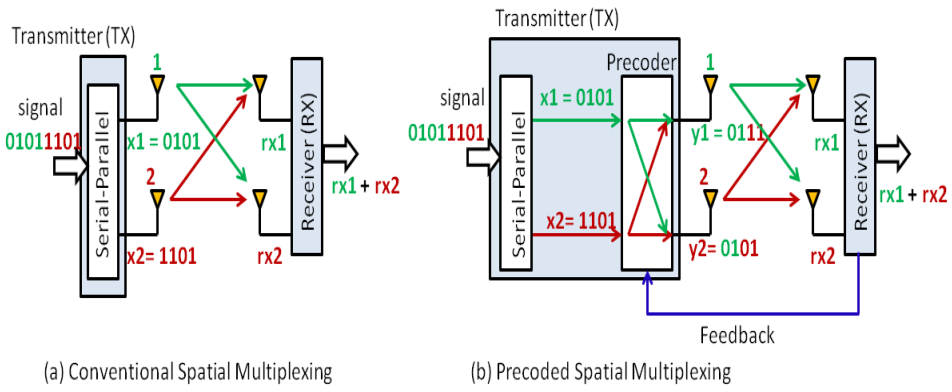

Figure 3.4: Schematic Diagram of Conventional Spatial Multiplexing and Preccoded Spatial Multiplexing

3.2.2 Space or Spatial Diversity (SD)

Space diversity uses redundancy to achieve transmitter diversity by sending orthogonal information set at two different timeslots from two different antennas. It can also be implemented by combining multiple signals obtained through an array of receive antennas. These signals are transmitted from the same source but have passed through statistically independent channels. Fig. 3.5 illustrates the techniques of spatial diversity and spatial multiplexing for a MIMO system with two transmission and two reception antennas.

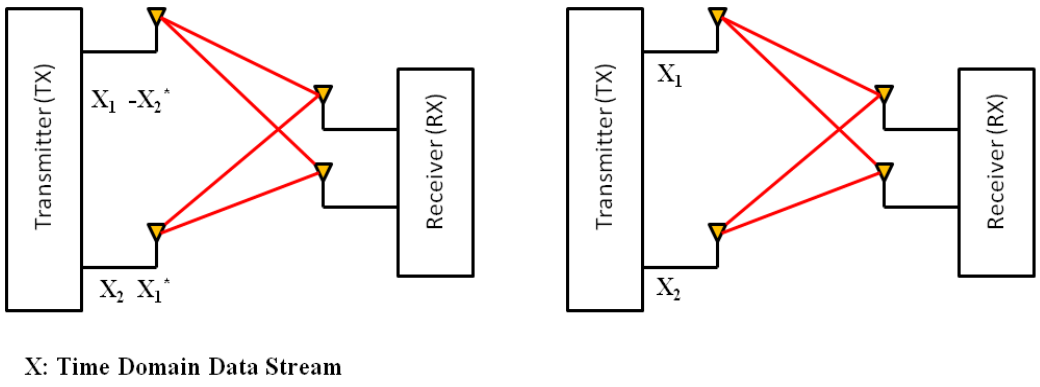

(a) Spatial Diversity (b) Spatial Multiplexing

Figure 3.5: Schematic Diagram of SD and SM for a 2x2 MIMO System

3.2.3 Beamforming

Beamforming or spatial filtering techniques uses the antenna array and advance signal processing algorithms to perform weighted processing on every physically separated antenna in the array. Beamforming is intended to maximize the power of the desired signals while minimizing or nulling the power of the interfering signals by

controlling the relative magnitudes and phases of the signals. Fig. 3.6 demonstrates how the beamforming technique uses an array of antenna elements to steer a signal energy or beam in a desired direction. The adaptive controller at the transmitter exploits the CSI feedback to select different transmission weights for each antenna element. Note, the transmission powers for each element in the array can also be adaptively allocated.

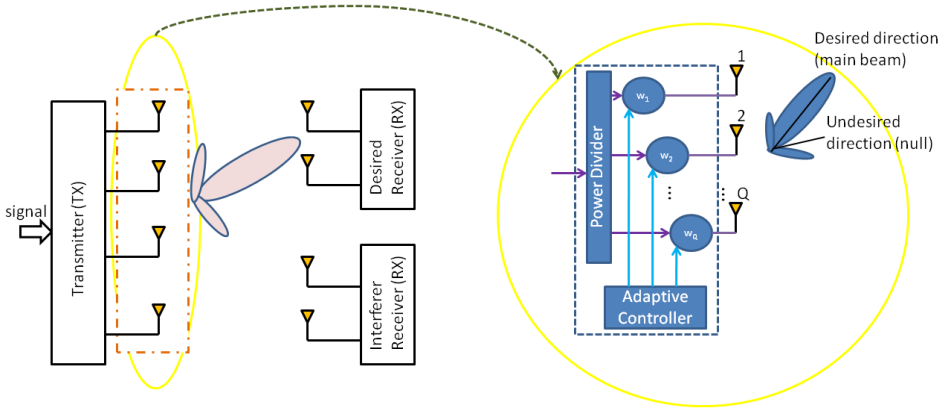

Figure 3.6: Schematic Diagram of Beamforming using an Adaptive Antenna Array

3.2.4 Hybrid MIMO and Beamforming

In order to leverage the benefits of MIMO and beamforming: increased transmission rate and signal reliability or diversity gain – both technologies are often combined. In such a hybrid system the physical antenna elements in the array at the transmitter are sub-divided into sub-arrays. On each sub-array, one virtual antenna or beam is formed with beamforming. These beams constitute spatial diversity or spatial multiplexing as illustrated in Fig. 3.7.

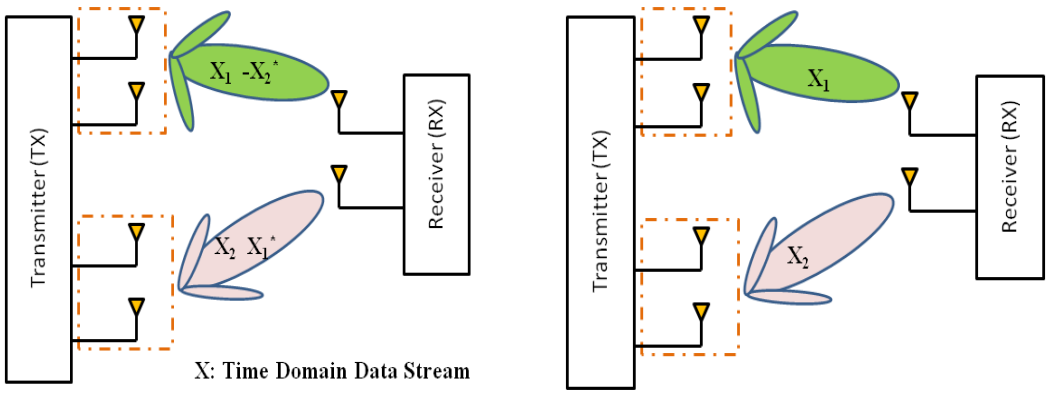

(a) Spatial Diversity + Beamforming (b) Spatial Multiplexing + Beamforming

Figure 3.7: Schematic Diagram of a Hybrid MIMO and Beamforming System for four Transmission Antennas and two Reception Antennas

CHAPTER 4: SYSTEM MODEL: MIMO-OFDM FOR WIRELESS TRANSMISSION

The MIMO architectures and techniques discussed in Chapter 3 are developed for flat fading channels. However, many of the current and future wireless communication systems are broadband in nature, i.e., the communication is over a frequency selective channel. Consequently, OFDM, which turns the frequency selective channel into multiple parallel flat fading channels, has been adapted as a companion for MIMO processing in next generation technologies [59]–[62]. This combined application of multi-antenna technology and OFDM modulation, resulted in the creation of a new architecture called MIMO-OFDM. Currently, MIMO-OFDM has been selected to be the air interface of several standards, such as WiMAX [63], LTE [64], and LTE-Advanced [65]. In this Chapter, we will briefly describe the principle of OFDM transmission and then, present the basic idea behind MIMO-OFDM processing for multi-antenna communication systems.

4.1 Orthogonal Frequency Division Multiplexing (OFDM)

OFDM is a type of multicarrier (MC) modulation technique for signal transmission over wireless channels first proposed by Chang in [66]. It is essentially identical to the Discrete Multi-tone Modulation (DMT) technique and is a Frequency Division Multiplexing (FDM) scheme. These techniques divide the total available bandwidth in a communication medium into a series of non-overlapping frequency sub-bands known as subchannels or subcarriers, each of which is used to carry a separate signal. This allows a single transmission medium such as a cable or a radio link to be shared by many signals.

Unlike FDM, OFDM uses the spectrum much more efficiently by spacing the subchannels closer together (refer to Fig. 4.1); this is achieved by making all the carriers orthogonal. The orthogonality of the subcarriers means that each subcarrier has an integer number of cycles over a symbol period. Due to this, the spectrum of each subcarrier has a null at the center frequency of each of the other subcarriers in the system. This results in no interference between the subcarriers. "Each subcarrier in an OFDM system signal has a very narrow bandwidth (e.g., 1 KHz), thus resulting in low symbol rate. This results in the signal having a high tolerance to multipath delay spread, as the delay spread must be very long to cause significant InterSymbol Interference (ISI) (e.g., >500 $\mu secs$) [53]."

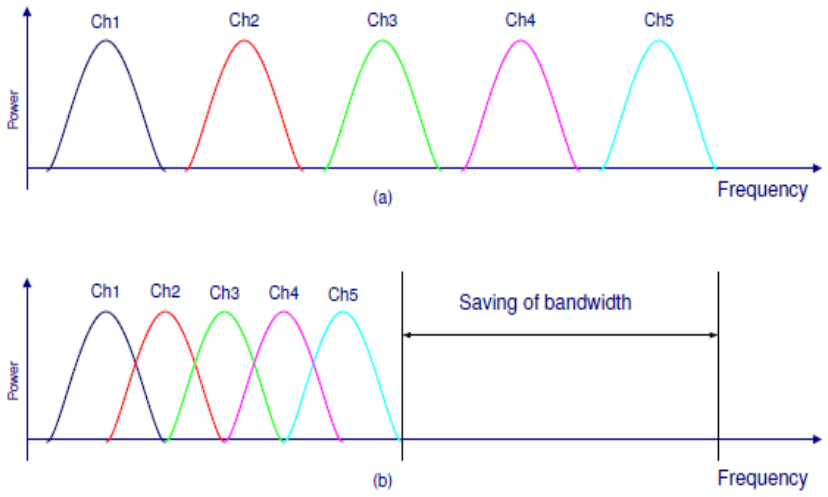

Figure 4.1: Comparison of FDM versus OFDM

One of the primary advantages of OFDM over single-carrier schemes is its ability to cope with severe channel conditions that arise from frequency-selective fading due to multipath, interference and attenuation of high frequencies. OFDM simplifies

channel equalization by turning a frequency selective channel into a set of parallel flat fading channels, and thus, avoids the use of equalizers in Inter-Symbol Interference mitigation [67]. Some of the pros and cons of OFDM includes:

- High spectral efficiency;
- Provides an opportunity to use link adaptation [68];
- Provides efficient and low complexity equalization using Fast Fourier Transform (FFT) processing;
- Robustness for high-data rate transmission over multipath fading channel;
- Sensitivity to synchronization errors – frequency offsets, timing errors and phase noise;
- Relatively high peak-to-average power ratio, which reduces the power efficiency of the RF amplifier [70].

4.1.1 OFDM Transceiver

Fig. 4.2 shows a block diagram of the baseband processing of an OFDM transceiver for a Single Input Single Output (SISO) system. Once the binary input data is processed by a data scrambler, channel encoding is applied to improve the bit error rate performance. The output of the encoder is then interleaved to reduce the burst symbol error rate. The bit stream is then mapped into symbols using Multi-level Quadrature Amplitude Modulation (M-QAM) schemes such as 4-QAM, 16-QAM, and 64-QAM. Depending on the channel fading conditions, these modulation rates can be selected adaptively to boost the data rate. The resulting complex symbols or spectrum is then converted to its time domain signal using and IFFT. The IFFT provides a

simple way of ensuring the orthogonality of the subcarrier signals in addition to the efficient transformation of the signal to the time domain.

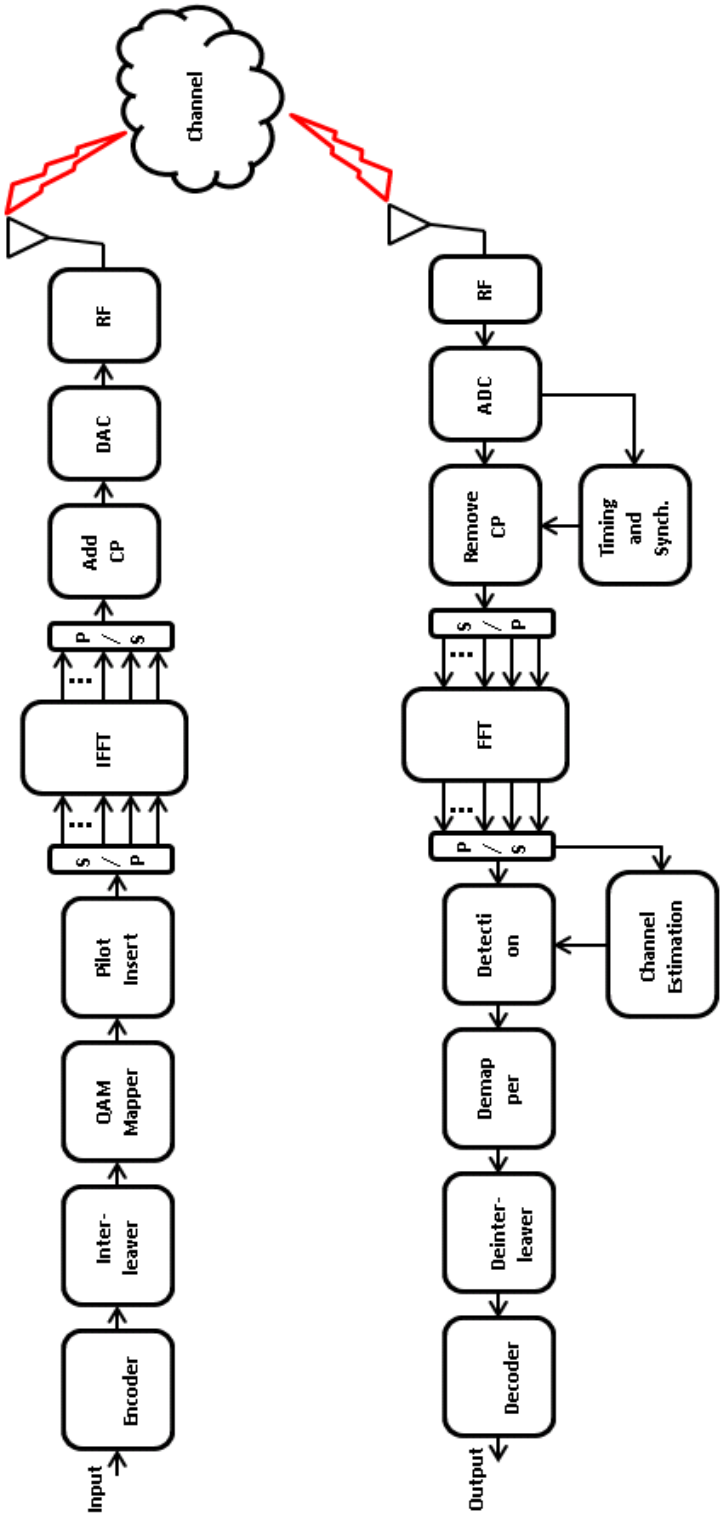

Figure 4.2: OFDM System Configuration for SISO

After OFDM modulation, a guard interval is inserted to suppress the ISI caused by multipath distortion [53]. The guard interval is also known as the *Cyclic Prefix* (CP). A cyclic prefix is a copy of the last part of the OFDM symbol, which is prepended to the transmitted symbol (refer to Fig. 4.3). This makes the transmitted symbol periodic, which plays a key role in identifying frames correctly. The addition of a guard interval allows time for the multipath signals from the previous symbol to die away before the information from the current symbol is received [71].

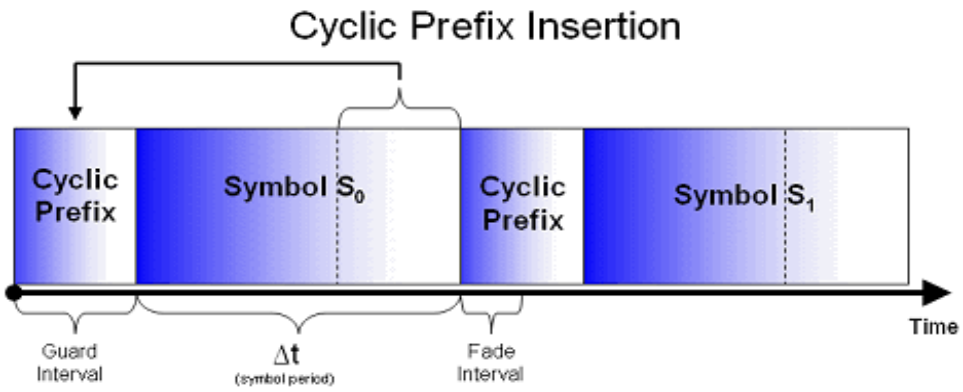

Figure 4.3: Cyclic Prefix Insertion

In addition to inserting a guard interval, OFDM also applies windowing - a technique to reduce the out-of-band radiation when the OFDM symbol would have a "discontinuous" end or beginning. The raised cosine window or filter is normally applied for pulse-shaping in order to minimize ISI [72]. Fig. 4.4 illustrates the time domain spectrum of two OFDM symbols that are separated by a guard interval and can easily be filtered using windowing. After the cyclic prefix block, the digital signal is converted in the DAC (digital to Analog converter) to produce the analog baseband signal. It is then upconverted to RF, and then transmitted by the antennas over the wireless channel.

At the receiver side, the reverse operation of the transmitter is performed. First, the received RF signal is down-converted to baseband and subsequently converted from analog to digital using the Analog-to-Digital (ADC) converter. The receiver corrects the frequency offset and symbol timing by using the training sequence inserted at the preamble by the transmitter. The CP is removed and then FFT is performed. The resulting signal is corrected for the channel influences, demapped, de-interleaved and finally decoded to obtain the transmitted binary output data.

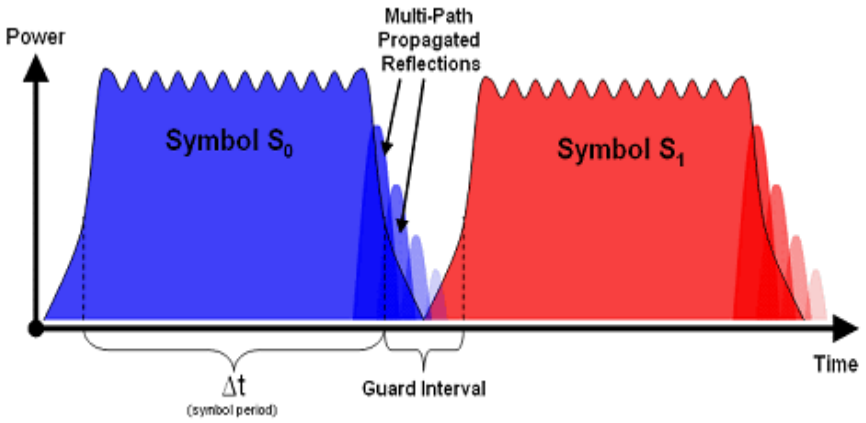

Figure 4.4: Depicts how Guard Interval reduces ISI (Adapted from [73]).

4.2 MIMO-OFDM System

When an OFDM signal is transmitted through a number of antennas in order to achieve diversity or capacity (higher transmission rate), the system is known as a MIMO-OFDM communication system. This system leverages the aforementioned advantages of MIMO systems and of the OFDM transmission technique to combat the frequency-selectivity of wireless communication channels. As already discussed,

OFDM transforms a frequency-selective channel into parallel flat-fading subchannels, and the MIMO technology exploits the multipath propagation resulting from slow fading to improve system performance. Thus, in addition to the spatial and temporal dimension of MIMO, OFDM adds one extra dimension to exploit: frequency dimension. MIMO-OFDM architecture therefore, enables the application of the same MIMO techniques for both narrowband and broadband communications [59], [74].

Fig. 4.5 shows a unified MIMO-OFDM system with 2 transmit (TX) and 2 receive (RX) antennas. It combines the functionality illustrated in Fig. 3.3 with that in Fig. 4.2. However, a couple of new features were added to this unified system. In addition to the regular encoder, interleaver and mapper, a MIMO demultiplexer and multiplexer are added to both the transmitter and receiver side, respectively. The MIMO demultiplexer (MIMO Demux) separates the single signal input from the mapper into multiple output signals corresponding to the number of transmit antennas. The multiplexer (MIMO Mux block) does the reverse process of merging the parallel streams from the received antennas into a single output.

The signal substreams from the MIMO demultiplexer are subjected to OFDM modulation as already explained in the previous section. First, it is split into parallel IFFT input using the S/P block (Serial to Paralell) where the pilot tones for channel training are inserted; the cyclic prefix is also added to help combat ISI. The IFFT output is then merged into a serial stream and converted from digital to analog at the D/A block. The resulting baseband signal is upconverted to the radio frequency (RF) before being sent to the antenna controller. The antenna controller selects the best antenna states or configurations for transmission based on some feedback from the transmitter. The RF signal is then transmitted over the wireless channel where it experiences multipath and noise. On reception, the reverse process is carried out on the signal as illustrated in Fig. 4.5.

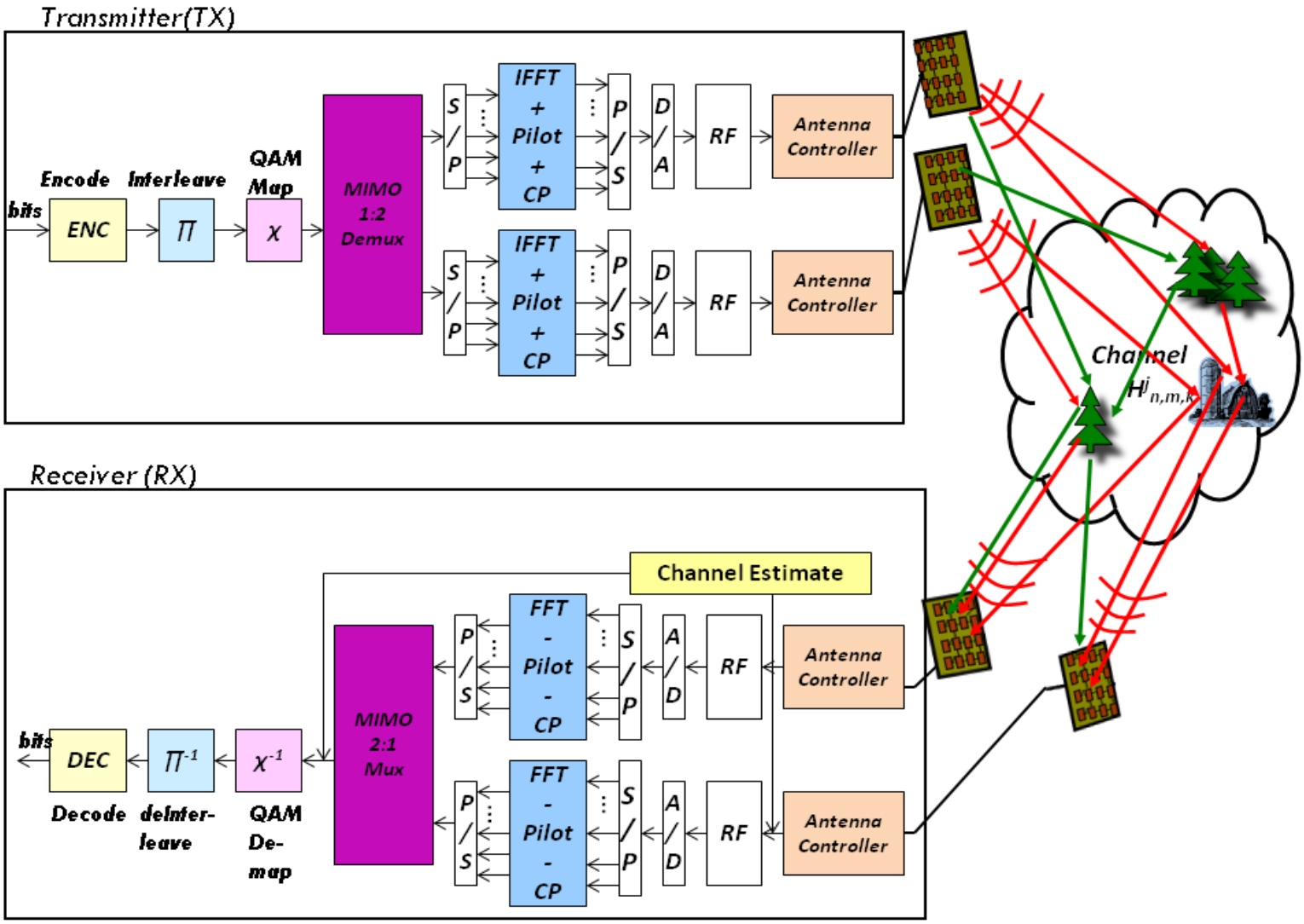

Figure 4.5: MIMO-OFDM System with Reconfigurable Antenna Arrays

CHAPTER 5: RECONFIGURABLE ANTENNAS FOR WIMAX/LTE

5.1 Introduction

With the emergence of high-speed data standards for wireless communications, the need for compact and efficient antenna systems for next generation communication technologies is on the rise. Tremendous progress has been made in the research of adaptive antenna systems such as reconfigurable antennas with numerous designs that are reconfigurable in frequency, pattern, polarization, or a combination of these parameters [20].

Pattern reconfigurable antennas are of special interest due to their ability to dynamically change their radiation properties to the wireless channel characteristics. These antennas are able to generate uncorrelated radiation patterns which can produce uncorrelated channel realizations in a multipath rich wireless channel for a given frequency [116]. As a result, "two co-located antennas with different patterns "see" differently weighted multi-path components so that they interfere differently resulting in better reception; this improves link reliability [10], and channel capacity [9].

In this part of the thesis work, we present two designs of pattern reconfigurable antennas for WiMAX application. We first present a characterization of each antenna solution and demonstrate through field measurements how the pattern reconfigurability of the antennas can be used to improve link reliability.

Related Work

Several other approaches have been presented in [43] – [45]. In [43], a pattern reconfigurable microstrip parasitic array based on Yagi–Uda antenna radiation principle, which uses four switches to reconfigure the radiation pattern into three variations,

is presented. However, its design is not straightforward due to the complex relationships between physical parameters such as element length, spacing, and diameter, and performance characteristics such as gain and input impedance. In [44], a pattern reconfigurable antenna array that consists of two symmetrically reconfigurable monopoles is proposed for operating frequencies between 2.05 – 2.18GHz. While, in [45], a planar electronically reconfigurable antenna based on parasitic microstrip structure for WLAN applications is presented. All these solutions either present antenna architectures that require intricate designs or are tailored for applications operating in the WLAN band. Our solution provides a compact and simple antenna design for WiMAX technologies such as wireless routers and possibly femtocell devices that operate at higher frequencies.

5.2 Reconfigurable Printed Dipole Array (RPDA) for WiMAX Applications

In this section, we present a design of a printed dipole pattern reconfigurable antenna for applications that operate in the WiMAX frequency band between 2.5 – 2.7 GHz. The proposed antenna system consists of an array of two reconfigurable microstrip dipoles, whose active elements can be reconfigured in length using PIN diode switches. The setting of the different switches results in different geometries of the antenna and, consequently, different levels of inter-element mutual coupling and array far-field radiation patterns. The characteristics of the antenna parameters and patterns is analyzed. And, through experimental field testing, the performance of the proposed antenna array is evaluated based on the received Carrier to Interference–plus–Noise Ratio (CINR) as a metric.

We evaluate the performance of the proposed antenna array against a commercial WiMAX antenna in an indoor environment. In the experimental setup, the antenna

array was interfaced to a WiMAX modem that is connected to a laptop computer via ethernet; this setup was used as a fixed WiMAX subscriber station. We measured the Carrier to Interference–plus–Noise Ratio (CINR) as a performance metric for the downlink reception channel from the fixed WiMAX subscriber station to the Base Station.

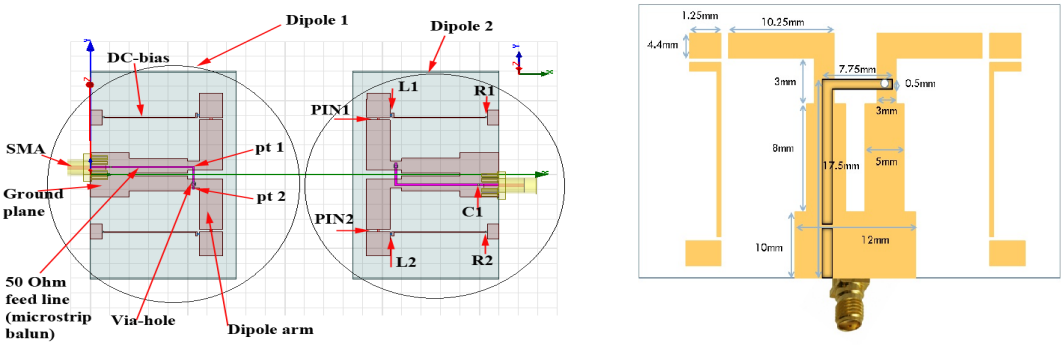

(a) (b)

Figure 5.1: The Design and Geometry of the Proposed Antenna: (a) General view; (b) Dimensions of the Proposed Antenna Element

5.2.1 Antenna Design and Prototyping

The geometrical specification of the proposed antenna design is illustrated in Fig. 5.1. The antenna structure was first designed using Ansoft electromagnetic simulator – High Frequency Structure Simulator (HFSS). The reconfigurable antenna array, consisting of two symmetrically microstrip dipoles is printed on a FR4-epoxy substrate with relative permittivity, ϵ_r, of 4.4 and dielectric loss tangent of 0.02. The detailed dimensions of the dipole are illustrated in Fig. 5.1(b). A quarter–wavelength microstrip balun acts as unbalanced–to–balanced transformer from the feed coaxial line to the two printed dipole strips [39]. The presence of a via-hole permits feed

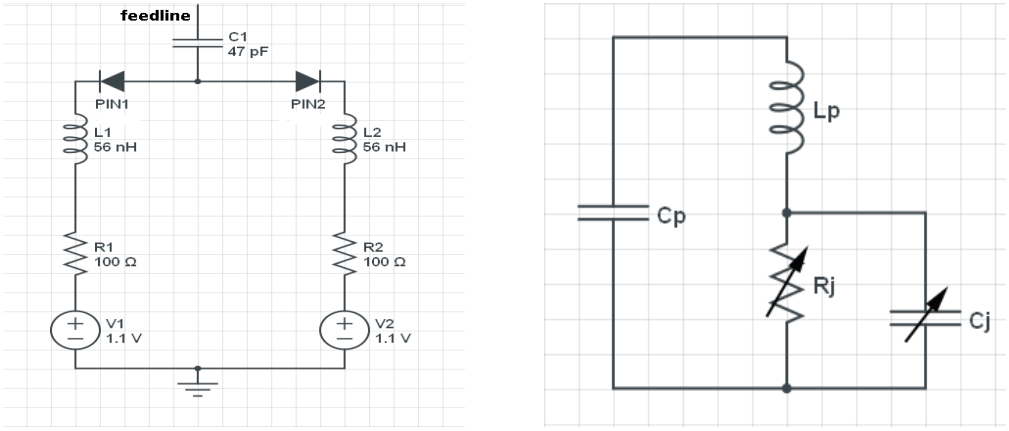

(a) (b)

Figure 5.2: Electrical circuits (a) Switching Circuit for PIN1 and PIN2 of the Antenna Element; (b) RF Equivalent Circuit for PIN diode including Packaging Effects

point, pt 2, to be shifted in phase by 180^o with respect to the feed point pt 1 of the other printed dipole strip (refer to Fig. 5.1(a)). "This occurs because of the 180^o phase difference between the top strip and the ground plane of the microstrip line" [10].

For each dipole, the geometry of the antenna, and thus, the length of the dipole-arm strip is changed using PIN diode switches; this changes the radiation structures which lead to different radiation patterns. The PIN diode model number is BAP64-03; it has an insertion loss of 0.3 dB and an isolation of 7.8 dB. The biased circuits are located at the sides of the 50–Ω microstrip feed line. When a direct bias voltage of 1.1 V is supplied with the two thin DC-bias traces the PIN diode switches are turned on; PIN1 and PIN2 are operating in the ON–state. Otherwise, the switches are turned off and are in the OFF–state. It is therefore, possible to define two configurations for each antenna, one when both of the switches are in the ON–state ("LONG" configuration) and another when they are in the OFF-state ("SHORT" configuration). Thus, the antenna array has four operating configurations. Other elements of the RLC circuit

include: a capacitor (C1), inductors (L1 and L2), and resistors (R1 and R2). To block the dc current from flowing back to the RF input, a surface mounted capacitor of 47 pF is placed on the microstrip balun. Similarly, a inductor of 56 nH is used to block the RF from flowing in the DC supply trace, and a resistor of 100 Ω is mounted to limit the voltage across the diodes. In simulation, the PIN diodes are modeled using the lumped RLC boundary conditions in HFSS; a lumped RLC boundary represents a combination of lumped resistor, inductor, and/or capacitor applied to a surface. The elements of the RF equivalent circuit of the switch come from the electric properties of the diode junction in the ON and OFF states as specified by the manufacturer [76].

Switch Modeling in Simulation

The PIN diodes are modeled using the lumped RLC boundary conditions in HFSS; a lumped RLC boundary represents a combination of lumped resistor, inductor, and/or capacitor applied to a surface. The elements of RF equivalent circuit of the switch come from the electric properties of the diode junction in the ON and OFF states as specified by the manufacturer [76]. Since, the PIN diode is essentially a current controlled variable resistor at RF and Microwave frequencies, it can be used as a switch [77]. the diode forward resistor R_D can be controlled over a wide range by varying the forward current, I_F. Therefore, when the current through the diode has been switched ON and OFF, it can be used as a switch, a phase modulator or as a phase-shifter [77]. In simulation implementation, the ON state of the switch is modeled by specifying a low forward resistance, $R_D = 1\ \Omega$, which, corresponds to the manufacturer specified forward current of the diode; and in the OFF state, R_D is set to 1 GΩ.

The RF equivalent circuit of the switch is depicted in Fig. 5.2(b) for both ON and OFF states. The reactive components Cp and Lp model packaging effect, while the

others come from the electric properties of the diode junction in the ON and OFF states as specified by the manufacturer [76]. Since, a PIN diode is essentially a current controlled variable resistor at RF and Microwave frequencies, the resistor R_j can be controlled over a wide range by varying the forward current, I_F. Therefore, when the current through the diode has been switched ON and OFF, it can be used as a switch, a phase modulator or as a phase-shifter [77]. In the simulation implementation, the ON state of the switch is modeled by specifying a forward resistance $R_j = 1\ \Omega$, which, corresponds to the manufacturer specified forward current of the diode; and in the OFF state, R_j is set to 1 GΩ.

Prototype Fabrication

The HFSS simulation design is exported in to IsoPro – a circuit prototyping software package that provides simple control and quick Circuit milling, drilling and routing procedures for the circuit board milling machine. The prototype of the antenna array with the switching circuits is fabricated and the surface mounted RLC elements are soldered on the antenna surface. The radiation patterns of the prototype are measured in the Anechoic Chamber Testing facility of Drexel University. An Agilent Technologies PNA-L network analyzer was used to measure the antenna S-parameters.

5.2.2 Antenna Parameters and Radiation Patterns

The performance of the antenna prototype is characterized over a wide frequency range through the analysis of the measured S(scattering) parameters and antenna radiation patterns. We further demonstrate the performance of an antenna array that consists of two RPDA elements by analyzing the effects of mutual coupling between the elements; mutual coupling has been demonstrated to degrade the performance of

a diversity antenna system.

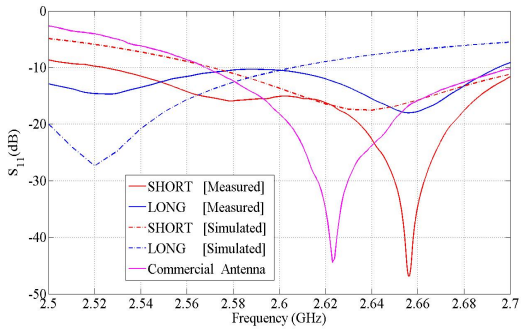

(a)

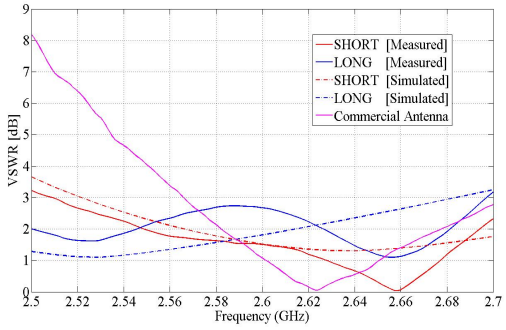

(b)

Figure 5.3: Measured Antenna Parameters of one Antenna Element: (a) Return loss (S11) (b) Voltage Standing-Wave Ratio (VSWR)

The S-parameters of the antenna element are measured using an Agilent PNA-L N5230A Network Analyzer. Fig. 5.3(a) shows the return loss or S_{11} and Fig. 5.3(b) depicts the Voltage Standing Wave Ratio (VSWR) of one antenna element. The two configurations (SHORT and LONG) share a common operating bandwidth, defined by $S_{11} < -10$ dB, from 2.525–2.685 GHz. At frequency 2.656 GHz, both configurations have their lowest S_{11} values of -18 dB for the LONG configuration and -46.8 dB for the SHORT configuration. During the shared band, the VSWR of

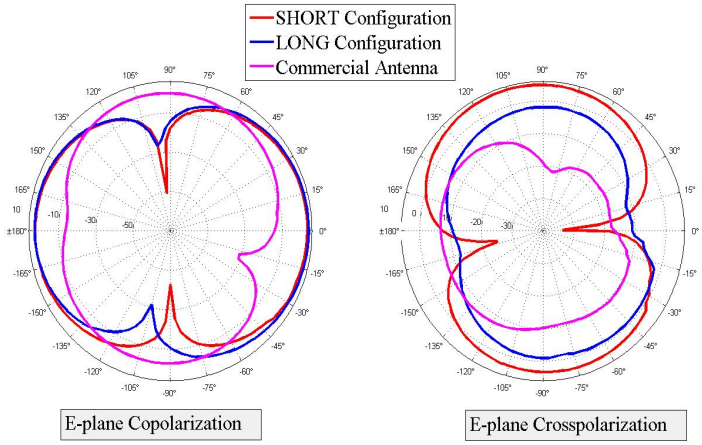

(a)

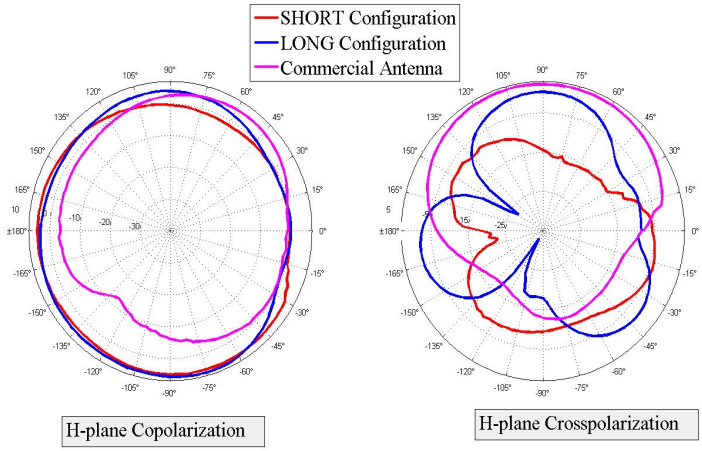

(b)

Figure 5.4: Radiation Patterns of an Antenna Element: (a) Measured Elevation Patterns (left: E-plane Copolarization; right: E-plane Cross Polarization) (b) Measured Azimuthal Patterns (left: H-plane Copolarization; right: H-plane Cross Polarization)

both configurations is below 2.6 as shown in Fig. 5.3(b). At the resonant frequency 2.656 GHz, the VSWR values are less than 1.2 which, indicates that the impedance of the antenna is nearly matched to the characteristic impedance of the transmission line. The commercial antenna performs poorly at frequencies lower than 2.57; this is reflected in Fig. 5.3(a) by return loss values of greater than -10 dB.

Fig. 5.4(a) illustrates the measured elevation radiation patterns for one element of the proposed antenna when operating a the SHORT and LONG configurations; and, the patterns for the commercial antenna. The antenna patterns were measured in the anechoic chamber facility of Drexel University. It depicts donut-shaped patterns for both antennas; however, the proposed antenna is horizontally polarized while the commercial antenna is vertically polarized. Fig. 5.4(a) also shows the cross polarization component of the elevation plane (E-plane) – this represents the polarization orthogonal to the copolarization (desired) component. This is included in order to demonstrate the fact that an antenna is never 100% polarized in a single mode (linear or circular, etc). The cross polarization may be specified for an antenna as a power level in negative decibels (dB), indicating how many decibels below the desired polarization's power level the cross-polarized component's power level is. Similarly, Fig. 5.4(b) indicates the azimuthal radiation patterns for a single element of the dipole array in the different states, benchmarked against the commercial antenna.

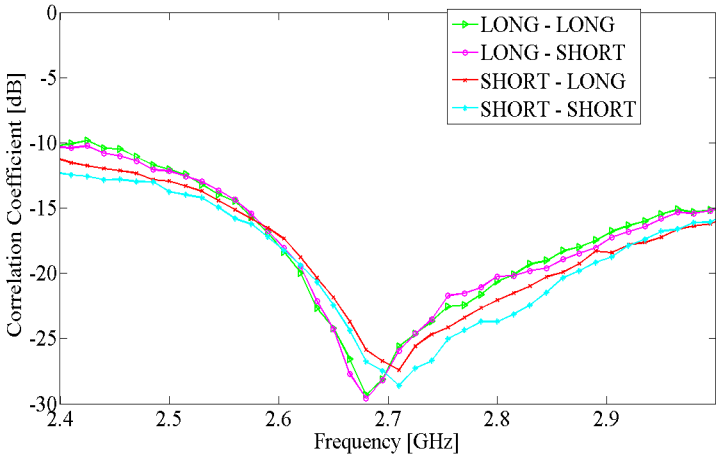

Figure 5.5: Envelope Correlation for two Collinear Quarter-wave Dipoles at different Frequencies

Fig. 5.5 demonstrates the spatial correlation as a function of resonant frequency for a two element array with inter-element separation of $\lambda/4$. The spatial correlation performance for the array elements in the different antenna states – LONG and/or SHORT configurations is plotted. The trend of the curves show that the negative effect of the mutual coupling between the two elements of the array is minimized near the resonant frequency at the frequency-band between 2.6 – 2.8 GHz. This fact is indicted by the dipping of the curves at this frequency range. The correlation values were based on the simple formulation derived in [78] using the S-parameter description of the system. This expression is included (5.1) below for reference. In [78], Blanch et al. showed that the approach of computing the envelope correlation from the S-parameter description of the antenna system generates the same results as the technique that derives it from radiation pattern measurements of the antenna system as in [79].

$$\rho_e = \frac{|S_{11} * S_{12} + S_{21} * S_{22}|^2}{(1 - (|S_{11}|^2 + |S_{21}|^2))(1 - (|S_{22}|^2 + |S_{12}|^2))} \tag{5.1}$$

where ρ_e is the correlation coefficient, S_{11} and S_{22} are the input and output port reflection coefficients, respectively, and S_{12} and S_{21} are the reverse and forward voltage gains, respectively. This equation yields the same results for envelope correlation as the computation from (5.2) below:

$$\rho_e = \frac{|\iint_{4\pi}[\overrightarrow{F}_1(\theta,\phi) \bullet \overrightarrow{F}_2(\theta,\phi)]d\Omega|^2}{\iint_{4\pi}|\overrightarrow{F}_1(\theta,\phi)|^2 d\Omega \iint_{4\pi}|\overrightarrow{F}_2(\theta,\phi)|^2 d\Omega} \tag{5.2}$$

where ρ_e is the correlation coefficient, $\overrightarrow{F}_i(\theta,\phi)$ is the field radiation pattern of the antenna system when port i is excited, $\bullet$ denotes the Hermitian product, and $\Omega = (\theta,\phi)$ is the solid angle.

5.2.3 Performance Testing: Experimental Setup and Results

Setup

In the experimental setup, the antenna array was hooked up to a WiMAX modem that is connected to a laptop computer via ethernet; this setup was used as a fixed WiMAX Subscriber Station. The Subscriber Station is then set to transmit 1500 pilot-based training packets using each of the four configurations of the antenna array: SHORT – SHORT; LONG – LONG; SHORT – LONG; and LONG – SHORT. The antenna array configuration, SHORT – SHORT, indicates that both antenna elements of the array are configured to use the "SHORT" configuration. The Carrier to Interference–plus–Noise Ratio (CINR) was then measured as a performance metric for the downlink reception channel. Similar measurements were made using the commercial WiMAX antenna of the service provider device. All experiments were carried out in a typical indoor laboratory environment (refer to Fig. 5.6); and, the test location is situated on the third floor of Bossone research center at Drexel University. The nearest base station is located on the rooftop of an 8–story building about 400 meters away from the test location.

Performance Results

Figs. 5.7 and 5.8 shows the percentile CINR performance for the proposed antenna array and the commercial WiMAX antenna. The four bar charts show the measurement results in different locations. Each bar indicates the percentage of time that a particular CINR value was measured using a given antenna array configuration during the training packets transmission interval. The results in Fig. 5.7(a) show an improved CINR performance with the proposed solution compared to the commercial antenna. The antenna array out-performs the commercial antenna 80% of the time and some of the antenna array configurations perform better than the others. Similar

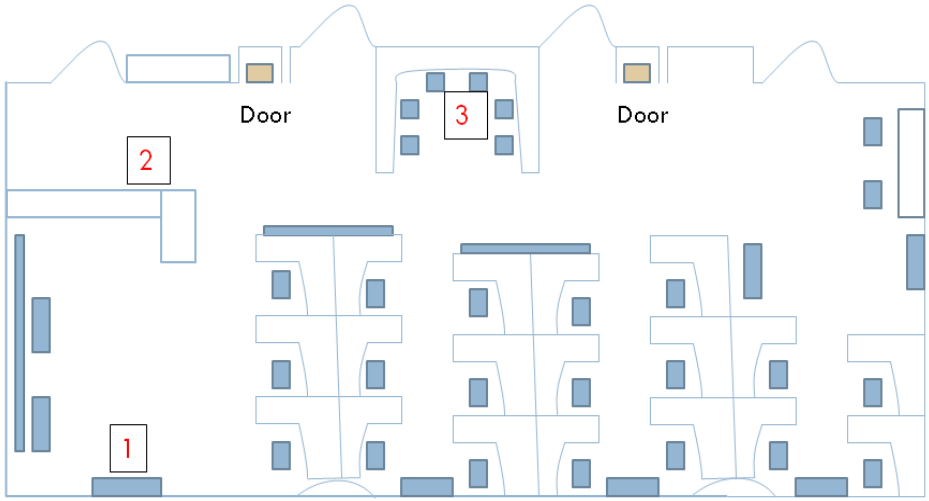

Figure 5.6: Office Layout for the Test Locations

result is obtained in the other measurement locations as indicated in Figs. 5.7(b), 5.8(a), and 5.8(b).

The proposed antenna solution, therefore, enables the flexibility of selecting a configuration that yield the highest received CINR for a given transmission period or environment. Each of the reconfigurable antenna element used is able to adaptively modify its radiation characteristics and thus can leverage pattern diversity to impact the manner in which the transmitter and receiver "perceive" the wireless channel. As established in [10], "two co-located antennas with different patterns "see" differently weighted multi-path components so that they interfere differently for the two antennas resulting in better reception." This enables us to merge the benefits of antenna diversity and antenna reconfigurability to improve link capacity and CINR or the signal strength at the receiver [9].

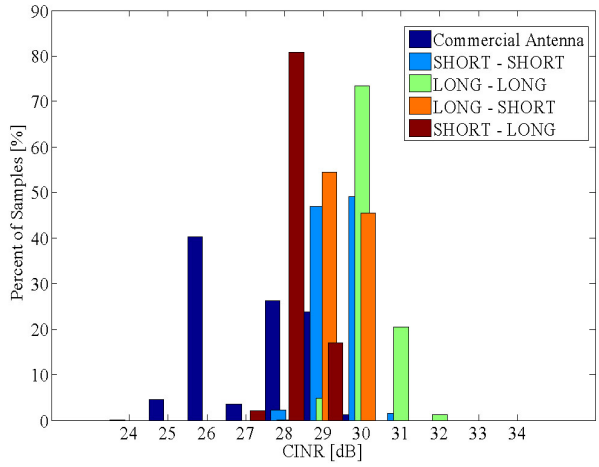

(a)

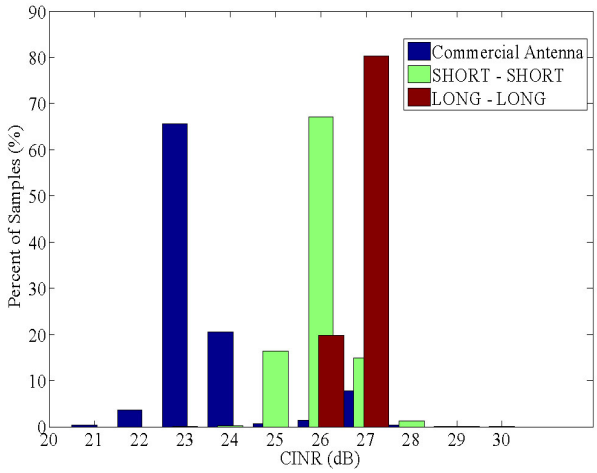

(b)

Figure 5.7: WiMAX Measurements: Percentile CINR Performance for the Reconfigurable Antenna and the Commercial Antenna (a) Measurement Location (1) (b) Measurement Location (2)

5.2.4 Summary and Conclusion

A pattern reconfigurable antenna array for adaptive systems that operate at frequencies between 2.5 – 2.7 GHz has been proposed. Measurement results demonstrate potential performance improvement from using the proposed antenna array in adaptive wireless communication systems. Our solution therefore, provides a great alter-

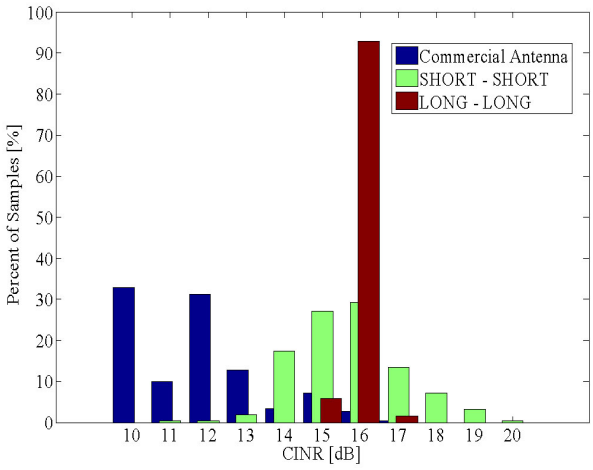

(a)

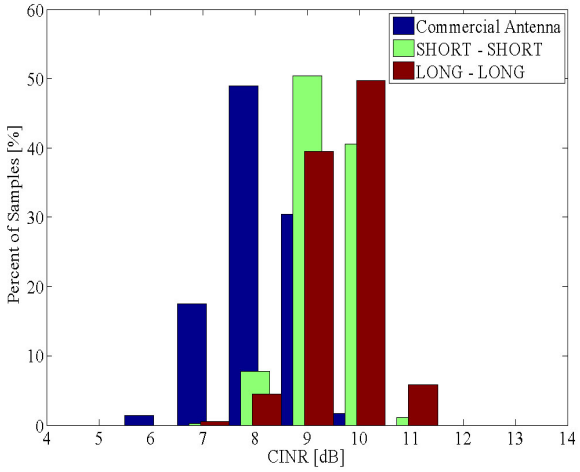

(b)

Figure 5.8: WiMAX Measurements: Percentile CINR Performance for the Reconfigurable Antenna and the Commercial Antenna (a) Measurement Location (3) (b) Measurement Location (4)

native that can easily be adopted for WiMAX commercial application. Further study will focus on configuration selection algorithms in real-time WiMAX applications.

5.3 Reconfigurable Alford for WiMAX/LTE

5.4 Motivation

Even though the RPDA is capable of generating multiple radiation patterns and its pattern diversity has been shown to improve system performance by Piazza et al. in [10], it has some inefficiency issues. In the same work, the authors have also shown that, at a given frequency some of the antenna patterns have lower radiation efficiency than others. Reduced radiation efficiency means low power is radiated from when the antenna is in certain states; this increases the pattern spatial correlation which conversely, reduces the pattern diversity gain and capacity [23]. These radiation efficiency issues motivated us to consider a new pattern reconfigurable antenna design known as the reconfigurable Alford shown in Fig. 5.9. This antenna design presents a more efficient alternative due to the fact that its different radiation patterns are generated through the excitation of fixed dipole arms rather than changing lengths of the dipole antennas as with the RPDA. The reconfigurable Alford antenna is capable of generating both omnidirectional and directional patterns at the WiMAX frequencies 2.5 –3 GHz.

5.4.1 Reconfigurable Alford Design

The design is based on the reference design in [128]; originally tuned to resonate at 3.8 GHz. As in the design of the RPDA discussed in section 5.1 above, the reconfigurable Alford is first modeled using the electromagnetic software simulator HFSS on an FR-4 dielectric substrate with relative permittivity, ϵ_r, of 4.4. The eight metallic elements (four at the top layer and four at the bottom layer) are connected to the feedline though an array of PIN diodes as switches. Each of these elements can be selectively connected or disconnected to the feed to generate different radiation

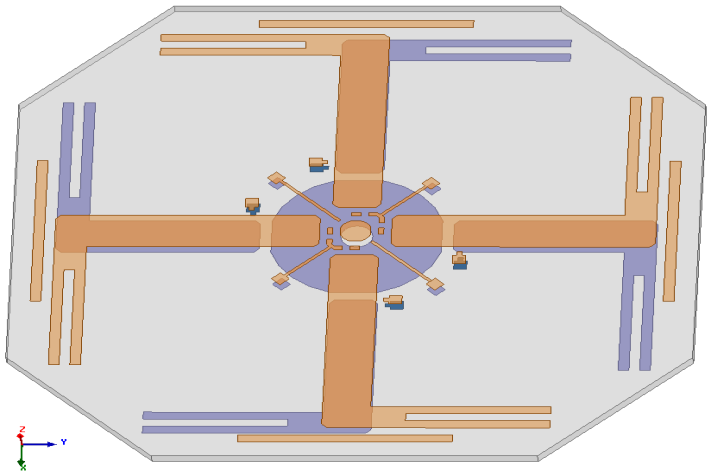

Figure 5.9: A Reconfigurable Alford Antenna

patterns. When adjacent microstrip elements are excited through connection to a voltage on the feedline, a directional pattern is generated. The energy toward the disabled branches undergoes reflections that focuses the beam in the direction of the excited pair. Similarly, when all the branches are connected to the feedline, an omnidirectional pattern is generated from the uniform current distribution on the antenna surface. Therefore, one element is capable of generating at least eight different antenna patterns.

5.4.2 Antenna Characterization

The scattering parameters of the prototypes and the effects of mutual coupling between the elements of an antenna array of two reconfigurable Alford elements were analyzed in [**?**]. This characterization enabled us to derive a relationship with the pattern spatial correlation between the Alford array elements as discussed in the prior section. This analysis helps us to draw inferences on how the antenna array characteristics affect the performance of a MIMO system that employs this array.

Fig. 5.10 shows the setup of the antenna array of two elements. The close prox-

imity ($\lambda/4$) of the two elements have deliberately selected such that there is a strong mutual coupling between them. This coupling is effectively leveraged to generate different radiation patterns for each array's geometry. In Fig. 5.10(a), antenna branches 1 and 2 of antenna element one and branches 2 and 3 of antenna element two are enabled or connected to the feedline –element one is in mode 1 and element 2 is in mode 2. Fig. 5.10(b) shows the second configuration where branches 1 and 4 of antenna element one and 3 and 4 of antenna element two are enabled to generate the directional pattern illustrated. In this configuration, antenna element one is in mode 4 and element two is in mode 3, respectively. Note, the element is in mode 5 when branches 1 and 3 are activated, and in mode 6 when branches 2 and 4 are enabled. When all of the branches of the element are active, the antenna element is said to be in mode 7.

The antenna array configurations are a permutation of the different modes. Table 5.1 illustrates nine different configurations for an antenna array with two elements. It also shows the average values of measured spatial correlation of the array when the elements are in the different states or modes for two frequency bands. Configurations 1 – 8 are for the antenna array that uses two reconfigurable Alford elements shown in Fig. 5.10. Configuration 9 is for antenna array system that uses conventional omnidirectional antennas.

Figs. 5.11 plots the antenna pattern correlation between the antenna array patterns for different array configurations at different frequencies. It illustrates the performance in both linear and non-linear scales. Fig. 5.12 is a bar chart that plots the average values of the correlation at two frequency sub-bands with their respective error bars ; this is intended to give a holistic view of the performance of the different configurations over the desired bands.

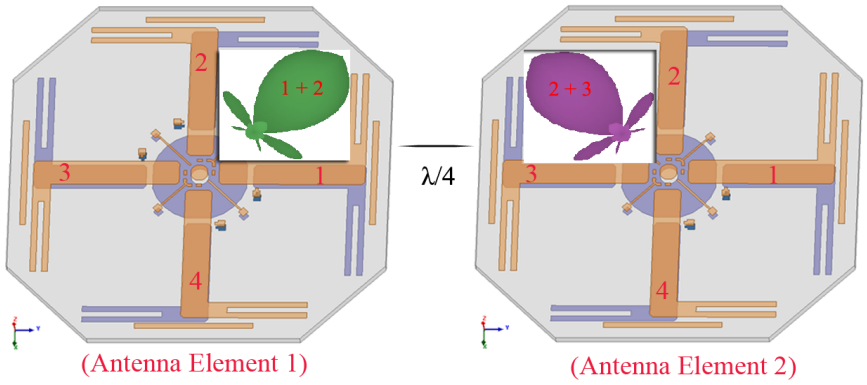

(a)

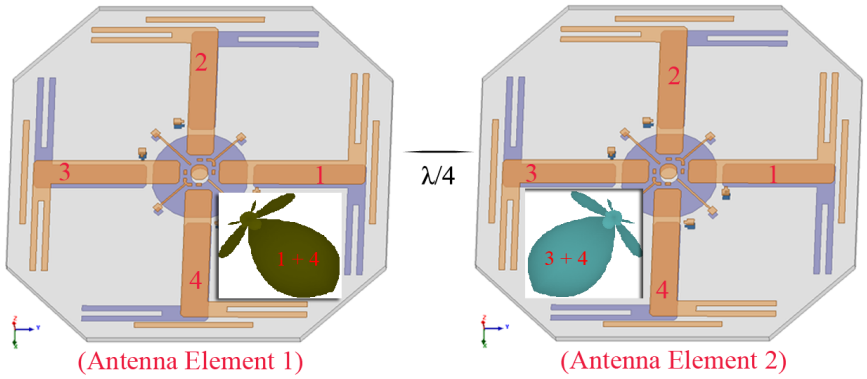

(b)

Figure 5.10: Measurement Setup for the S-parameters (a) Configuration 1 (b) Configuration 2

5.5 Summary

The trends of the antenna pattern correlation curves for the configurations of the reconfiguration Alford (configurations 1 –8) indicate that on the correlation of the array patterns is <0.006 or -22 dB. This is very low compared to the correlation values of the conventional antenna array that uses omnidirectional antennas. In the

Table 5.1: The antenna Correlation of different Antenna Array Configurations

	Antenna State		Average Spatial Correlation	
	Element 1	Element 2	Band: 2.4–2.59 GHz	Band: 2.6–2.8 GHz
Configuration 1	Mode 1	Mode 2	3.5e-4 ± 2.9e-4	3.5e-4 ± 2.9e-4
Configuration 2	Mode 4	Mode 3	3.8e-4 ± 3.6e-4	9.4e-4 ± 1.3e-3
Configuration 3	Mode 1	Mode 3	6.8e-4 ± 8.3e-4	1.2e-3 ± 1.6e-3
Configuration 4	Mode 4	Mode 2	8.5e-4 ± 7.8e-4	5.1e-4 ± 4.5e-4
Configuration 5	Mode 6	Mode 6	2.4e-4 ± 4e-4	4.7e-4 ± 6.6e-6
Configuration 6	Mode 5	Mode 5	1.1e-3 ± 8.2e-4	1.4e-3 ± 1e-4
Configuration 7	Mode 5	Mode 6	1e-4 ± 1.1e-4	1.5e-4 ± 11e-4
Configuration 8	Mode 7	Mode 7	3.5e-4 ± 2.8e-4	1.4e-3 ± 1.6e-3
Configuration 9	Omni Ant	Omni Ant	4.2e-2 ± 2e-1	5e-1 ± 3e-1

latter case, the maximum value is as high as 0.5 or -3 dB which indicates that the patterns generated by this antenna array is highly correlated. This high pattern correlation is directly related to the spatial MIMO spatial channel correlation and is known to reduce channel capacity [9] and [23]. In contrast, the consistently lower spatial correlation of the pattern configurations of the reconfigurable Alford array can be used to maximize channel capacity through adaptation. The proper choice of the transceiver array configuration for a particular multipath environment can be made based on the available channel information.

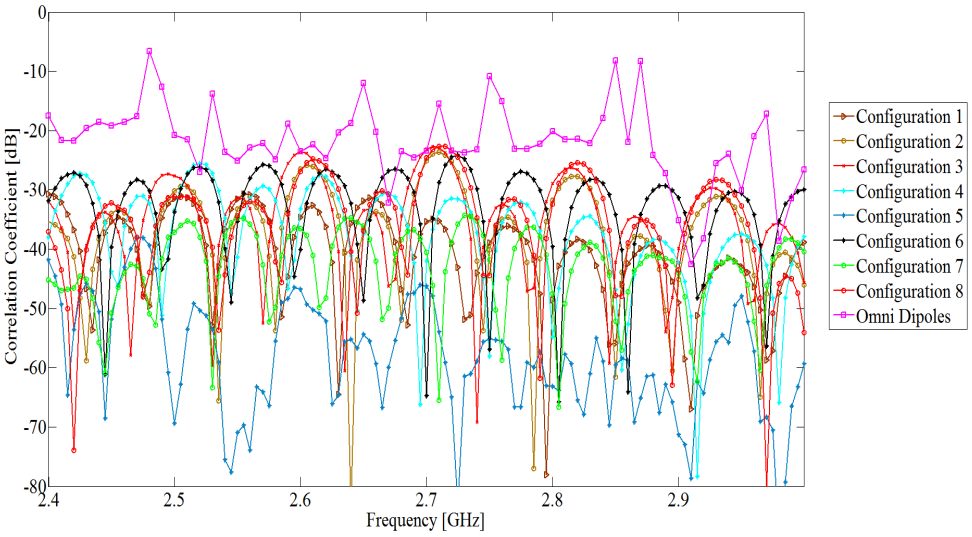

(a)

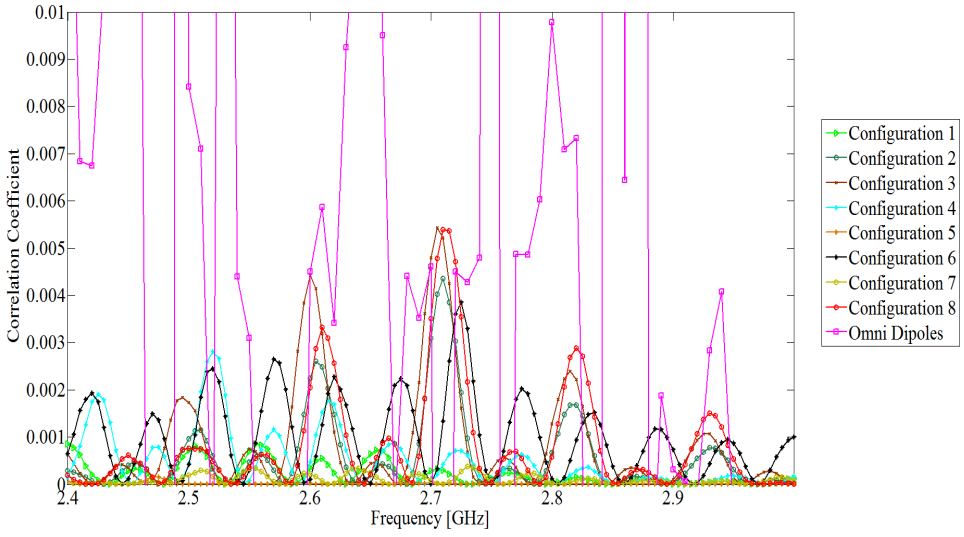

(b)

Figure 5.11: Envelope Correlation for two Collinear Quarter-wave Alfords at different Frequencies for different Configurations (a) decibel (dB) scale (b) Linear scale

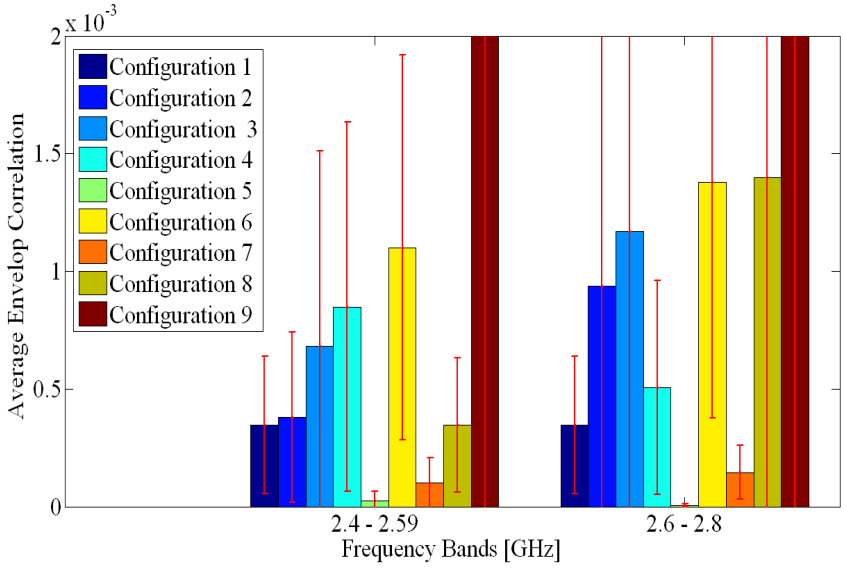

Figure 5.12: Average Envelope Correlation for two Collinear Quarter-wave Alfords at two Frequency bands for different Configurations

CHAPTER 6: Spatially Adaptive Algorithm for Pattern RAS

In this Chapter, we study design improvements for Multiple Input Multiple Output (MIMO) communication systems that make use of Orthogonal Frequency Division Multiplexing (OFDM). Various Adaptive Modulation and Coding (AMC) techniques were developed for such systems that load bits onto the subcarriers in a channel adaptive fashion in order to increase throughput. However, these techniques assume that the channel itself cannot be manipulated. Reconfigurable antennas are capable of adaptively modifying their radiation characteristics and thus leverage pattern diversity to affect how the transmitter and receiver perceive the wireless channel. In this work, we propose a low complexity spatial AMC algorithm that uses the advantages of reconfigurable antennas in concert with link adaptation to improve MIMO-OFDM link throughput. First, this algorithm searches for the antenna configuration that yields the highest post-processing Signal-to-Noise Ratio (ppSNR). Then it applies AMC based on the ppSNR of the selected configuration and a Bit Error Rate (BER) constraint. The AMC stage uses fixed link tables defined by ppSNR regions for supportable spectral efficiencies to select the modulation and coding scheme for transmission. We experimentally evaluate the performance of the proposed scheme for a 2x2 MIMO-OFDM wireless system in an indoor environment.

6.1 Introduction

Adaptive multiple input-multiple output wireless systems have been demonstrated to increase spectral efficiency and provide flexible data rates in multipath fading channels [7, 51]. Recent research in this area has either focused on adaptive antenna systems such as pattern reconfigurable antennas [8], [9], [10], and [85] or adaptive

physical layer (PHY) techniques such as link adaptation [15]–[16], to enhance data rates.

Several studies [8]–[10] have proposed pattern reconfigurable antennas for MIMO-OFDM systems. These antennas are capable of dynamically changing their radiation properties or patterns according to the wireless channel characteristics. Pattern reconfigurability has been shown to be effective in improving Signal-to-Noise Ratios (SNR) at the receiver [9] and the channel capacity [10] in MIMO-OFDM systems.

Although several works [9], [10], and [85] have demonstrated the benefits of reconfigurable antennas, translating the benefits of these antennas into a practical realizable MIMO communication system is very challenging. The use of reconfigurable antennas introduce the need for efficient antenna state or configuration selection schemes to optimize channel capacity or throughput. Specifically, the key challenge is in the selection of the optimal radiation pattern or state from all the available states for a transceiver pair in different wireless conditions. This challenge is compounded by the large antenna state search space that grows with the number of reconfigurable antenna elements used at the transmitter and receiver. In this work, we attempt to redress this issue by employing a low-complexity spatially adaptive scheme for joint antenna state selection and Adaptive Modulation and Coding (AMC) for throughput enhancement in MIMO-OFDM links with bit error rate constraint. We develop and test the proposed scheme in a software defined radio framework that leverages the capabilities of reconfigurable antennas and physical layer adaptation algorithms. This framework can potentially be used to integrate these antennas into practical MIMO communication systems.

6.1.1 Related Work

Current generation standards such as 3GPP LTE have employed similar techniques such as joint MIMO precoder and AMC to improve diversity gain through directional gain and interference reduction [86], [87]. Precoding signal processing exploits the channel state information by operating on the transmit signal using a weighting vector that essentially assigns more transmit power along beams with strong channel and vice verse; it functions as a multimode beamformer [88]. Antenna configuration selection uses a channel dependent metric such as channel capacity or Signal-to-Noise Ratio [9] to determine the optimal radiation pattern that helps achieve diversity gain. Through the use of weighting matrices, precoding couples transmission layers to the multiple antennas – a portion of each signal layer is transmitted through each antenna [87]. However, antenna state selection relies on spatial multiplexing to map each layer to a single antenna dedicated to transmitting that layer. Therefore, although the conceptual signal modeling of precoding and antenna state selection are equivalent, the key difference lies in the system-level implementation of each signal processing technique. From the hardware perspective, precoding is hardware agnostic - can be used with various antenna systems. On the other hand, antenna state selection is hardware specific and depends on the reconfigurable antenna type [10].

The literature on AMC is vast, and for brevity we consider the representative approaches found in [16]–[18]. These approaches provide the framework upon which other AMC techniques were modeled. The works in [16] and [17] propose bit allocation schemes that attempt to maximize throughput over a set of modulation types given that the mean bit error rate (BER) is below a prescribed threshold. The model in [16] uses a peak BER threshold which cannot be exceeded by each subcarrier; the peak BER is adjusted iteratively until the throughput is maximized. Adaptive bit allocation is achieved by varying the signal constellation size according to the

measured SNR values in each subcarrier; this allocation uses a different modulation type per subcarrier but does not consider coding. The model in [17] employs adaptive power allocation and bit loading on a per subcarrier basis, using an iterative technique known as Water-Filling AMC (WF-AMC).

The AMC algorithm proposed in this work employs instead a fixed modulation type and coding rate across all subcarriers; it uses look-up tables known to both the transmitter and receiver to minimize the volume of feedback to the transmitter, and reduce the computational complexity resulting from the iterative process used in [16], [17]. Another technique named Block AMC (BL-AMC), presented in [18], builds on the model in [17] to reduce the volume of feedback information by performing AMC adaptation based only on a single OFDM symbol rather than on all subcarriers. It employs an exhaustive search algorithm for adapting a fixed modulation type and coding scheme across all subcarriers. The adaptation algorithm used in our study attempts to reduce the computational complexity by replacing the exhaustive search with fixed lookup tables.

We evaluate the experimental performance of the proposed scheme for a 2x2 MIMO-OFDM wireless system in an indoor environment. We demonstrate that the computational complexity of the proposed scheme is significantly lower than the relative values for the adaptation algorithms in [17],[18]. Furthermore, we demonstrate the advantage of using reconfigurable antennas in synergy with link adaptation for performance enhancement in MIMO systems. The proposed algorithm provides a sub-optimal but practical alternative to established algorithms that may prove difficult to implement in a realistic wireless communications system.

The Chapter is organized as follows: Section 6.2 describes the system model. Section 6.3, discusses the proposed algorithm for spatial adaptation in detail. Section 6.4 presents the experimental setup and the implementation framework including the

hardware. Section 6.5 presents the performance results and analysis, and Section 6.6 provides a brief summary.

6.2 MIMO-OFDM System Model

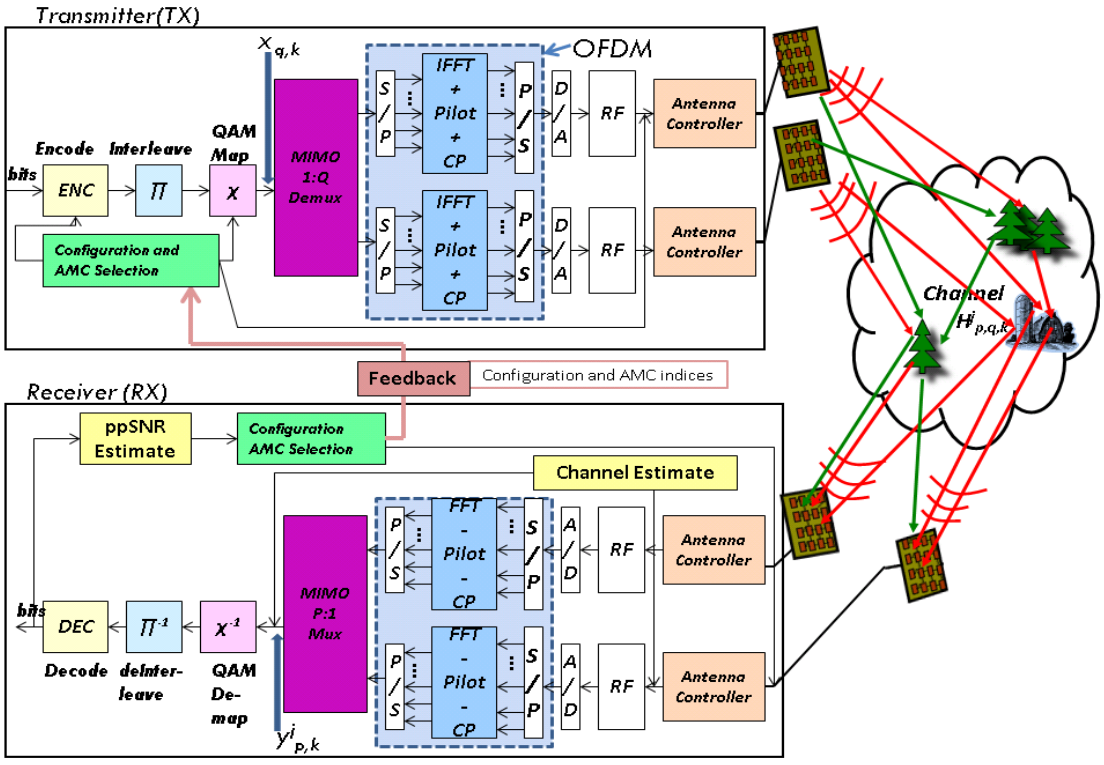

Figure 6.1: System Model for MIMO-OFDM using Reconfigurable Antennas

Fig. 6.1 shows a high-level MIMO-OFDM model of the spatially adaptive system. The system is constructed by concatenating a convolutional encoder with an interleaver and a symbol mapper. After the mapping, the symbols in M-QAM are modulated by the Inverse Fast Fourier Transform (IFFT) and the appropriate Cyclic Prefix is added to reduce inter-symbol interference. The data are then split into two spatial streams that are fed into the antenna controller before transmission; the con-

troller sets the correct antenna transmission configuration or mode. The two streams are separately transmitted from the two transmit antennas over the radio channel using spatial multiplexing technique. At the receiver, the cyclic prefix is removed and the signal is transformed back into frequency domain with an FFT prior to de-interleaving and subsequently decoded to reconstruct the received symbols.

The receiver estimates the ppSNR to be used for adaptation and then, runs the Spatially Adaptive Modulation and Coding (SAMC) control algorithm to determine the antenna configuration and transmission rates. The controller uses the lookup tables to select the indices of the configuration and AMC mode that consists of a modulation type and coding rate. It sends this indices to the transmitter via the feedback channel and transmitter uses its lookup tables to match the selected parameters.

Each of the reconfigurable antennas used in this MIMO system is able to adaptively modify its radiation characteristics and thus leverage pattern diversity to impact the manner in which the transmitter and receiver perceive the wireless channel. As established in [10], "two co-located antennas with different patterns "see" differently weighted multi-path components so that they interfere differently for the two antennas resulting in better reception." This observation motivated us to merge the benefits of antenna diversity and antenna reconfigurability to improve link capacity and SNR at the receiver [9].

We consider a MIMO-OFDM system with Q transmit and P receive antennas sending data across K subcarriers using the j^{th} $(j = 1, ..., J)$ antenna configuration. The OFDM sequence transmitted from the q^{th} $(q = 1, ..., Q)$ transmit antenna on the k^{th} $(k = 1, ..., K)$ OFDM subcarrier is represented by $\mathbf{x}_{q,k}$. The received sequence is given by

$$\mathbf{y}_{p,k}^{j} = \sum_{q=1}^{Q} \sqrt{\frac{\varepsilon_s}{Q}} \mathbf{H}_{p,q,k}^{j} \mathbf{x}_{q,k} + \mathbf{n}_{p,k}, \tag{6.1}$$

where $\mathbf{y}_{p,k}^{j}$ is the P x 1 received vector at the p^{th} receive antenna, $\mathbf{H}_{p,q,k}^{j}$ is the P x Q channel response matrix between the q^{th} transmit and the p^{th} receive antenna for the k^{th} subcarrier and the j^{th} antenna configuration, and $\mathbf{n}_{p,k}$ is the P x 1 Additive White Gaussian Noise (AWGN) at the p^{th} receive antenna for the k^{th} subcarrier. J is the total number of antenna configurations and ε_s is the transmit energy. Expression (1) can be written as $\mathbf{y}_{p,k}^{j} = \sum_{q=1}^{Q} \mathbf{H}_{p,q,k}^{j} \mathbf{s}_{q,k} + \mathbf{n}_{p,k}$ where $\mathbf{s}_{q,k} = \sqrt{\frac{\varepsilon_s}{P}} \mathbf{x}_{q,k}$. After Zero-Forcing with Successive Interference Cancellation (ZFSIC) equalization,

$$\hat{\mathbf{s}}_{q,k} = [\mathbf{H}_{p,q,k}^{j}]^{-1} \mathbf{y}_{p,k}^{j} = \mathbf{s}_{q,k} + [\mathbf{H}^{j}{}_{p,q,k}]^{-1} \mathbf{n}_{p,k}, \tag{6.2}$$

where $[\mathbf{H}_{p,q,k}^{j}]^{-1}$ is the pseudo-inverse of $\mathbf{H}_{p,q,k}^{j}$. The ppSNR for the p^{th} stream at subcarrier k and antenna configuration j is defined as:

$$ppSNR_{p,k}^{j} = \frac{1}{var(\hat{\mathbf{s}}_{q,k} - \mathbf{s}_{q,k})} = \frac{1}{\sigma_k^2} \tag{6.3}$$

where σ_k^2 is the noise variance of the received symbols.

The overall ppSNR for configuration j is determined as the average across transmit antennas and subcarriers.

$$ppSNR^{j} = \frac{1}{P} \sum_{p=1}^{P} (\frac{1}{K} \sum_{k=1}^{K} ppSNR_{p,k}^{j}). \tag{6.4}$$

6.3 Spatially Adaptive Modulation and Coding (SAMC) Algorithm

The proposed SAMC algorithm is described in **Algorithm 1**. It is carried out in two main stages: 1) Antenna configuration selection and 2) AMC selection.

1) Antenna configuration selection: During this stage, the algorithm selects an optimal configuration J^* that yields the highest average ppSNR. This process requires channel training and is carried out during one of the following training intervals: i) Initial training interval, and ii) Re-training Interval. The initial training interval is necessary when no prior channel training has been done. Conversely, the re-training interval prior to some initial training is only used in order to abate the effects of channel fading over time and for up-to-date channel adaptation.

i) Initial training interval: In this interval, initial channel training is carried out over all the J possible configurations; 10 training packets are transmitted using QPSK modulation for each of the J possible configurations. After each training packet transmission, the ppSNR is calculated by taking the mean of the subcarrier ppSNR values. The average ppSNR of a specific configuration is then obtained by taking the mean of the 10 transmissions. In total, 160 packets will be transmitted in this phase, and 16 average ppSNR values will be obtained. The algorithm then selects configuration j^* that with the highest average ppSNR. We sort these 16 average ppSNR values and store the top 5 along with their corresponding configurations.

In this interval, there is need to transmit multiple training packets at a given configuration in order to obtain a meaningful statistic of the Channel Quality Indicator (CQI) from post processing. However, a major challenge arises in selecting the period of the training interval: the use of a long training interval will lead to parameter adaptation based on out-dated channel characteristics; meanwhile a short interval fails to yield a realistic statistic. Determining the optimal training period requires further analysis that deviates from the main focus of this work. Therefore, a fixed training period of 10 packets was only used to obtain a CQI statistic from post processing the channel measurements. Similarly, in an attempt to minimize the re-training interval time we selected a subset of the total configuration for the re-training phase.

Table 6.1: AMC modes and their operating Regions

AMC Mode	Modulation Type	Overall Coding Rate	Data rate (bps/Hz)	Regions for Target BER 10^{-3} (dB)
AMC1	BPSK	1/2	0.5	$2.2 \leq ppSNR^{j^*} < 6.8$
AMC2	4-QAM	1/2	1	$6.8 \leq ppSNR^{j^*} < 8.6$
AMC3	4-QAM	3/4	1.5	$8.6 \leq ppSNR^{j^*} < 13.6$
AMC4	16-QAM	1/2	2	$13.6 \leq ppSNR^{j^*} < 15.3$
AMC5	16-QAM	3/4	3	$15.3 \leq ppSNR^{j^*} < 21$
AMC6	64-QAM	2/3	4	$21 \leq ppSNR^{j^*} < 23$
AMC7	64-QAM	3/4	4.5	$ppSNR^{j^*} \geq 23$

ii) Re-training Interval: during this interval we re-train over the top 5 configurations stored in interval i); and transmit 1 training packet per configuration - thus, a total of 5 training packets. We then select the configuration that yields the highest average ppSNR out of these top 5 configurations.

2) AMC selection: in this stage, the algorithm selects the AMC scheme using the $ppSNR^{j^*}$ associated with the optimal configuration in Stage 1.

The selected antenna configuration and AMC scheme are then used to transmit a scheduled number of packets. In order to minimize the loss of throughput during the training interval in stage 1 of the algorithm, we append a payload of 1KB to each training packet. The size of the training packet is reduced to 32 bytes. Additionally, if the optimal configuration found during the training interval is consecutively selected, the number of packets scheduled for transmission at the optimal configuration and AMC scheme is doubled. These measures helped reduce the negative impact of training overhead on throughput gains; and not only minimized training time but provided data transmission opportunity.

Algorithm 2 SAMC for MIMO–OFDM

1: $J = 16$
2: **for** $j \leftarrow 1, J$ **do**
3: Transmit 1 training packet
4: **for** $k \leftarrow 1, K$ **do**
5: $ppSNR^j_{p,k} = \frac{1}{var(\hat{\mathbf{s}}_{q,k} - \mathbf{s}_{q,k})}$
6: **end for**
7: $ppSNR^j = \frac{1}{P}\sum_{p=1}^{P} \frac{1}{K}\sum_{k=1}^{K} ppSNR^j_{p,k}$
8: **end for**
9: Select the optimal configuration j^* such that $\arg\max_j ppSNR^j$
10: Choose the corresponding AMC mode for data transmission from the link table in Table I so that $\bar{P}_b \leq P_e$
11: Schedule 2 packets for transmission
12: If the same optimal configuration j^* is consecutively selected, schedule 2 more packets for transmission at j^*
13: Re-train over the best five configurations; *set* $J = 5$ and **Repeat** steps 2 through 8
14: **Repeat** steps 9 through 13 until data transmission is done.

6.3.1 AMC Selection Algorithms

We propose two AMC selection algorithms: 1) Highest rate selection; and 2) Robust rate selection. The first is a throughput maximization algorithm that selects the AMC mode with the highest data-rate satisfying a target BER constraint. This AMC mode represents a fixed modulation and coding scheme across all subcarriers. The second algorithm optimizes throughput subject to constraints of target BER (P_e) and target data rate (Ψ_0). It sacrifices some throughput gain for robustness and the satisfaction of the target constraints. Robustness is achieved through optimization of the AMC mode selection.

In lieu of the exhaustive search algorithms in [17],[18], we propose the use of predetermined link tables to obtain the best AMC in solving (6). First, we assign each of the modes to operate within a particular post processing Signal-to-Noise Ratio (ppSNR) region R_χ. Each region is defined by two thresholds. The thresholds are

obtained by using the upper bound expression for the symbol error probability in AWGN channels [93]:

$$P_{\sqrt{M}} \approx 2(1-\frac{1}{\sqrt{M}})Q(\sqrt{\frac{3m}{(M-1)}\frac{E_b}{N_0}\frac{1}{r}}) \leq 2e^{-(\frac{3m}{(M-1)}\frac{E_b}{N_0}\frac{1}{r})}; \tag{6.5}$$

where M defines the constellation size, r the coding rate, $\frac{E_b}{N_0}$ is the SNR per bit, and $m = log_2(M)$. The BER can be approximated by $\frac{1}{m}(1-(1-P_{\sqrt{M}})^2)$.

As shown in Fig. 6.2, each region is delimited by the thresholds ξ_χ and $\xi_{\chi+1}$, such that $\xi_\chi \leq ppSNR < \xi_{\chi+1}$. The receiver (RX) feeds back the index χ representing the AMC mode to the transmitter (TX) for adaptation. This AMC mode represents the fixed modulation and coding rate employed across all the subcarriers. When the ppSNR falls into the outage region, we keep the AMC which corresponds to region R_1, even though the target BER will not be satisfied. We restrict the set of different modulation type and coding rates to those specified in [90] (see Table I which shows the AMC modes and their regions of operation). Mode AMC1, for example, uses BPSK and a coding rate of 1/2 and operates within the region $2.2 \leq ppSNR^{j^*} < 6.8$ dB, where $ppSNR^{j^*}$ is the post processing SNR for the selected configuration j^*.

Figure 6.2: Switching Thresholds

The AMC selection procedures are explained below:

Highest Rate Selection Algorithm

Each AMC mode will be denoted by χ, where $\chi = 1, \ldots, \chi_{max}$ and χ_{max} is the total number of modes. For each χ, a convolutional encoder ς_χ with coding rates $R_c(\varsigma_\chi)$ and constellation size M_χ, where $log_2 M_\chi = m_\chi \in \{1, \ldots, m_{\chi_{max}}\}$, are defined. Spectral efficiency, Ψ, is then obtained by solving the optimization problem [17], [18]:

$$\begin{aligned} \underset{\chi}{\text{maximize}} \quad & \Psi(\chi) = R_c(\varsigma_\chi) log_2 M_\chi \\ \text{subject to} \quad & \bar{P}_b(\chi) \leq P_e, \end{aligned} \tag{6.6}$$

where

$$\bar{P}_b(\chi) = \frac{1}{P} \sum_{p=1}^{P} \frac{1}{K} \sum_{k=1}^{K} \frac{1}{m_\chi} Q\left(\sqrt{\frac{|\, \mathbf{H}_{p,q,k}^{j} \,|^2 |\, \hat{\mathbf{s}}_{q,k} - \mathbf{s}_{q,k} \,|^2}{4\sigma_k^2}}\right),$$

and P_e are the estimated and target bit error rates respectively ([95], [72]).

Robust Rate Selection Algorithm

In the design of this algorithm, we observed that the feedback information is often transmitted through a fading channel and is therefore itself prone to errors. There is a non-zero probability of feedback packet loss which may result in a mismatch of switching decisions (the transmitter may not be able to determine the correct AMC mode that the receiver sent). To decrease the occurrence of a mismatch, a change in an AMC level should only be initiated when the BER constraint cannot be achieved. Switching is minimized when the AMC mode used in the previous packet transmission is still a candidate for a subsequent transmission. The optimization problem becomes a slightly modified version of (6) with an additional constraint: $log_2(1+ppSNR) \geq \Psi_0$. This constraint ensures that the achieved data rate, $log_2(1 + ppSNR)$, is at least equal to the target data rate, Ψ_0. The introduction of the new constraint may lead to more switching between AMC modes. However, the frequency of switching due to

the additional constraint is preferable to the requirement of sending feedback after every packet transmission due to the resulting throughput savings.

The pseudocode describing the AMC selection algorithms is shown in **Algorithm 2**. It depicts the steps used for implementing the proposed AMC algorithms. First, the algorithm takes in the initial value of the target bit error rate (P_e) constraint. It then computes the AMC performance thresholds as illustrated in step 3 of Algorithm 2. These thresholds are used to determine the performance regions of the lookup Tables. If the objective is to maximize throughput, the "Highest rate" selection algorithm is employed to choose the AMC mode. The "Highest rate" selection algorithm uses Table I, to look-up the AMC index that corresponds to the region where the measured $ppSNR^{j^*}$ falls; thus, selecting the maximum AMC mode that satisfies the target BER constraint.

However, if robustness is preferred to throughput maximization, we utilize the "Robust rate" selection algorithm to select the AMC mode. This algorithm introduces a second constraint: a target data rate that must be satisfied in addition to the target BER requirement. It first, establishes the minimum required ppSNR threshold, ξ_χ, and then determines a ppSNR range over which to optimize the AMC mode selection. If the measured ppSNR is greater than this threshold value, the range consists of ppSNR values starting with the threshold value and incremented by an arbitrary value of 0.5 dB until $ppSNR^{j^*}$. Otherwise, the range is equal to $ppSNR^{j^*}$. Since the threshold value is the minimum requirement to satisfy both target BER and target data rate constraints, an AMC mode based on any of the ppSNR values within this range is a candidate for selection. Next, we populate 2D lookup tables for each ppSNR in the range with the AMC candidates; Table II shows a table for two possible target BERs and various target data rates at a ppSNR of 10dB. Note: an empty box in the table II means that the corresponding constraints cannot be satisfied at the measured

ppSNR.

As an example, suppose the target BER is 10^{-3}, target data rate equals 1.5 bps/Hz and the measured ppSNR is 10dB. From Table I, we determine that AMC3 (QPSK and coding rate 3/4) is the minimal AMC mode that would satisfy the specified target data rate. We then calculate the minimum threshold for the target BER as in step 3 of Algorithm 2, and find that ξ_χ is 8.6dB; the ppSNR Range is therefore, [8.6 9.1 9.6 10]dB. We populate four 2D look up tables (one for each ppSNR value in this range) as in Table II for the specified target BER and target data rate constraints. And finally, select the AMC mode with the highest number of occurrence across the four lookup tables. This is the mode that minimizes the need to carry out the selection process on subsequent packet transmission.

The proposed methods significantly reduce feedback overhead since only one index representing the AMC to be used is fed back. The feedback information in our model is independent of the total number of subcarriers (K) and requires only $\lceil log_2(\chi_{max})\rceil$ compared to $K\lceil log_2(m_{\chi_{max}})\rceil + N_q + \lceil log_2(\chi_{max})\rceil$ in [17], where N_q is the number of bits to represent the quantized power level. The price of the reduced complexity is lower accuracy – from using average channel statistics rather than the channel conditions of each subcarrier. The Water-Filling AMC (WF-AMC) and the Block AMC (BL-AMC) are two of the alternative AMC selection algorithms with improved degree of accuracy. However, as will be demonstrated through experimental results, WF-AMC and BL-AMC, are computationally more expensive and may prove difficult to implement in real wireless systems.

6.3.2 Computational Complexity of SAMC

We measure computational complexity of our algorithm by the number of elementary operations (*ops*) required for the algorithm to run, and express it as a function

Algorithm 3 AMC Selection Algorithms

Initialize P_e

for $\chi \leftarrow 1, \chi_{max}$ **do**

  Compute AMC performance thresholds and regions $thresholds(\chi) = \frac{-r_\chi(M_\chi-1)}{3m_\chi}\mathbf{ln}(\frac{1-\sqrt{(1-m_\chi * P_e)}}{2})$

end for

Select algorithm to execute

if (Highest rate selection Algorithm) **then**

  for $\chi \leftarrow 1, \chi_{max}$ **do**

    if $ppSNR^{j^*} > thresholds(\chi)$ **then**

      Select AMC mode χ

    else

      Select AMC mode 1

    end if

  end for

else if (Robust rate selection Algorithm) **then**

  Possible target data rates (bpHz): $\Psi_0 =$ [0.5 1 1.5 2 3 4 4.5]

  for $\chi \leftarrow 1, \chi_{max}$ **do**

    if $\Psi(\chi) == \Psi_0(\chi)$ **then**

      $\xi_\chi = bounds(\chi)$

    end if

  end for

  Find the ppSNR Range to optimize over

  if $ppSNR^{j^*} > \xi_\chi$ **then**

    $ppSNR\_Range = [\ [\xi_\chi : 0.5 : ppSNR^{j^*}]\ ppSNR^{j^*}]$

  else

    $ppSNR\_Range = ppSNR^{j^*}$

  end if

  Pre-populate the 2D lookup table

  for $\chi \leftarrow 1, \chi_{max}$ **do**

    for *each value in the SNR_Range* **do**

      Populate the columns of the 2D lookup tables with AMC candidates that satisfy both constraints as in Table II

    end for

  end for

  Select the AMC mode χ with the maximum occurrence across the lookup tables. This is the mode that minimizes switching

end if

Save the index of the selected AMC mode. This will be fedback to the transmitter for adaptation.

Table 6.2: A 2D lookup table for "Robust rate" selection algorithm for ppSNR=10dB

	possible target rates Ψ_0 (bps/Hz)						
	0.5	1	1.5	2	3	4	4.5
BER	Candidate Modes						
10^{-3}	AMC1 AMC2 AMC3	AMC2 AMC3	AMC3				
10^{-4}	AMC1 AMC2	AMC2					

of the problem size K (the total number of subcarriers). For the Water-Filling AMC (WF-AMC) model in [17], the complexity, denoted by $T(K)$ *ops*, is given by

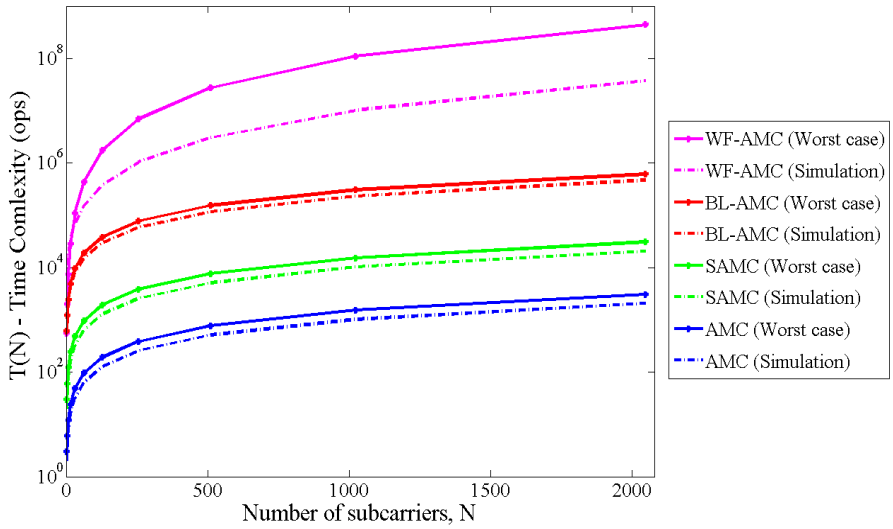

Figure 6.3: Computational Complexity Comparison

$$T(K) = O(J * \varsigma_{max}(2K + 2N_{EF} * K + N_{ET} * K)), \tag{6.7}$$

where J is the total number of antenna configurations; ς_{max}, the number of coding rates; and K is the total number of subcarriers. N_{EF} and N_{ET} denote the number of iterative searches needed in order to obtain the solutions for the "Efficientizing" and "E-tightening" subroutines in the Levin-Campello algorithm, respectively. These two parameters can grow up to K in the worst case, depending on the initial bit allocation [68]. For the BL-AMC model in [18],

$$T(K) = O(J * \chi_{max} * K). \tag{6.8}$$

The dependence of (8) on the number of subcarriers is due to the computation of the instantaneous Bhattacharyya factor in the bit error probability estimation. In the proposed model, the computational complexity is given by

$$T(K) = O(J * K + \chi_{max}). \tag{6.9}$$

The two terms in (9) represent the serial selection of the optimal configuration followed by the AMC. The first term represents the complexity of selecting the optimal configuration. The second represents the AMC selection complexity, which turns out to be a constant due to the use of pre-determined lookup link tables [101]. Fig. 6.3 illustrates the worst case scenarios of expressions (7) –(9) alongside simulations of the AMC selection algorithms. We compare, the Water-Filling AMC (WF-AMC) [17], Block-AMC (BL-AMC) [18], the proposed SAMC algorithm, and AMC with no antenna state selection. The MATLAB function "FLOPS" [102] was used for determining the number of operations required by the selection algorithms. The results show that the computational complexity of the proposed algorithms is at least two orders of magnitude lower than the values for WF-AMC [17] and BL-AMC [18].

6.4 Experimental Setup and Implementation

6.4.1 Software Defined Radio (SDR) Testbed

We use the Wireless open-Access Radio Platform (WARP) designed at Rice University for protocol implementation at the PHY layer. Three main components of the WARP testbed are of interest: (a) Xilinx Virtex-II Pro FPGA (Field-Programmable Gate Array), (b) MIMO-capable radios, and (c) 10/100 Ethernet port. The FPGA allows for MAC protocols to be written in C code. The platform supports up to (4) 2.4/5GHz radio boards which can be configured for applications similar to 802.11g standards. Source/Sink traffic and feedback of the protocols is handled over the Ethernet port [83].

6.4.2 Reconfigurable Printed Dipole Array (RPDA) Antennas

We use the Reconfigurable Printed Dipole Array (RPDA) [84] shown in Fig. 6.4 for both signal transmission and reception. These antennas have beam configurations that can be electronically controlled by adjusting the length of each dipole in the two-element array. A change in length is accomplished by biasing PIN diodes embedded in the structure of the antenna. Multiple radiation patterns are generated as a result of varying the levels of mutual coupling between array elements when the array geometry is changed [10]. We note in passing that although changing the electric length of the antenna changes the resonant frequency of the antenna, the configuration states of the array elements have been shown to resonate at a common frequency and reflection coefficient. Fig. 6. in [10] illustrates a reflection coefficient of -12.5 dB at a common resonant frequency of 2.484GHz.

The RPDA antennas use PIN diode switches to achieve four different operating states. The “Short” (S) configuration is used when the switches on the antenna are inactive. The active switches cause the antenna to operate in a “Long” (L)

Table 6.3: Possible configurations for 2x2 MIMO-OFDM system

		Configurations															
		1	2	3	4	5	6	7	8	9	10	11	12	13	14	15	16
TX	Ant 1	S	S	L	S	S	S	L	L	L	L	L	L	L	S	S	S
	Ant 2	S	S	L	S	L	L	L	L	L	S	S	S	S	S	L	L
RX	Ant 1	S	L	S	S	S	L	L	L	S	S	L	L	S	L	S	L
	Ant 2	S	L	S	L	L	L	S	L	L	S	S	L	L	S	S	S

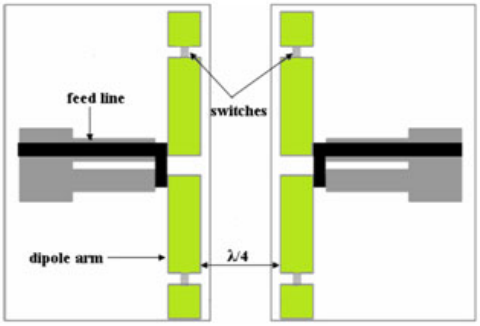

Figure 6.4: Reconfigurable Printed Dipole Array (RPDA)[84]

configuration. One array at each end of the link therefore uses a combination of the individual antenna states to form different configurations. Table III shows the 16 possible combinations for the 2x2 antenna structure; Fig. 6.5 shows 4 different radiation pattern combinations for a 2 antenna array system. The blue radiation pattern corresponds to antenna 1 and the red corresponds to antenna 2 of the array. The radiation patterns on the left of Fig. 6.5 are generated from the Short–Short configurations, for Antenna 1 and Antenna 2, respectively. The rest are from Short–Long, Long–Short, and then Long–Long configurations respectively.

To determine the pattern diversity of these antenna configurations, we evaluated the correlation coefficients based on the S-parameters as outlined in [78] and [80]. Fig. 6.6 shows the measured correlation coefficient as a function of resonant frequency

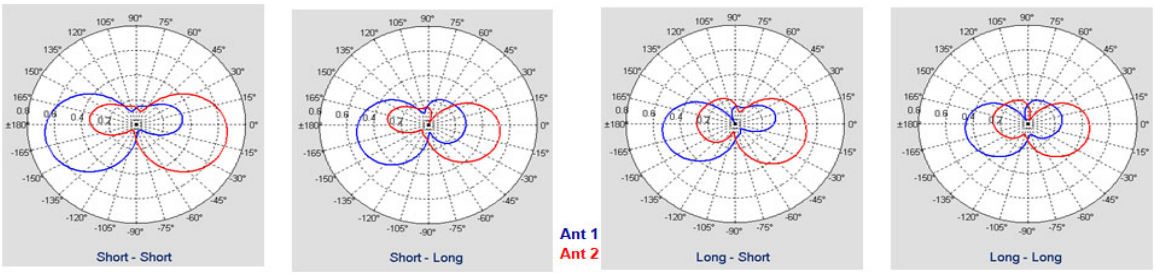

Figure 6.5: Radiation Patterns Combinations for a 2 Antenna Array System for all the Possible Antenna Configurations

for the LONG and SHORT configurations in a 2 element array with inter-element separation of $\lambda/4$. These values were computed from the S-parameters for the 2 element array of the RPDA using expression (5.1) [78]:

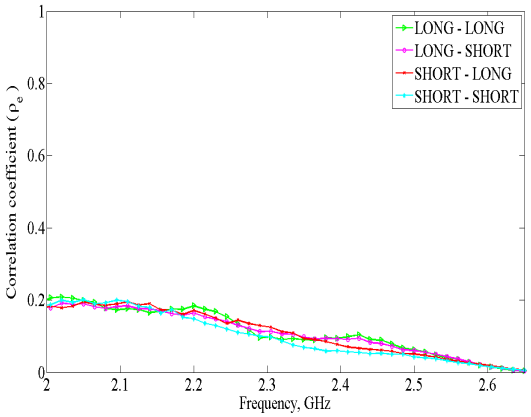

Figure 6.6: The Measured Correlation Coefficient as a Function of Resonant Frequency for the LONG and SHORT Configurations in a 2 Element Array with inter-element Separation of $\lambda/4$

6.4.3 Measurement Setup

The experimental setup used two stations. Each station is equipped with a laptop, a Wireless open-Access Radio Platform (WARP) board [83], and two Reconfigurable Printed Dipole Array (RPDA) antennas [84]. One of the stations is designated as the transmitter node and the other as the receiver node. Fig. 6.7 shows the setup of a transmitter station. A WARP board has two radio cards, each with one antenna slot. The laptop runs the software that drives the WARP radios and the reference code for signal processing. In this work, we assumed that the indoor environment where

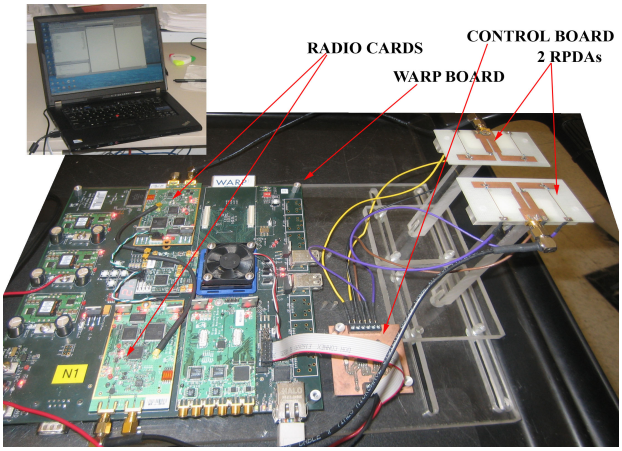

Figure 6.7: An Experimental Communication Node or Station

the experimental testing was carried out experiences slow fading - coherence time of the channel is large relative to the delay - where the channel can be considered to be roughly constant over the packet transmission period. And, based on the set of WLAN channel models developed by Medbo et. al. [91], we believe Model C best describes the experimental setting for this work. Model C defines and characterizes a typical indoor environment in non-line-of-sight (NLOS) conditions with rms delay spread of 150 ns and coherence bandwidth of 1.1 MHz [92]. Fig. 6.8 shows the

magnitude of the channel response over 1000 packet transmissions at each subcarrier for the measurement channel environment.

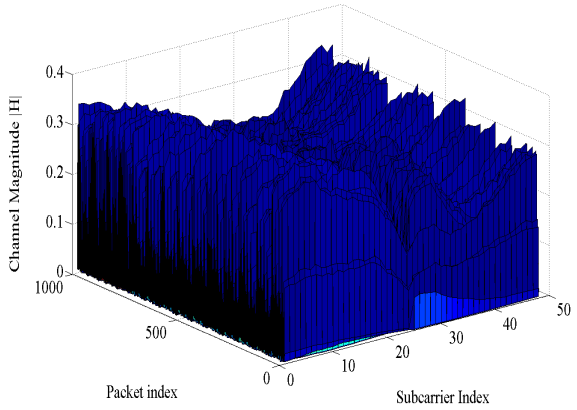

Figure 6.8: Measured Channel Magnitude over time per Subcarrier

Our implementation uses spatial multiplexing for signal transmission between the 2x2 MIMO link established by the two stations. Specifically, we implement V-BLAST MIMO signal processing technique in concert with OFDM because of its ability to cope with severe channel conditions such as frequency-selective fading due to multi-path. The transmission packets are based on the 802.11n OFDM format. The total bandwidth of 20 MHz is divided into 64 subcarriers: 48 for data and 16 for pilot symbols and preamble. Each OFDM symbol has 80 samples (64 samples for each subcarrier plus 16 samples for cyclic prefix). Based on the manufacturer's specification for WARP radio transmission rate of 10^7 samples per second, the sampling rate is approximately 8μs per OFDM symbol [93].

Data are encoded using punctured convolutional codes and modulated at a carrier frequency of 2.484 GHz using one of the four signal constellations: BPSK, QPSK, 16QAM, and 64QAM. The convolutional encoder uses a constraint length of and code

generator polynomials of 133, and 171 (in octal numbers). The puncturing matrices for the relevant coding rates (1/2, 2/3, 3/4) are specified in [94]. All transmissions consisted of a 24 byte header which includes a Cyclic Redundancy Check (CRC) modulated with BPSK and bits were coded at rate 1/2. The header carries a fixed channel training sequence [90] and a payload of 1KB is followed by a 4 byte CRC check.

6.5 Performance Results and Analysis

We evaluate the experimental performance of the proposed SAMC algorithm using the measurement setup presented in section IV-C above. The SAMC algorithm uses the highest rate transmission AMC. We also analyze the performance of the highest rate AMC without antenna selection procedure. This is considered as the non-reconfigurable scenario where the 2x2 MIMO system is equipped with RPDA antennas that uses a fixed configuration (all antenna states are set to SHORT configuration). We compare the performance of these two approaches with that of two other algorithms: WF-AMC [17], BL-AMC [18].

Fig. 6.9 illustrates the empirical ppSNR Cumulative Distribution Functions (CDFs) of two measurement campaigns. In the first campaign, we used RPDA antennas for signal transmissions and measured the channel SNR. In the second, we repeated the same measurements by using non-reconfigurable (reconfigurable antenna with fixed state) antennas for signal transmissions. The curves indicate a relative gain in ppSNR of 4 dB when the RPDA antennas were used compared to the results from the second campaign with non-reconfigurable antennas.

The throughput performance curves of the WF-AMC, BL-AMC, and the proposed algorithms are shown in Fig. 6.10. The WF-AMC [17] model outperforms all the other schemes. This slightly better performance is due to the water-filling adaptation

which is known to be optimal relative to other power allocation techniques. The proposed model, SAMC, performed better than both the spatial BL-AMC algorithm [18] and the non-reconfigurable AMC models. We note in passing that the effect of training overhead on these throughput measurements was not investigated as part of this work.

Similarly, the BER is calculated from the coarse approximation used in the optimization process based on the header information in each packet. Fig. 6.11 plots the BER performances of the proposed models and the other models from [17] and [18]. The non-reconfigurable AMC always satisfies the target BER requirement. The other models follow similar curves but only meet the BER constraint of 10^{-3} at ppSNRs greater than 7 dB. This behavior is partly due to the necessary training required for the configuration selection. Training introduces a delay which causes adaptation on outdated channel information. The random jumps above the target BER line can be explained by the use of BPSK even when the ppSNR fell in the outage region (see Fig. 6.2). Despite the relatively close throughput and BER performances, our approach is superior in its computational complexity performance. The computational complexity of our model is at least two orders of magnitude lower than the measured values for the other models in [17] and [18] (see Fig. 6.3).

In Fig. 6.12 we show the adaptive modulation types in terms of their fraction of usage – the percentage of time a modulation type is used during the experiment. As expected, at low ppSNR, BPSK is used most often; at moderate ppSNR (10dB) to middle-range ppSNR (17dB), QPSK and 16-QAM are frequently used. At high ppSNR, 64-QAM dominates in usage although lower modulation types make up a combined usage of at least 30%. Fig. 6.13 illustrates the fraction of usage for the top five configurations. The horizontal axis represents the configurations used at both the transmitter and receiver. For example, SS-SS indicates that all the antennas

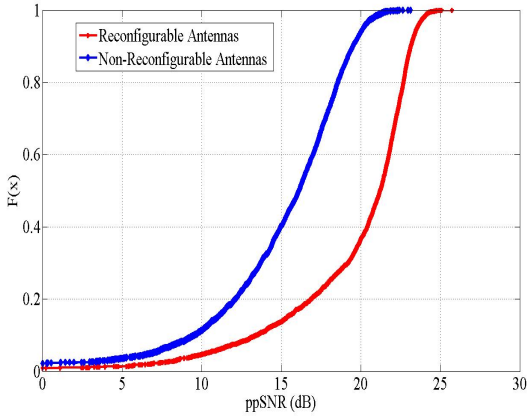

Figure 6.9: Empirical ppSNR CDFs for Reconfigurable AMC and Non-Reconfigurable AMC

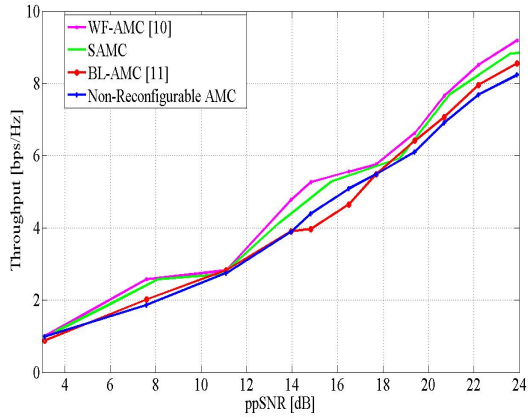

Figure 6.10: Throughput Comparison for 2x2 MIMO-OFDM System

operated in a "Short" configuration. The SS-SS configuration was favored over the rest of the configurations and is chosen for more than 45% of the transmissions. The other configurations are preferred for the rest of the time due to their relatively higher ppSNR with respect to the SS-SS configuration. The benefit from switching is lower BER performance, which results in improved throughput; however, the overall throughput performance maybe suboptimal due to the use of average ppSNR for

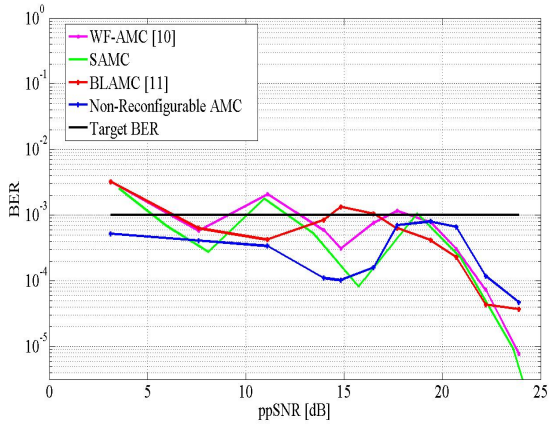

Figure 6.11: BER Performance Comparison

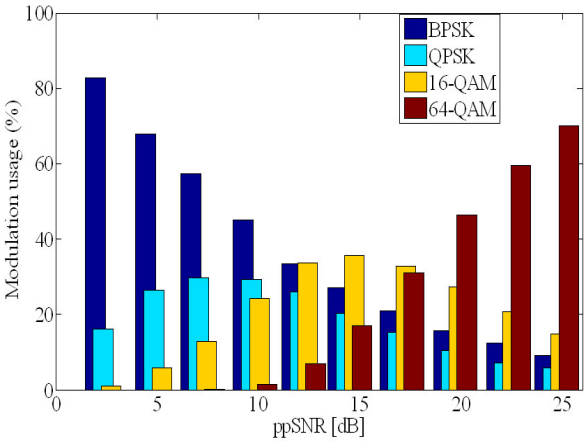

Figure 6.12: The Distribution of Modulation use in SAMC

all the subcarriers. Finally, Fig. 6.14 illustrates the channel variation over time as measured using the active antenna configurations. It shows the flat fading nature of the wireless channel environment without deep fades.

6.6 Summary

A Spatially Adaptive Modulation and Coding algorithm was proposed and implemented in a Software Defined Radio testbed. Multiple techniques of link adaptation

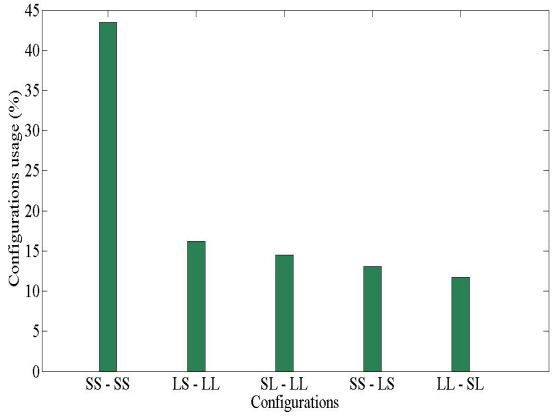

Figure 6.13: Configurations Usage in the Proposed Algorithm

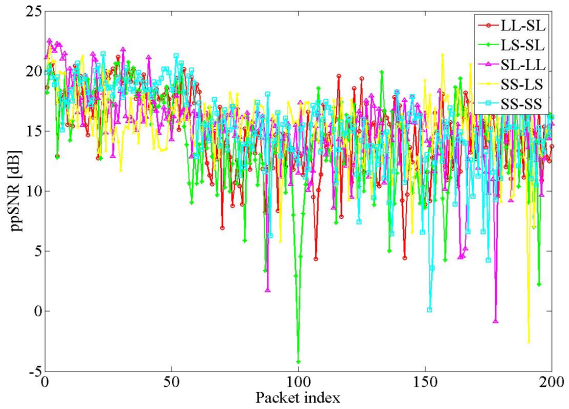

Figure 6.14: Channel Variation over time as Measured using the active Antenna Configurations

were employed to develop a low computational complexity, throughput enhancing model. The capabilities of Reconfigurable Printed Dipole Array (RPDA) antennas in MIMO-OFDM systems were harnessed to improve spectral efficiency. It was shown via field implementation that our model can increase post processing Signal-to-Noise Ratio and therefore system reliability over a multiple-antenna slow fading channel. Future work will investigate the effects of feedback delay on the proposed algorithm.

CHAPTER 7: BENEFITS OF PATTERN DIVERSITY IN RECONFIGURABLE ANTENNAS

In this Chapter, we investigate the benefits offered by radiation pattern diversity in reconfigurable antenna arrays and place these benefits in context with spatial diversity provided by conventional antenna arrays. The motivation for this new class of adaptive antenna arrays stems from the findings of previous studies, which have shown that the capacity of conventional multi-element arrays (MEAs) is adversely affected by spatial correlation. Reconfigurable antennas provide pattern diversity that can improve capacity and offer a unique opportunity for antenna system miniaturization for portable wireless devices.

We first use a common modeling framework to study the impact of spatial and pattern correlation on the performance of the multi-antenna array systems. We consider a geometry-based MIMO channel cluster model to investigate the effects of the channel spatial characteristics and antenna array geometry/radiation patterns on the spatial correlation and system performance. Next, through experimental evaluation, we study the benefits of pattern diversity derived from reconfigurable antenna arrays over spatial diversity from conventional arrays. Our findings demonstrate relative diversity performance improvement of at least 3 dB from using pattern diversity over space diversity.

7.1 Introduction

Information–theoretic analysis in [5], and [7] have shown that using multi-element antenna arrays (MEAs) at both the transmitter and receiver can lead to a linear growth in capacity with the number of antenna elements, for fixed power and band-

width. However, these MEA arrays rely on a rich-scattering multipath channel, antenna element placement and signal processing techniques to achieve spatial diversity or spectral efficiency. As demonstrated in [158], the diversity gain is significantly limited when the fading channels are not independent and are correlated. In practice, a correlation arise if the elements are not sufficiently spaced far apart or when a dominant line of sight (LOS) component is present in the transmission scenario [155]. Similarly, the spectral efficiency of these MEAs system is diminished: due to their inability to simultaneously transmit independent data streams over the multiple antenna elements without decoding errors at the receiver [157].

For the above reasons, MIMO antenna arrays must be designed to reduce spatial correlation to yield the additional degrees of diversity and spectral efficiency to improve system performance. The design and analysis of these multi-antenna arrays must also be coupled to the physical layer capabilities of the MIMO system to realize any further improvements. This is due to the complex dependence of spatial correlation on both spatial characteristics – angular spread, scatterers– and antenna array geometry/parameters such as element spacing and radiation pattern [153].

Traditional MEAs arrays use antenna element spacing to combat the effects of spatial correlation and channel fading. This array element spacing is a constraint that makes these arrays impractical to deploy in portable wireless devices such as routers or access points. This limitation is the main motivation for research efforts in the design of a compact alternative solution using reconfigurable antenna arrays system (RAS). Reconfigurable antenna technology has been shown to offer performance gains in MIMO systems by increasing channel capacity [10] and Signal-to-Noise Ratio (SNR) [9] at the receiver. RAS antennas are capable of dynamically changing their radiation characteristics and enable MIMO systems to adapt to physical link conditions. These antennas also provide space and cost benefits in incorporating multiple elements in a

single physical device by reducing the number of RF chains [112].

The goal of this work is to explore this new class of adaptive antenna array systems in lieu of traditional MEAs arrays as a suitable solution to achieve the benefits of MIMO arrays in small wireless handheld devices. The design flexibility of reconfigurable antenna arrays enables us to exploit the antenna geometry and mutual coupling between radiating array elements to generate different uncorrelated radiation patterns [27]. These uncorrelated radiation patterns can produce uncorrelated channel realizations in a multipath rich wireless environment which improves link reliability and channel capacity [116].

7.1.1 Related Works

Various research efforts in MIMO antenna arrays have either separately focused on developing techniques that use conventional antennas as adaptive arrays [21] – [23], or building compact reconfigurable antenna arrays for adaptive MIMO as an alternative to conventional arrays [20] – [26]. A few quantitative studies have also considered the system-level performance benefits of pattern reconfigurability [10] [9], and [112] – [115]. These works however do not benchmark the benefits of pattern diversity in RAS with models that employ adaptive conventional antenna arrays with physical layer adaptation algorithms. And in so doing fail to take full advantage of multi-antenna systems when applied in spatially correlated channel environments.

In this work, we propose a methodology that couples the antenna-selection algorithm design for reconfigurable antenna arrays with physical layer adaptation algorithms to improve system performance. Specifically, we implement a MIMO system model that leverages the capabilities of reconfigurable antennas in concert with various physical layer signal processing and link adaptation algorithms. The algorithms are designed and developed with computational complexity in mind in order to opti-

mize the performance benefits of these antenna arrays.

Among the myriad of MIMO signal processing techniques, approaches that take advantage of spatial multiplexing, spatial diversity, Beamforming or spatial filtering, were implemented and benchmarked against other works in literature. Notably, the approaches in [21], [23], and [104] which employ spatial multiplexing and transmit beamforming, antenna grouped algorithms are implemented. The work in [21] proposes a multimode antenna selection algorithm that dynamically adjusts both the number of substreams and the mapping of substreams to antennas, for a fixed data rate, to the channel conditions. It also discusses a dual-mode selection algorithm that switches between spatial multiplexing and beamforming. It also derives several expressions that characterize the various criteria for selecting the number of substreams and the optimal mapping of substreams to transmit antennas. In [23], an adaptive algorithm that selects between beamforming, multimode antenna selection and spatial multiplexing is presented. This model extends the work in [21] to demonstrate capacity gains derived from adaptively switching between MIMO schemes. The work in [104] introduces several mode selections criteria and a low complexity criterion which is derived from a low complexity antenna grouping algorithm.

We use a common modeling framework to study the impact of either spatial or pattern correlation on the performance of the multi-antenna array system. We consider a geometry-based MIMO channel cluster model to investigate the effects of the channel spatial characteristics and antenna array geometry/radiation patterns on the spatial correlation and system performance. This allows for the benchmarking of conventional antenna array techniques such as antenna grouping, and selection, against pattern reconfigurability. And, motivated us to study the benefits of pattern diversity derived from reconfigurable antennas arrays over spatial diversity from conventional arrays and their relevant signal processing techniques through field experimentation.

7.2 MIMO Channel Model:

A Geometry-based MIMO Cluster Modeling

7.2.1 Cluster Channel Model: WINNER Model

We consider a geometry-based stochastic channel model (GSCM) first presented in [120]. This is a double-directional cluster model that uses advanced modeling techniques to capture the propagation characteristics of the wireless environment and the effects of antenna array patterns, their polarization and the mutual coupling between array elements. We chose the WINNER model because it covers a wide range of propagation scenarios and environments and is antenna independent; which makes it suitable for evaluating adaptive radio systems. This is a key distinction with other models such as the SCM/SCME models proposed for 3GPP systems in [121].

Fig. 7.1 shows the graphical representation of the a single link cluster model. Multiple clusters in the scattering region surrounding the transmit and receive array are represented by the circles with dots. The number of clusters, paths, and rays or subpaths varies with the scenario.

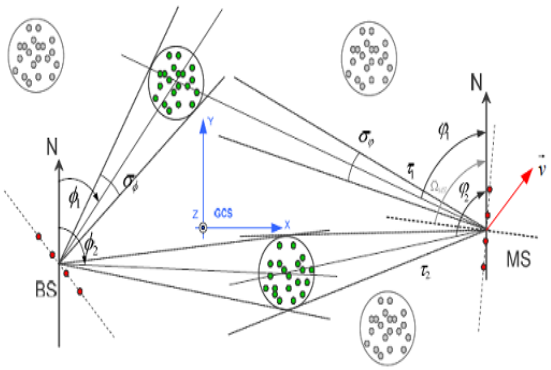

Figure 7.1: A Graphical Representation of a Single Link WINNER Cluster Model [120]

7.2.2 3D Antenna Array Modeling in WINNER

The WINNER model uses an antenna array modeling methodology proposed in [124] that allows for a 3D description of the antenna array characteristics such as polarization, directional filtering, and spatial displacement. It supports arbitrary geometries and allows the BS and MS to use different antenna arrays. The antenna array elements are represented in the element-coordinate-system (ECS) and can be placed and oriented anywhere with respect to the array-coordinate-system (ACS). The positioning of the array can be done arbitrarily in the global-coordinate-system (GCS), which is used to define the radio-network system layout and as a reference for polarization [120]. Additionally, the antenna element beam patterns are represented by effective-aperture-density-functions (EADF)– a 2D fourier transform of the field pattern– to provide an effective way of interpolating the field pattern for an arbitrary elevation and azimuth angles (θ, ϕ) respectively.

7.2.3 Channel Selectivity and Spatial Correlation

The time-variant impulse response for a P×Q MIMO channel as modeled in [120] is given by (7.1). The channel matrix is composed of the antenna array response matrices $\mathbf{F}_{tx}$ and $\mathbf{F}_{rx}$ for the transmitter and receiver respectively. It defines the channel from the Tx antenna element q to the Rx element p, for a given cluster n with R number of rays (subpaths).

The spatial characteristics of the propagation channel are described by the angular parameters AoA/AoD, which are distributed according to a certain probability distribution function (PDF) that models the power angular spectrum (PAS). Numerous field experimentation works including [129]–[130], have shown that the PAS is accurately modeled by the truncated Laplacian PDF, defined by

$$\mathbf{H}_{p,q,n}(t;\tau) = \sum_{r=1}^{R} \begin{bmatrix} \overrightarrow{F}_{rx,p,V}(\varphi_{n,r}) \\ \overrightarrow{F}_{rx,p,H}(\varphi_{n,r}) \end{bmatrix}^{T} \begin{bmatrix} \alpha_{n,r,VV} & \alpha_{n,r,VH} \\ \alpha_{n,r,HV} & \alpha_{n,r,HH} \end{bmatrix} \begin{bmatrix} \overrightarrow{F}_{tx,q,V}(\phi_{n,r}) \\ \overrightarrow{F}_{tx,q,H}(\phi_{n,r}) \end{bmatrix} \times exp(j2\pi\lambda_0^{-1}(\overrightarrow{\varphi}_{n,r} \,.\, \overrightarrow{\iota}_{rx,p})) \times exp(j2\pi\lambda_0^{-1}(\overrightarrow{\phi}_{n,r} \,.\, \overrightarrow{\iota}_{tx,q})) \times exp(j2\pi\upsilon_{n,r})\delta(\tau - \tau_{n,r}) \quad (7.1)$$

where

t is time, τ is the propagation delay;
$\overrightarrow{F}_{rx,p,V}$ and $\overrightarrow{F}_{rx,p,H}$ are the antenna element p field radiation patterns for vertical and horizontal polarization, respectively;
$\alpha_{n,r,VV}$ and $\alpha_{n,r,VH}$ are the complex gains of vertical-to-vertical and horizontal-to-horizontal polarizations of ray n,r respectively;
λ_0 is the wavelength of the carrier frequency;
$\overrightarrow{\phi}_{n,r}$ is the angle of departure (AoD unit vector;
$\overrightarrow{\varphi}_{n,r}$ is the angle of arrival (AoA) unit vector;
$\overrightarrow{\iota}_{rx,p}$ and $\overrightarrow{\iota}_{tx,q}$ are the location vectors of elements p and q, and;
$\upsilon_{n,r}$ is the Doppler frequency component of ray n, r.

$$PAS(\Omega) = \sum_{n=1}^{N} \frac{\beta_n}{\sigma_k\sqrt{(2\pi)}} exp\left[-\frac{\sqrt{(2)}|\Omega - \bar{\Omega}_n|}{\sigma_n}\right] \times U\left[\Omega - (\bar{\Omega}_n - \Delta\Omega_n)\right] - U\left[\Omega - (\bar{\Omega}_n + \Delta\Omega_n)\right] \quad (7.2)$$

where N is the number of clusters, $\Omega = (\theta, \phi)$ is the solid angle, $\bar{\Omega}_n$ is the mean arrival/departure angle of the nth cluster, $U(\theta)$ is the step function, and the constant β_n is derived to fulfill the normalization requirement such that $\int_{-\pi}^{\pi} PAS(\Omega)d\Omega = 1$. Note, "Truncated" here refers to the fact that each mode is only defined within a limited interval $\left[\bar{\Omega}_n + \Delta\Omega_n - \bar{\Omega}_n + \Delta\Omega_n\right]$

The variance of the PAS which measures the size of the cluster, also defines the spread of the AoDs ($\overrightarrow{\phi}_{n,r}$)/AoAs ($\overrightarrow{\varphi}_{n,r}$) and is referred to as the angular spread (AS). The AS causes spatial selectivity and depends on the characteristics of the multipath scattering environment. When the environment has few scatters or the scatters are

positioned far apart, the AS is narrow. Conversely, when a large number of local scatters exists around the BS/MS, a wide angular spread results.

Spatial Correlation

When the channel consists of few multipaths, the measured signals at the different antennas of the multi-antenna system can become spatially correlated. Spatial correlation–a correlation between the signal's spatial direction and the average received signal gain –degrades the performance of multi-antenna systems and limits the number of antennas that can be used for a given MIMO link. For this reason, MIMO antenna arrays must be designed to reduce spatial correlation to yield the additional degrees of diversity and improve system performance [155]. The spatial correlation between the qth and pth antenna array elements, denoted by $\rho_{p,q}$, is defined by (7.3) as in [79] and [126]:

$$\rho_{p,q} = \frac{\iint_{4\pi}[e^{-j2\pi\frac{d_{p,q}}{\lambda}sin(\Omega)}PAS(\Omega)|\overrightarrow{F}_p(\theta,\phi)\bullet\overrightarrow{F}_q(\theta,\phi)|^2]d\Omega}{\iint_{4\pi}PAS(\Omega)|\overrightarrow{F}_p(\theta,\phi)|^2d\Omega\iint_{4\pi}PAS(\Omega)|\overrightarrow{F}_q(\theta,\phi)|^2d\Omega} \tag{7.3}$$

where
$d_{p,q}$ is the distance between antenna elements p and q,
λ is the wavelength corresponding to the carrier frequency of the system,
$PAS(\Omega)$ is the PAS of the scattered fields and
$\overrightarrow{F}_i(\theta,\phi)$ is the field radiation pattern of the antenna system when port i is excited,
$\bullet$ denotes the Hermitian product.

It can be observed that the spatial correlation is a function of the channel or spatial characteristics through $PAS(\Omega)$, and antenna array parameters such as polarization, radiation patterns through $\overrightarrow{F}(\theta,\phi)$ as well as the array element spacing

or geometry. This fact demonstrates the need to tune and optimize both channel and antenna array parameters to reduce spatial correlation. In this work, we exploit this dependence through a joint design approach that simultaneously tunes antenna array parameters as well physical layer algorithms that improve system performance in correlated MIMO channels.

7.3 Antenna Design and Characterization

This material in this section has been discussed in detail in Chapter 5 but for quick reference and relevance, we have briefly included the main details.

7.3.1 Reconfigurable Alford Loop Antenna Design

Fig. 7.2 shows the reference antenna design first published in [128]. Each of these elements can be selectively connected or disconnected to the feed to generate different radiation patterns. When adjacent microstrip elements are excited through connection to a voltage on the feedline, a directional pattern is generated. The energy toward the disabled branches undergoes reflections that focuses the beam in the direction of the excited pair. Similarly, when all the branches are connected to the feedline, an omnidirectional pattern is generated from the uniform current distribution on the antenna surface. Therefore, one element is capable of generating at least eight different antenna patterns.

7.3.2 Antenna Characterization Setup

This characterization of the scattering parameters enables us to derive a relationship with the pattern antenna correlation between the alford loop array elements as discussed in the prior sections. The antenna correlation is based on (7.3) without the PAS distribution since we are only concerned about the inter-element correlation.

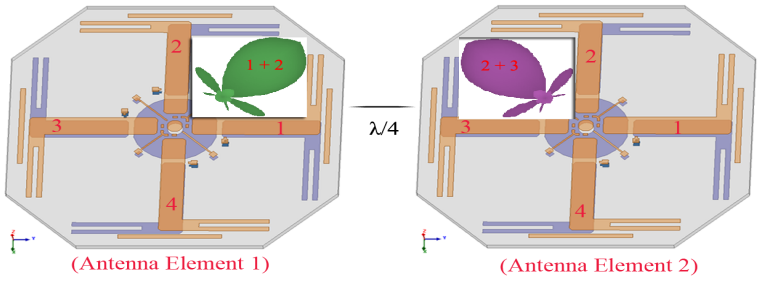

Figure 7.2: Measurement Setup for the S-parameters (a) Configuration 1 (b) Configuration 2 [128]

This analysis helps us to draw inferences on how the antenna array characteristics affect the performance of a MIMO system that employs this array.

The setup of the antenna array of two elements is illustrated in Fig. 7.2. The close proximity ($\lambda/4$) of the two elements have deliberately been selected so that there is strong mutual coupling between them. This coupling is effectively leveraged to generate different radiation patterns for each array's geometry. For the discussion of the antenna modes and the antenna configurations, we refer the reader to Chapter 5, Section 5.4.2.

7.3.3 Pattern Correlation Results

For convenience, we include the pattern correlation result in Fig. 5.11(a) as Fig. **??** below. It depicts the pattern correlation between the antenna array patterns for different array configurations at different frequencies.

The pattern correlation curves for the states of the reconfigurable alford loop (configurations 1 –8) indicate that on the correlation of the array patterns is <0.006 or -22 dB. This is very low compared to the correlation values of the conventional antenna array that uses omnidirectional dipole antennas for an antenna spacing of $\frac{\lambda}{4}$. In the latter case, the maximum value is as high as 0.5 or -3 dB which indicates

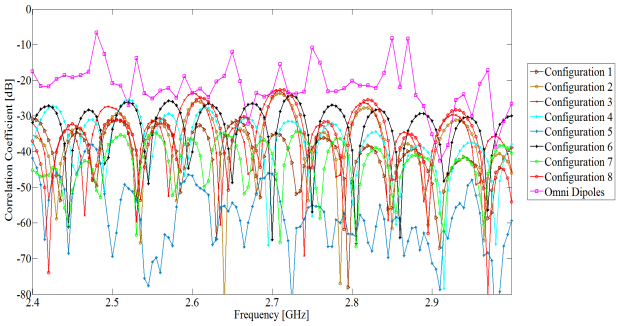

Figure 7.3: Antenna Envelope Correlation for two Collinear Quarter-wave Alfords at different Frequencies for different Configurations in decibel (dB)

that the patterns generated by this antenna array is highly correlated. This result is similar to the findings in [127] for the same antenna spacing. This high pattern correlation is directly related to the spatial MIMO spatial channel correlation and is known to reduce channel capacity [23]. In contrast, the consistently lower spatial correlation of the pattern configurations of the reconfigurable Alford array can be used to maximize channel capacity through adaptation. The proper choice of the transceiver array configuration for a particular multipath environment can be made based on the available channel information.

7.4 Performance of MEAs in Clustered MIMO Channels

In this section we evaluate the capacity and diversity performance of both conventional MEAs and the proposed reconfigurable antenna arrays in clustered MIMO channels described above. To avoid any inconsistencies and for a fair comparison, we use the same antenna array structure for both conventional and reconfigurable array scenarios. The reconfigurable alford loop described above, generates both omnidirectional and directive radiation patterns. For the conventional array scenario, we fix the state of all the array elements in the omnidirectional mode, whereas in

the reconfigurable scenario, the antenna array can switch between any of the 49 possible configurations. This ensures that the conventional array scenario solely relies on the space diversity between the elements while the reconfigurable array system leverages the pattern diversity of the antenna system. We analyze these two systems to demonstrate the benefits of pattern diversity relative to space diversity.

Using the correlated channel model described in [120], we generate the channel matrix as in (7.1) above. To define the ergodic capacity of the MIMO link, a Frobinius normalization of the channel matrix was computed to remove the differences in path loss among a number of channel matrices [10]. This normalization is necessary to preserve the relative antenna gain effects of each configuration. All the channel matrices for each receiver were normalized with respect to the channel matrix generated from the omnidirectional configuration. The normalization factor η_F is given by

$$\eta_F = \sqrt{\frac{||H_{Omni}||_F^2}{P\ Q}} \tag{7.4}$$

The capacity of the $Q\times$ P MIMO system without transmitter channel knowledge and uniform power allocation across transmit antennas is then given by

$$C = E\left\{log_2\ det\left[I_P + \frac{SNR}{Q}\frac{H\ H^\dagger}{\eta_F^2}\right]\right\} \tag{7.5}$$

where $H^\dagger$ is the Hermitian transpose of $\mathbf{H}$.

We also use diversity gain as another performance metric to show the improvement of the diversity receiver. Theoretically, the diversity gain is maximal at the receiver when the different received antenna signals are uncorrelated and minimal when the signals are correlated. The performance of diversity systems is often based on the cumulative distribution functions of the output SNR for a given outage probability as analyzed in [161]. Based on the selection combining technique and the assumption

that the AoAs of the the multipath waves are uniformly distributed, the probability that the instantaneous combiner output SNR γ is below some value γ_s is described by

$$\begin{aligned} Prob(\gamma < \gamma_s) = 1 - 2\ exp(\frac{\gamma_s}{\Gamma})Q(\sqrt{(}\xi\gamma_s), |\rho_s|\sqrt{(}\xi\gamma_s)) \\ +exp(-\xi\gamma_s)I_o\left[|\rho_s|\sqrt{(}\xi\gamma_s)\right] \end{aligned} \tag{7.6}$$

where Γ is the mean SNR and ρ_s is the correlation coefficient between two channels. The functions Q and I_o–the modified Bessel function– are given in [161] and $\xi = \frac{2}{\Gamma(1-|\rho_s|^2)}$.

7.4.1 Simulation Results

We simulate the MIMO channel for a typical indoor environment using the WINNER II model consistent with the WINNER II scenario A1 [120]. In this scenario, the Base station (BS) or Access Points(AP) are assumed to be in the corridors of an office setting, where the LOS case is realized in corridor-to-corridor and the NLOS in corridor-to-room. And, in the NLOS case, the basic path-loss is calculated into the rooms adjacent to the corridor where the AP is located. Wall-losses and floor losses are also appropriately modeled and added to the general path-loss model.

The channel parameters for each snapshot is determined stochastically, based on statistical distributions. Each cluster is approximated by a truncated Laplacian PAS distribution with each path in the cluster being modeled by a unique spatial distribution characterized by a fixed angular spread and variable mean AoAs/AoDs. Antenna patterns for each MIMO radiating element are both simulated in Ansoft HFSS and directly measured in the anechoic chamber. The patterns are then added to the propagation and fading model in the WINNER simulation channel model.

The link capacity of the channel for the reconfigurable antenna system is computed using (7.5) for all possible configurations of the transmitting and receiving array per

simulation scenario. The channel capacity from the reconfigurable antenna scenario is then compared with the capacity achieved from when the antenna system is used as a conventional array. For the diversity performance, we vary the spacing between the antenna elements when it is being used as a conventional array in order to study the effect of antenna spacing on performance.

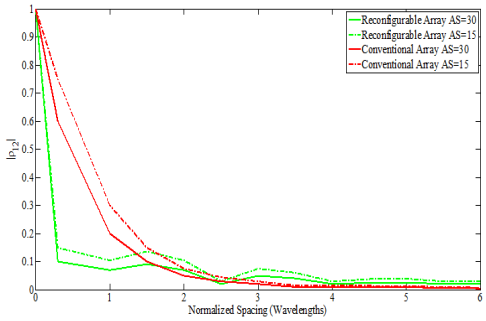

Figure 7.4: Correlation Coefficient of two Antenna Elements for using Laplacian PAS

Fig. 7.4 illustrates the absolute value of the correlation coefficient as a function of antenna spacing for different antenna modes and azimuth angular spread. These curves assumed a single mode-Laplacian PAS with mean AoA of 20^o and $\Delta\theta$ set to 180^o. It can be observed that the correlation coefficient decreases as the antenna spacing between the two elements increases as well as when the AS increases. The graphs also show the performance of the reconfigurable array relative to the conventional array. As shown, for a given antenna spacing and AS the conventional array elements tend to be more correlated than the reconfigurable array ones.

These results illustrate that the angular spread affects spatial correlation–a narrow AS leads to high correlation. Also, at narrow angular spread, a greater antenna spacing is required in order to achieve low spatial correlation. This could be a major

limitation for deployment of antenna arrays in physically small wireless devices. Conventional MEAs have fixed antenna spacing and have no remedy for wireless scenarios that lead to narrow AS. However, reconfigurable antenna arrays require a fixed element spacing and a single structure to provide a wide range of radiation patterns to combat spatial correlation. The flexibility in their design enables the fine tuning and optimization of the array geometry to minimize spatial correlation by exploiting the element mutual coupling, and polarization. This flexibility and advantages are not offered by conventional arrays that rely on antenna grouping or placement algorithms to reduce spatial correlation.

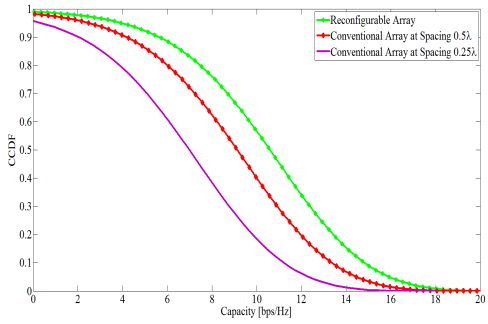

Figure 7.5: The CCDF of Capacity for a 2×2 MIMO/MEA using Conventional and Reconfigurable Arrays for an SNR of 20dB

Fig. 7.5 shows the complementary cumulative distribution function (CCDF) performance of the capacity for the conventional and reconfigurable arrays for $AS = 15^o$ and antenna spacing of 0.25λ. The CCDF shows the percentage of time that the capacity is at or above the values specified by the horizontal axis. The curves show improved performance with the MEA system using reconfigurable arrays relative to the conventional array structure. For the capacity of the reconfigurable array system, the capacity of the channel is found for each possible configuration of the transmitting

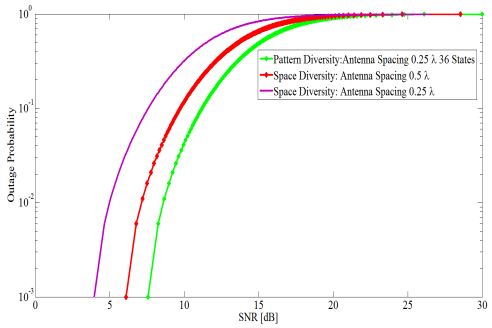

Figure 7.6: The Diversity Gain CDFs for the a 2×2 MIMO/MEA System in Conventional and Reconfigurable Array Modes

and receiving array. And, the optimal solution of the reconfigurable antenna array was the one that guaranteed the highest channel capacity.

Fig. 7.6 compares the diversity gain from space diversity derived from the conventional array structure versus the antenna-pattern diversity derived from reconfigurable antenna arrays. The pattern diversity is realized from using 49 combined states for each array pair –each element is capable of generating 7 different patterns, therefore, with a 2 element array we are able to realize 7×7 radiation pattern configurations. If the receiver uses a reconfigurable array as well, a total of 2401 combined states are realizable. But for this study we only consider the case when only the transmitter uses the reconfigurable array. We only use the top 6 configurations since using all 49 antenna states is impractical. This reduction in the number of configurations was obtained by finding the states with the lowest correlation between the two antenna signals. The curves show that for a given antenna spacing of 0.25λ, antenna-pattern diversity outperforms the space diversity by more than 3dB at an outage probability greater than 0.01. This performance gain may increase with the number of patterns used but at the cost of antenna selection complexity.

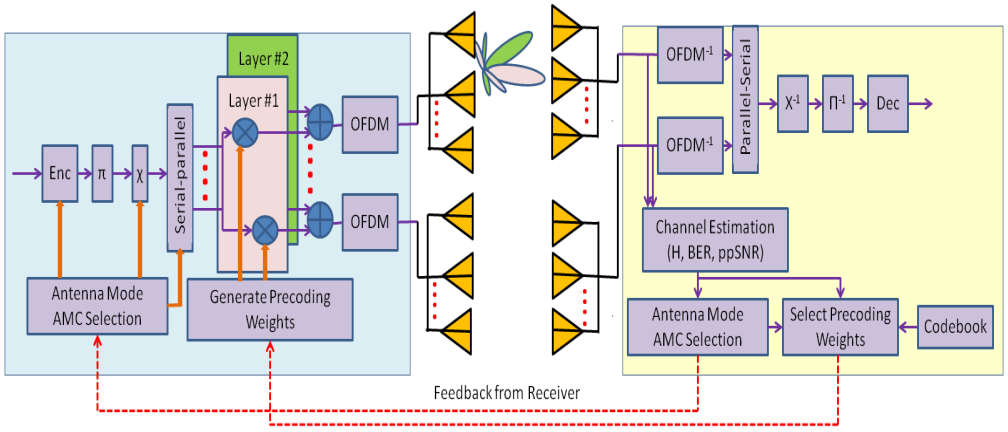

Figure 7.7: Conventional Antenna Array System: Closed-loop Single User MIMO Transmission System using Code-book-based Precoding and Antenna Grouping

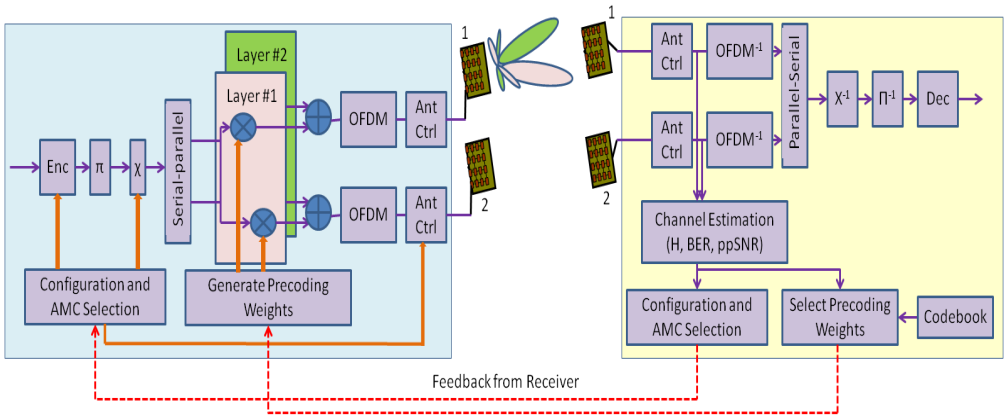

Figure 7.8: Reconfigurable Antenna Array System: Closed-loop Single User MIMO Transmission System using Code-book-based Precoding

7.5 MIMO System Model

In previous sections, we used a simulation framework that employs MIMO cluster modeling to study the impact of spatial correlation and channel spatial characteristics on the performance of MEAs systems. Our findings shown in Figs. 7.5 and 7.6 demonstrate that for a fixed antenna spacing of $\frac{\lambda}{4}$, the capacity and diversity gain from RAS based MEAs outperforms that from conventional MEAs. However, as the

antenna spacing for conventional MEAs is increased to 0.5λ, this performance gap diminishes. It can be inferred from Fig. 7.4 that this performance gap will vanish if the antenna spacing for the conventional MEAs is increased to 1.8λ. At this spacing, the spatial correlation coefficient for the angular spread of 30 degrees is equal for both RAS MEAs and conventional MEAs systems. These simulation findings allow us to quantify the benefits of RAS against conventional MEAS for the same value of spatial correlation. In this section and the rest of paper, we study and analyze through field experimentation the benefits of pattern diversity in RAS MEAs against space diversity in conventional MEAs at a given spatial correlation.

We consider a MIMO-OFDM system illustrated in Fig. 7.7 that transmits R bits per channel using conventional antenna arrays. Fig. 7.8 shows the same system employing reconfigurable antenna arrays. Although the two models are illustrated on two different figures, they are actually implemented in parallel in a common framework. The same antenna arrays are used in both scenarios: for the conventional antenna array setup, the reconfigurable antenna array operates in a fixed state where as in the RAS setup, the reconfigurable antenna array can operate in all possible states described.

The system consists of Q transmit and P receive antennas sending data across K subcarriers. The system consists of serial to parallel spatial multiplexer that produces G substreams, a precoding mapper that maps these streams to transmit antennas, a channel matrix that is function of the of the wireless environment, and a space-time receiver that uses the estimate of the channel state information to decide on the transmitted bit stream. The feedback channel is used to send a low-rate feedback comprising of the precoding matrix index, antenna mode index and the adaptive modulation and coding index.

The symbol vector $\mathbf{s}_{q,k}^{t}$ produced from the spatial multiplexer during each symbol

period t for a given subcarrier is denoted by $\mathbf{s}_{q,k}^{t} = [s_{1,k}^{t}, s_{2,k}^{t}, ..., s_{Q,k}^{t}]$. R bits are demultiplexed into Q different bit streams and modulated using the same constellation. The number of bits per substream is R/G so that R bits are transmitted irrespective of the value of G. This symbol vector is precoded by a $Q \times G$ precoding matrix $\mathbf{W}_{Q,g}\ \epsilon$ $\omega(G, Q)$ where $\mathbf{W}_{Q,g}$ represents a substream-to-antenna group g mapping. It is the g^{th} entry in $\omega(G, Q)$, the ordered set of $Q \times G$ matrices constructed by all combinations of G columns of the identity matrix $\mathbf{I}_Q$. The cardinality $|\omega(G, Q)| = \binom{Q}{G}$. For a $Q = 2$, $\omega(1,2) = \left\{ \begin{bmatrix} 1 \\ 0 \end{bmatrix}, \begin{bmatrix} 0 \\ 1 \end{bmatrix} \right\}$, $\omega(2,2) = \left\{ \begin{bmatrix} 1 & 0 \\ 0 & 1 \end{bmatrix} \right\}$ The columns of the mapping matrices are simply selection diversity vectors that select the antenna to transmit the corresponding substream. This ordered set is $\omega(G, Q) = \left\{ \mathbf{W}_{Q,1}, \mathbf{W}_{Q,2}, ..., \mathbf{W}_{Q,\binom{Q}{G}} \right\}$.

Assuming that the transmitter has no knowledge of the forward-link channel, the optimal values of the parameter G (the number of substreams and the precoding group g are determined at the receiver and fedback to the transmitter. Suppose, the OFDM symbol transmitted from the q^{th} $(q = 1, ..., Q)$ transmit antenna on the k^{th} $(k = 1, ..., K)$ OFDM subcarrier is represented by $\mathbf{s}_{q,k}$. During the t symbol period, the received sequence at the p^{th} $(p = 1, ..., P)$ receive antenna is given by

$$\mathbf{y}_{p,k} = \sqrt{\frac{\varepsilon_s}{Q}} \mathbf{H}_{p,q,k} \mathbf{W}_{Q,g} \mathbf{s}_{q,k} + \mathbf{n}_{p,k}, \tag{7.7}$$

where $\mathbf{H}_{p,q,k}\mathbf{W}_{Q,g}$ is the equivalent channel. After precoding, the q^{th} transmit antenna transmits the g^{th} of $\mathbf{W}_{Q,g}\mathbf{s}_{q,k}$.

For the system in Fig. 7.8 that uses reconfigurable antenna arrays with J antenna configurations or patterns, the system is modeled by:

$$\mathbf{y}_{p,k}^{j} = \sqrt{\frac{\varepsilon_s}{Q}} \mathbf{H}_{p,q,k}^{j} \mathbf{W}\ \mathbf{s}_{q,k} + \mathbf{n}_{p,k}, \tag{7.8}$$

where $\mathbf{y}_{p,k}^{j}$ is the P x 1 received vector at the p^{th} receive antenna, $\mathbf{H}_{p,q,k}^{j}$ is the P x Q channel response matrix between the q^{th} transmit and the p^{th} receive antenna for the k^{th} subcarrier and the j^{th} antenna configuration, and $\mathbf{n}_{p,k}$ is the P x 1 Additive White Gaussian Noise (AWGN) at the p^{th} receive antenna for the k^{th} subcarrier. J is the total number of antenna configurations and ε_s is the transmit energy. In both system models, the transmission bandwidth is assumed to be much less than the coherence bandwidth of the channel and that the symbol period is much less than the coherence time. A zero-delay limited capacity feedback link is assumed to be available from the receive to the transmitter. The receiver uses a Zero-Forcing linear equalizer.

7.5.1 System Model I: Review of the Antenna Mode Selection Criteria

While several criteria have been discussed in detail in [21] and [104], in this section, we only present two such criteria: i) Post-Processing SNR-based selection criterion for dual-mode antenna selection, and ii) Eigenmode-Based Selection for multimode antenna grouping. In the former case, the system switches between two antenna modes of space diversity and spatial multiplexing; the system is either using the sub-arrays to send independent data streams or sending redundant copies of the same stream through all the sub-arrays. In the latter case, the multimode selection introduces the possibility of selecting certain sub-arrays for transmission and not using the rest. It uses either spatial multiplexing or space diversity on various antenna groups that are adaptively selected based on the eigenmode of the equivalent channel matrix.

Post-Processing SNR-based Selection

It has been established in [21] that the performance of spatial multiplexing with a Zero-Forcing linear receiver is a function of the effective SNR for each stream is

given by

$$SNR_p^{(ZF)} = \gamma_0 \frac{1}{[\mathbf{H}_{p,q,k}^H \mathbf{H}_{p,q,k}]^{-1}} \tag{7.9}$$

The ergodic capacity for the spatial multiplexing with linear receivers is then given by [23]

$$C_{(SM)} = \sum_{p=1}^{P} E\left[log_2(1 + SNR_p^{(ZF)})\right] \tag{7.10}$$

Similarly, the performance of spatial diversity with a Zero-Forcing receiver is dependent on the equivalent channel matrix $\mathbf{H}_{p,q,k}\mathbf{W}_{1,g}$ and is given by

$$SNR^{(ZF)} = \gamma_0 \parallel \mathbf{H}_{p,q,k}\mathbf{W}_{1,g} \parallel^2 \tag{7.11}$$

And, the corresponding ergodic capacity for the spatial diversity with linear receivers is then given by [23]

$$C_{(SD)} = E\left[\frac{1}{2}\sum_{p=1}^{P} log_2\left(1 + SNR_p^{(ZF)}\right)\right] \tag{7.12}$$

These values of SNR determine the performance of the system as measured by the average probability of vector symbol error. Also, $SNR^{(ZF)}$ is related to the singular value decomposition vector as below

$$\max_{1\leq g\leq Q} \quad SNR^{(ZF)}(Q,g) \leq \frac{\varepsilon_s}{N_0}\lambda_{max}^2(\mathbf{H}_{p,q,k}) \tag{7.13}$$

where $SNR(Q,g)$ denote the post-processing SNR for a stream given the precoding matrix $\mathbf{W}_{Q,g}$. Another parameter of importance is $d_{min}^2(Q,R)$, which denotes the squared minimum Euclidean distance of the constellation used for transmission on one of the Q substreams. This parameter is often used to derive the probability of

detection error in maximum-likelihood detection of the signal. This is modeled by either of these equations:

$$Pr(error|\mathbf{H}_{p,q,k}) \leq (2^R - 1)Q\left(\sqrt{\frac{\varepsilon_s}{2N_o}d^2_{min}(\mathbf{H}_{p,q,k})}\right) \tag{7.14}$$

$$Pr(error|\mathbf{H}_{p,q,k}) \leq (2^R - 1)Q\left(\sqrt{SNR(G,g)d^2_{min}(Q,R)}\right) \tag{7.15}$$

Based on the above derivations in [21] by Heath et al., the following approximation provides a selection criterion that chooses spatial multiplexing over space diversity if

$$d^2_{min}(Q,R)\min_{1\leq g\leq Q} \quad SNR(Q,1) \geq d^2_{min}(1,R)\max_{1\leq g\leq Q} SNR(1,g) \tag{7.16}$$

Else, choose space diversity transmission from the best transmit antenna.

Eigenmode-based Selection

The eigenmode-based selection criterion is used for the multimode transmission where both the number of substreams and the antenna subset are optimally chosen. By considering a Zero-Forcing receiver, the same work in [21] leverages a result from matrix theory to derive the criterion for multimode selection by using the singular value of $\mathbf{H}_{p,q,k}\mathbf{W}_{Q,g}$. The eigenmode selection rule solves for $\{G^*, g*\}$ that maximize the minimum singular value; this requires he computation of $\lambda_{min}(\mathbf{H}_{p,q,k}\mathbf{W}_{Q,g})$ for all possible $\mathbf{W}_{Q,g}\ \epsilon\ \omega(G,Q)$. The eigenmode-based selection criterion first choose G^* such that

$$G^* = arg\max_{1\leq G\leq Q}\lambda_G(\mathbf{H}_{p,q,k})d^2_{min}(G,R) \tag{7.17}$$

and then find the g^* that solves

$$g^* = arg \max_{1 \leq g \leq \binom{Q}{G^*}} \lambda^2(\mathbf{H}_{p,q,k}\mathbf{W}_{G^*,g}), \tag{7.18}$$

7.5.2 System Model II: Antenna Configuration Selection Criteria

This system model uses post processing SNR (ppSNR) as the metric of configuration selection. The algorithm selects an optimal configuration J^* that yields the highest average ppSNR. This process requires channel training and is carried out during one of the following training intervals: i) Initial training interval, and ii) Re-training Interval. The initial training interval is necessary when no prior channel training has been done. Conversely, the re-training interval prior to some initial training is only used in order to abate the effects of channel fading over time and for up-to-date channel adaptation.

i) Initial training interval: In this interval, initial channel training is carried out over all the J possible configurations; several training packets are transmitted using QPSK modulation for each of the J possible configurations. After each training packet transmission, the ppSNR is calculated by taking the mean of the subcarrier ppSNR values. The average ppSNR of a specific configuration is then obtained by taking the mean of the transmissions at that configuration. The algorithm then selects configuration j^* that with the highest average ppSNR. We sort these average ppSNR values and store the top 5 along with their corresponding configurations.

In this interval, there is need to transmit multiple training packets at a given configuration in order to obtain a meaningful statistic of the Channel Quality Indicator (CQI) from post processing. However, a major challenge arises in selecting the period of the training interval: the use of a long training interval will lead to parameter adaptation based on out-dated channel characteristics; meanwhile a short interval

fails to yield a realistic statistic. Determining the optimal training period requires further analysis that deviates from the main focus of this work. Therefore, a fixed training period was used to obtain a CQI statistic from post processing the channel measurements. Similarly, in an attempt to minimize the re-training interval time we selected a subset of the total configuration for the re-training phase.

ii) Re-training Interval: during this interval we re-train over the top 5 configurations stored in interval i); and transmit a training packet per configuration - thus, a total of 5 training packets. We then select the configuration that yields the highest average ppSNR out of these top 5 configurations.

7.6 Experimental Implementation

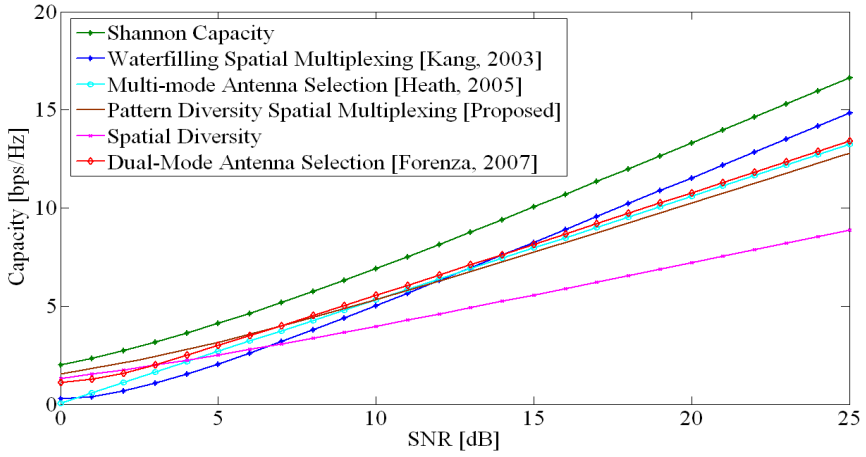

Figure 7.9: Average Capacity for Single User MIMO Transmission System; Shannon Capacity, Waterfilling Technique, Antenna Selection Approaches, Pattern Diversity Scheme

7.6.1 Measurement Setup

The experimental setup used two stations. Each station is equipped with a laptop, a Wireless open-Access Radio Platform (WARP) board [83], and two Reconfigurable antennas. A WARP board has two radio cards, each with one antenna slot. Each of the WARP boards are equipped with a Field-Programmable Gate Array (FPGA) that allows for flexible configuration to different 802.11 standards. The laptop runs the software that drives the WARP radios and the reference code for signal processing. The WARP based testbed therefore, provides a flexible software-defined-radio platform for implementing the PHY/MAC protocols.

We implement a 2x2 MIMO link established by the two stations in concert with OFDM because of its ability to cope with severe channel conditions such as frequency-selective fading due to multipath. The transmission packets are based on the 802.11n OFDM format. The total bandwidth of 20 MHz is divided into 64 subcarriers: 48 for data and 16 for pilot symbols and preamble. Each OFDM symbol has 80 samples (64 samples for each subcarrier plus 16 samples for cyclic prefix). Based on the manufacturer's specification for WARP radio transmission rate of 10^7 samples per second, the sampling rate is approximately 8μs per OFDM symbol [93].

Data are encoded using punctured convolutional codes and modulated at a carrier frequency of 2.484 GHz using one of the four signal constellations: BPSK, QPSK, 16QAM, and 64QAM. The convolutional encoder uses a constraint length of and code generator polynomials of 133, and 171 (in octal numbers). The puncturing matrices for the relevant coding rates (1/2, 2/3, 3/4) are specified. All transmissions consisted of a 24 byte header which includes a Cyclic Redundancy Check (CRC) modulated with BPSK and bits were coded at rate 1/2. The header carries a fixed channel training sequence [90] and a payload of 1KB is followed by a 4 byte CRC check.

7.7 Performance Results

Several algorithms were considered for implementation: i) Proposed model using pattern reconfigurable antennas illustrated in Fig. 7.8. The proposed spatially adaptive algorithm is implemented as part of this model. ii) The model in Fig. 7.7 using conventional arrays. With this model three algorithms: The waterfilling spatial technique [117], multimode [23], and dual-mode [105], approaches are implemented.

Fig. 7.9 presents the ergodic capacity curves for the different techniques with Zero-Forcing receivers. The results were based on channel measurements in an indoor environment. In the figure, we can see that at SNRs below 5dB the proposed technique generates the highest capacity, with respect to the other approaches. For SNRs less than 10dB it outperforms both multimode antenna selection and the waterfilling spatial technique. This advantage can be attributed to the pattern diversity gain associated with the use of the reconfigurable antennas. At low SNRs, the spatial diversity techniques also performs better than the other techniques except the proposed model. However, at higher SNRs it consistently performs below the other models.

At SNR range higher than 10dB, the all the models perform closely except the that for the waterfilling technique. The slight advantage of the waterfilling technique can be attributed to the optimal power allocation between antenna elements of the transmission array. Also, the 1dB gap between the antenna grouping algorithms with the pattern diversity based technique can be explained by the spatial diversity advantage realized from selecting the optimal antenna grouping scheme. The minor difference between the dual-mode and multimode schemes may be attributed to the fact that implemented system uses only two transmit and receive antenna arrays. We believe the use of a larger number of antenna array elements would have influenced the performance of the two schemes.

The results in Fig. 7.9 corroborate our capacity simulation results shown in Fig. 7.5 above. It shows that the performance of pattern reconfigurability at a fixed antenna spacing of $\frac{\lambda}{4}$ is comparable to that of spatial diversity from other conventional MEAs techniques for spatial waterfilling [117], multimode [23], and dual-mode [105]. However, these conventional MEAs algorithms require antenna spacing greater than 1.8λ so as to achieve the same performance as the proposed reconfigurable array model. The performance of conventional MEAs for a fixed antenna spacing of $\frac{\lambda}{4}$ is significantly diminished relative to the pattern diversity performance due to high spatial correlation as illustrated by the spatial diversity curve in magenta. These results reinforce the tremendous benefits of pattern diversity for portable devices due to its minimal antenna spacing requirement – a spacing of $\frac{\lambda}{4}$ which is at least 7 times less than the required spacing for conventional MEAs to achieve the same diversity/capacity performance.

7.8 Summary

In this chapter, an analysis of the benefits of a new radiation pattern diversity system is presented. We characterize spatial correlation in a clustered MIMO channel using a geometry-based stochastic model to motivate these benefits. Through this study, we have shown the complex dependence of spatial correlation on both spatial characteristics and antenna array geometry and radiation patterns. And, subsequently, its adverse impact on systems capacity and diversity performance. Our findings show, that for fixed antenna placement or spacing conventional antenna arrays experience high spatial correlation relative to reconfigurable antenna arrays. This difference is attributable to the fact that RAS array designs integrate spatial geometry and spatial effects such as mutual coupling and polarization to reduce element correlation. Conversely, conventional antenna arrays only rely on greater antenna

spacing to low correlation between array elements.

The implications of these findings motivated us to propose and implement a model that couples the antenna state selection for reconfigurable antenna arrays with the physical layer adaptation algorithms to improve system performance. Specifically, we implement adaptive antenna selection algorithms from MEAs to RAS within a common framework. We experimentally analyze and present the model that leverages the pattern diversity of reconfigurable antennas and benchmark it against a model that uses conventional antenna arrays with its relevant signal processing techniques. Our findings show that at low SNRs, pattern diversity provides a better diversity gain relative to space diversity.

The main contribution of our work is the demonstration of the benefits of pattern diversity reconfigurable antenna arrays to motivate their integration in portable MIMO wireless systems – systems that are too small to employ conventional antenna arrays due to space and design limitations.

CHAPTER 8: INTEGRATING PATTERN RAS IN 4G SYSTEMS

8.1 Introduction

Although several reconfigurable antenna designs and prototypes have been analyzed and tested in the laboratory settings [24]–[27], the transition from laboratory testing to deployment is still a challenge. The integration and deployment of this antenna prototypes in real-world wireless systems have been inhibited by the prohibitively high costs of implementation and integration infrastructure. As a result, many research institutions have turned to Software-Defined Radio solutions to implement radio communications systems [11], [116], [132]–[134]. In this Chapter, we discuss various examples of relevant cost-efficient platforms for integrating these antenna systems. We present the proposed platform and discuss some preliminary performance analysis.

Technically, SDR solutions enable the replacement of hardware specific components with their software implementation [135]. "SDR defines a collection of hardware and software technologies where some or all of the radios operating functions (also referred to as physical layer processing) are implemented through modifiable software or firmware operating on programmable processing technologies. These devices include field programmable gate arrays (FPGA), digital signal processors (DSP), general purpose processors (GPP), programmable System on Chip (SoC) or other application specific programmable processors. The use of these technologies allows new wireless features and capabilities to be added to existing radio systems without requiring new hardware [136]." Fig. 8.1 shows a generalized functional SDR architecture with some of the key features.

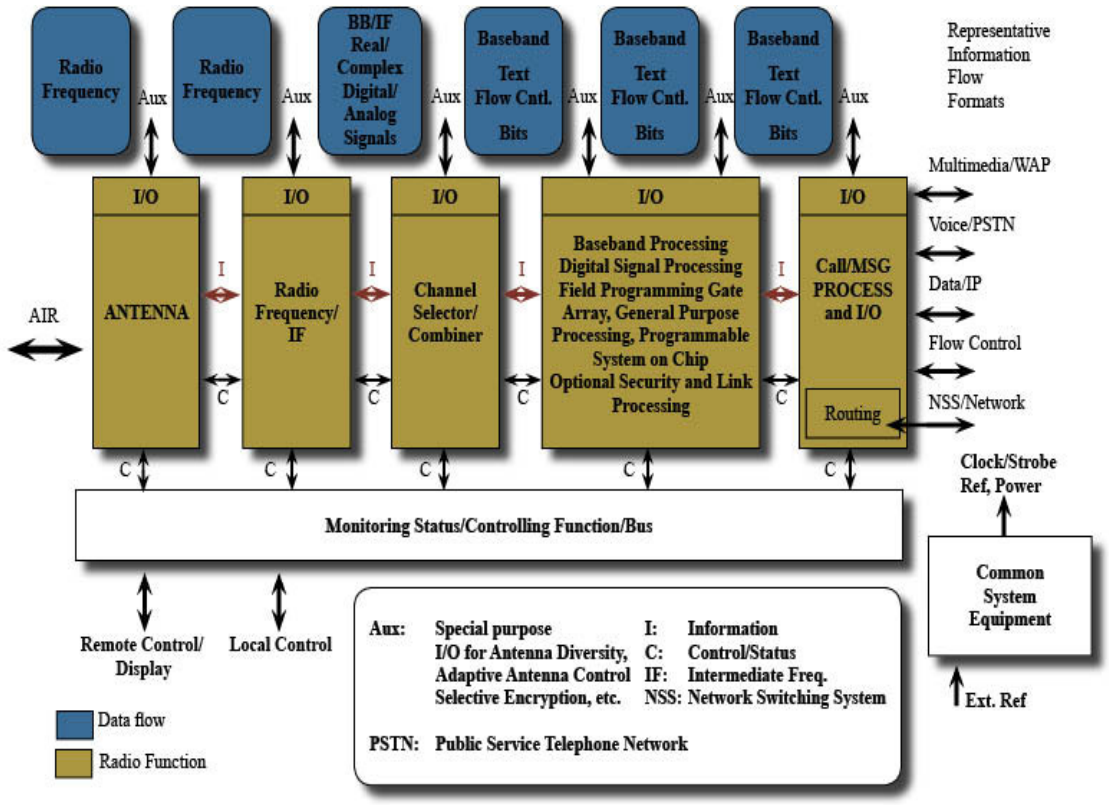

Figure 8.1: A Schematic of a Generalized Functional Software Defined Radio

8.2 Software Defined Radio Solutions

8.2.1 Hardware: Commercial-Off-The-Shelf Technologies

Commercial Off-The-Shelf (COTS) technologies have been used to provide a cost-efficient alternative infrastructure for testing SDR based communications systems. Recent advances in COTS radios have made them valuable in applications ranging from deployed sensors on unsecured borders, to networked RFID tracking, to organizing emergency response teams. Additionally, the reduced cost and availability of these technologies make them viable for custom development and enable quick solution design cycles. Several research works [137]–[141] have leveraged COTS to build state-of-the-art wireless communication testbeds for testing the performance

of various wireless radios and algorithms. These testbed prototypes are generally built around high-performance hardware such as FPGAs and DSPs, the Universal Software Radio Peripherals (USRP) and readily-available wireless base stations. Below, we briefly describe one of the commonly used COTS technologies for wireless communications.

Universal Software Radio Peripherals (USRP)

The USRPs are a family of computer-hosted hardware designed by Ettus Research [142]. A USRP node shown in Fig. 8.2(a) consists of a motherboard and daughterboard that acts as the RF front-end. The daughterboard is controlled by an Altera FPGA, and different daughterboards that operate at various frequency ranges can be used with the same unit. Fig. 8.2(b) is a block diagram that demonstrates the internal features of the USRP unit. Each USRP board features four high-speed Analog to Digital Converters (ADC) and Digital to Analog Converters (DAC), and general purpose interfaces for connection to a Linux terminal and other external hardware. The front-ends are used for operations such as up and down conversions, and filtering. The ADC, DAC and the FPGA perform the digital signal processing operations and signal conversions from baseband to RF frequencies. The code for the FPGA is open-source and can be modified or reprogrammed to provide additional functionality.

8.2.2 SDR Platforms using Open-Source Frameworks and COTS

Although several works [137]–[141] have leveraged COTS to build a state-of-the-art wireless communication testbeds, most of them, [137] –[139] implement PHY layer protocols only and decouples the other OSI layers of the communications system such as the data link/MAC, network/IP, or transport layers. The testbed in [140], however, uses a suite of open-source software frameworks to develop and implement all the

(a)

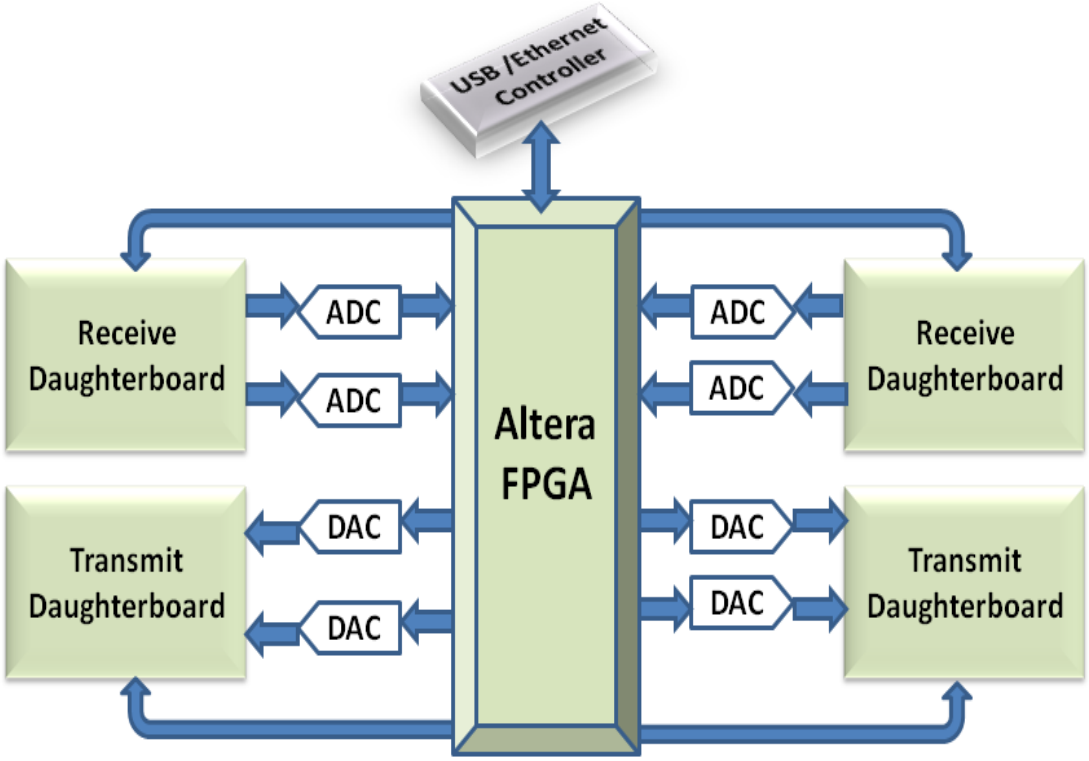

(b)

Figure 8.2: USRP: (a) Hardware; (b) Block Diagram of Internal Features of USRP

OSI layers in a MIMO testbed known as Hydra. This testbed leverages the readily available USRP hardware – designed primarily for accessibility and based on open

source software suites – for testing the performance of a MIMO wireless protocols. Below is a brief description of two of the commonly used open source frameworks.

(I). GNU Radio Software: PHY/MAC Layers Processing

GNU Radio is a free software development toolkit that provides signal processing blocks to implement software radios [145]. It can be used for signal processing from the physical layer with low-cost external RF hardware such as the USRP developed by Ettus Research [142]. Fig. 8.3(a) shows a high-level architecture of a Gnuradio-based SDR platform.

The GNU Radio architecture is based on a set of reconfigurable library of functions or modules called signal processing blocks. Although, the GNU Radio applications are primarily written using the Python programming language, the blocks are written in C++ for high speed performance. The developer can therefore implement real-time high-throughput radio architectures. As shown in Fig. 8.3(b) GNU Radio also provides a Python interface for each C++ block. These blocks are connected via a simplified wrapper and interface generator (SWIG). Specifically, the SWIG is used for parsing the C++ interfaces and to generate the 'glue code' required for Python to call into the C++ code. GNU Radio utilizes USRP – a programmable computer-based transceiver – to serve as the RF front-end of the software defined radio. The USRP Hardware Drivers (UHD) provide an application programming interface (API) for the USRPs and enables information exchange with computers via an Ethernet interface.

(II). CLICK Modular Router Software: MAC/Data Link and IP Layers Processing

Click modular router is an open source software architecture for building flexible and configurable routers. "A Click Router is assembled from packet processing

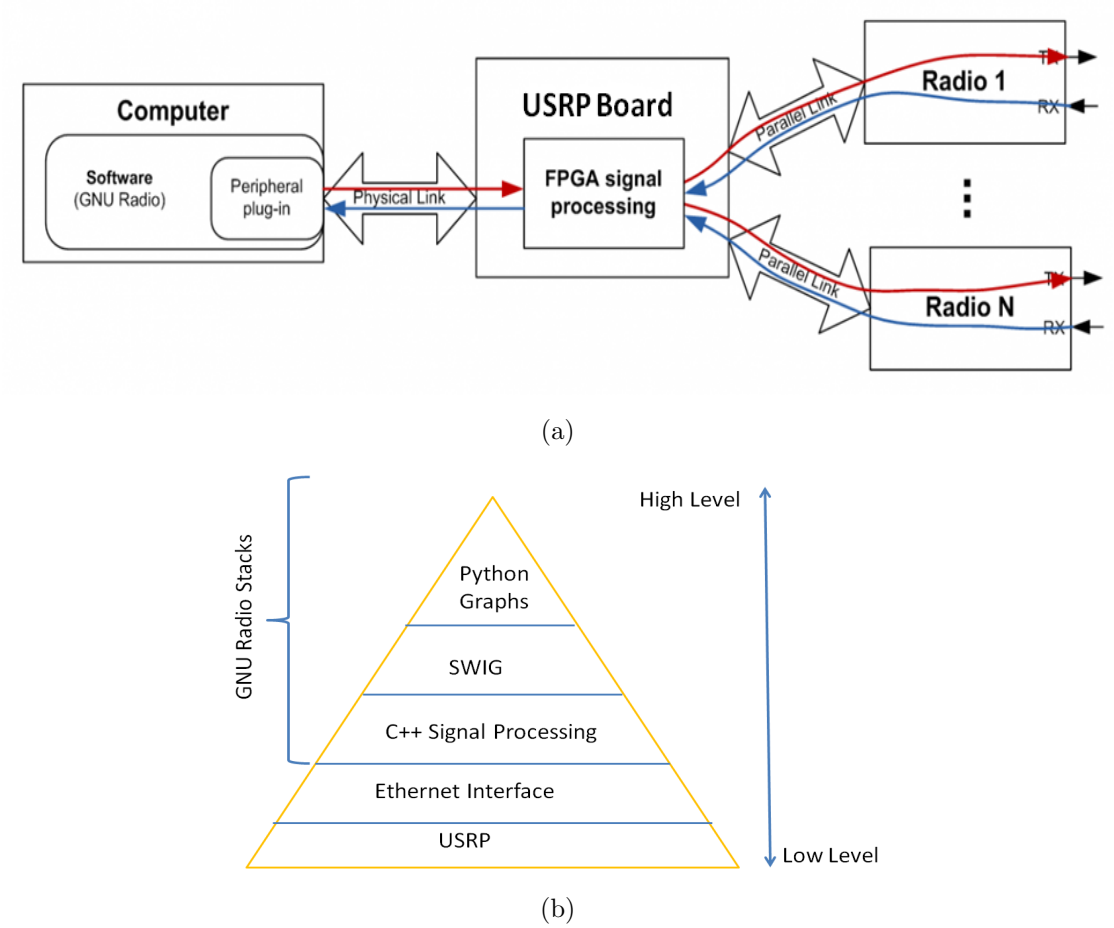

Figure 8.3: GNU Radio Framework: (a) A High-level Architecture of GNURadio-Based SDR; (b) GNU Radio Stacks

modules called elements. Individual elements implement simple router functions like packet classification, queuing, scheduling, and interfacing with network devices. A router configuration is a directed graph with elements at the vertices; packets flow along the edges of the graph. Several features make the individual elements more powerful and complex configurations easier to write,including pull connections, which model packet flow driven by transmitting hardware, and flow-based router context, which helps an element locate other interesting elements [146]."

Protocol Stack for an Example SDR Platform based on Open Source Frameworks

Most SDR platforms based on open-source frameworks described above, are composed of an open-source reconfigurable radio frequency front-end provided enabled by the USRP hardware driver suite, GNU Radio software for PHY/MAC processing and Click modular router to provide the wireless routing. For the rest of the upper layers, transport and applications, they leverage the Linux TCP/IP and applications stack to facilitate end-to-end system testing. Fig. 8.4 illustrates the protocol stack for a typical SDR platform build on open source frameworks.

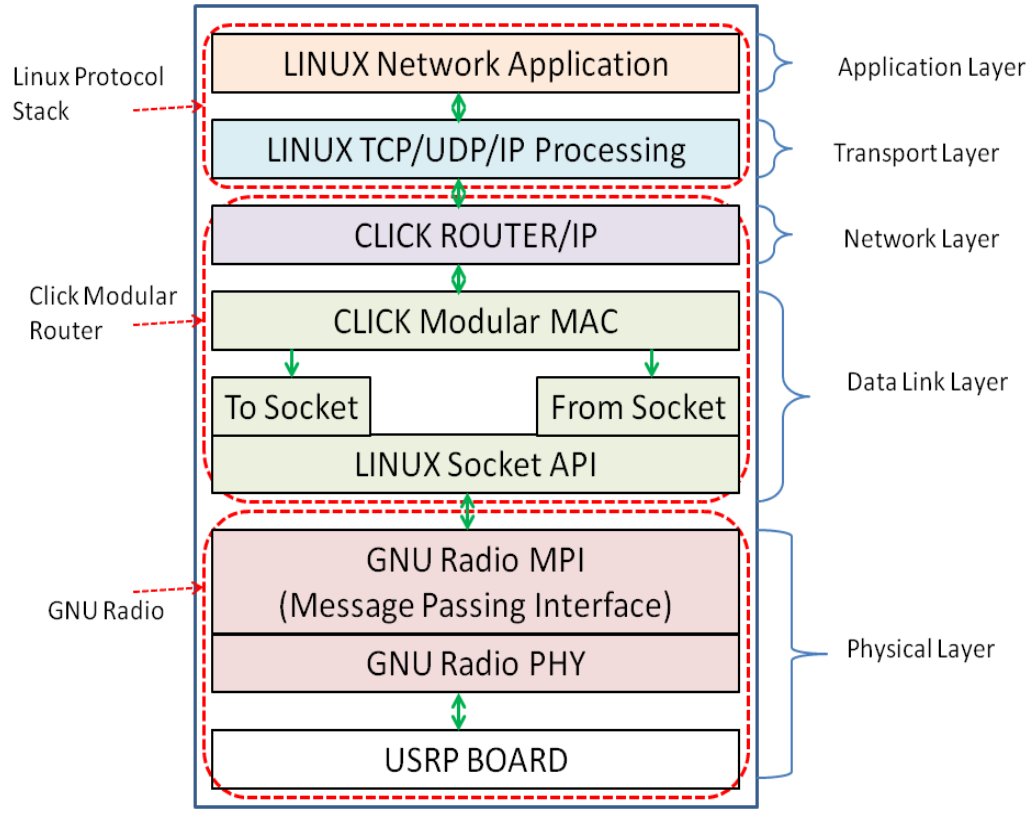

Figure 8.4: A Protocol Stack for the SDR Testbed based on Open Source Software

8.2.3 Other SDR Platforms

The work in [141] leverages the capability of a WiMAX femto base station, an Access Service Network (ASN) gateway, and Linux servers that are readily available to develop a WiMAX network testbed. The base station is a programmable PicoChip [143] WiMAX platform based on the IEEE 802.16e standard [144]. The testbed was specifically used for testing multicast video delivery schemes for 4G wireless networks. However, SDR platform solutions similar to that in [141] tend to be more costly than anticipated and may not be affordable by many research laboratories.

8.3 Proposed Solution: Platform and Experimental Testbed

The flexibility and cost-efficiency of the aforementioned wireless testbeds motivated us to pursue similar COTS technologies to develop a testbed for integrating our novel pattern reconfigurable antennas. Initially, we had sought to take advantage of open source hardware drivers and frameworks such as GNU Radio to develop the relevant software-defined radios similar to the testbed in [133] and [140]. However, due to the nonexistence of the implementation of higher layer protocols in the Click modular router for WiMAX applications, we were not able to pursue this option. This motivated us to pursue a testbed similar to the one presented in [141].

We leverage a state-of-the-art IEEE 802.16e Air4G WiMAX base station from Airspan. This base station device is an open, programmable and virtualizable node, and is one of the key enabling technologies for a collaborative project known as GENI – Global Environment for Network Innovations– WiMAX project [148]. GENI is a multi-institutional project to provide researchers with tools to build next-generation Internet. The Drexel Wireless System Laboratory at Drexel University joined this initiative and was able to procure its own base station using NSF-supported research funding. Each WiMAX base station operates in the educational broadband services

band using experimental licenses approved by FCC and provides a wide-area coverage to support both mobile and fixed users. In this section, we briefly introduce the GENI WIMAX framework and then describe the proposed platform for integrating the reconfigurable antennas in a real wireless system.

8.3.1 GENI WiMAX Platform: Open Access Next Generation Wireless Network Testbed

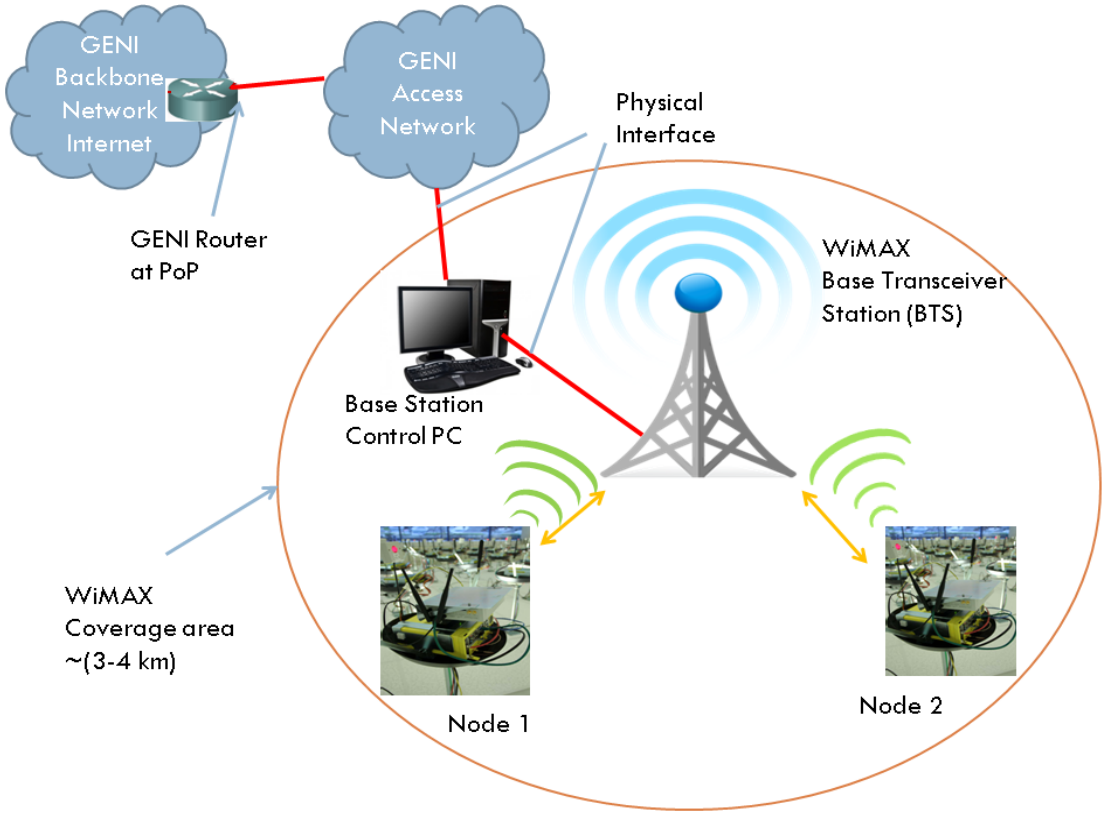

Figure 8.5: A High level Schematic of the GENI WiMAX System and its Interfaces

Fig. 8.5 shows a high level schematic of the GENI WiMAX base station and its interfaces for connecting to the GENI network. The base station is connected to the

GENI access Network using Ethernet or optical fiber technology. This connection point also provides a control interface for researchers to access the base station via the GENI-supported ORBIT Management Framework (OMF). Researchers are able to use ORBIT scripting, experimental control, management and measurement tools to run experiments. The base station is directly connected to the base station controller computer via another physical interface. This interface exposes the features of the base station such as the assignment of PHY/MAC resources (thus, OFDMA, TDMA, scheduling slots, power levels, service classifications, etc.) to each traffic flow. The controller is equipped with a Netspan server software which manages the WiMAX network elements. This server also manages interfaces for initial configuration, scheduler policy selection, queue management and diagnostic access to every radio network element.

WiMAX Base Station Hardware

The Air4G base station is a multi-platform technology that integrates both WiMAX and LTE-Advanced. It is equipped with Quad port and 90 degree sector antennas. It operates in the 700 MHz, 1.4 GHz, 2.3 – 2.7 GHz and 3.3 – 3.8 GHz bands. It has four receivers and four transmitters. It supports both TDD and FDD standards for multiplexing; in the TDD mode the subchannels for the Downlink (DL) and Uplink (UL) can be partitioned into multiple time-frequency configurations. In the mobile WiMAX mode, Air4G supports 3.5, 7, and 10 MHz bandwidth channel sizes. However, it is capable of supporting up to 20 MHz PHY/MAC channels when in the LTE mode. It can run both WiMAX and LTE modes concurrently. It supports standard adaptive modulation schemes based on QPSK, 16QAM, and 64QAM.

8.4 Proposed WiMAX Testbed

Our proposed testbed comprises of an Air4G WiMAX base station, a control server, and multiple wireless clients as depicted in Fig. 8.6. The base station is tuned to operate in a 10 MHz bandwidth with the licensed center carrier frequency of 2.59 GHz. The control server runs Windows Server 2008 operating system with a 2.33 GHz processor and 2 GB of RAM memory. The clients run on Windows operating systems and one of the clients, Node 1, is connected to a 4G WiMAX dongle via a USB interface. The dongle has two external antenna ports that enables the connection of the reconfigurable antenna array to it; the array is in turn connected to a control board for switching between different modes. The other client, Node 2, is also equipped with a Tecom 2.5 GHz WiMAX USB dongle [149].

The WiMAX clients can be associated with the WiMAX base station through the control server which acts as the Access Service Network gateway. The controller also hosts a DHCP server and dynamically assigns IP addresses to new clients from a pool of available addresses. Additionally, it controls and maintains both downlink and uplink connections between the base station and the clients through service flow configuration.

8.4.1 Experimental Evaluation

Parameters: WiMAX PHY/MAC Profiles

The BS PHY profile is set to the TDD mode and the OFDMA channel properties are set as follows: Downlink to Uplink ratio of 29:18, bandwidth of 10 MHz, OFDMA FFT size is set to 1024 and the frame period to 5 ms, and HARQ is set to enabled. The downlink channel is set to operate at carrier frequency of 2.59 GHz, EIRP of 30 dBm and transmit power of 30 dBm. For the purpose of mimicking a 2x2 MIMO system, the BS RF profile is set to use 2 antennas. The downlink sub-frame mode

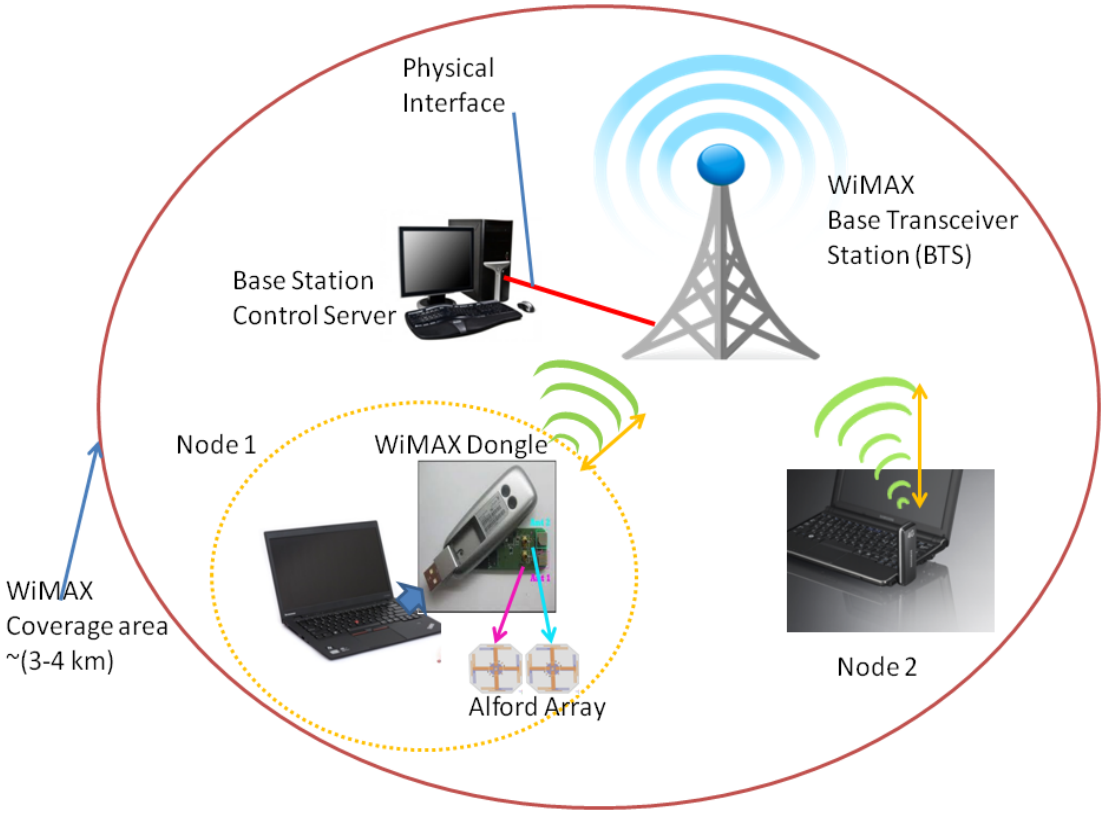

Figure 8.6: A High level Schematic of the Proposed Testbed

property is set to full channel and the MIMO matrix is set to dynamic when testing in the performance of the system the in multimode MIMO state; where it switches between three modes: beamforming, spatial diversity, and spatial multiplexing. The MIMO matrix is set to MIMO matrix B for the state where spatial multiplexing technique is required. The uplink subframe mode property is also set to full channel and the maximum HARQ ACK subchannels is set to 15. Both uplink and downlink burst profiles are set to adaptive modulation and coding based on the modes defined in [144]. This modulation or constellation range from {QPSK , 16QAM, 64QAM }, while the FEC coding rates are {1/2, 2/3, 3/4, 5/6}. Both convolutional code and convolutional turbo code with variable code rate and repetition coding are supported; in this experiments we used convolutional turbo code. Tables 8.1 and 8.2 summarizes

Table 8.1: System Parameters

Parameters	Value
Frequency	2.59 GHz
Duplex	TDD
Bandwidth	10 MHz
BS Antenna Gain	17 dBi
MS Antenna Gain	1.8 dBi
BS Max Power	43 dBm
BS Noise Figure	4 dB

Table 8.2: OFDMA Parameters

Parameters	Value
Channel Bandwidth	10 MHz
Sampling Frequency	11.2 MHz
FFT Size	1024
Subcarrier Spacing	10.94 kHz
Symbol Time	91.4 μs
Cyclic Prefix	11.4 μs
Symbol Duration	102.9 μs
Frame Duration	5 ms
OFDMA Symbols	48

the main system and OFDMA parameters used.

Measurement Methodology

Throughput measurements are commonly performed by sending a large file from one peer to another. In this methodology, the file size is divided over the transfer time duration and the achieved throughput in bits per seconds is measured. However, this method measures application throughput of the established link, which essentially

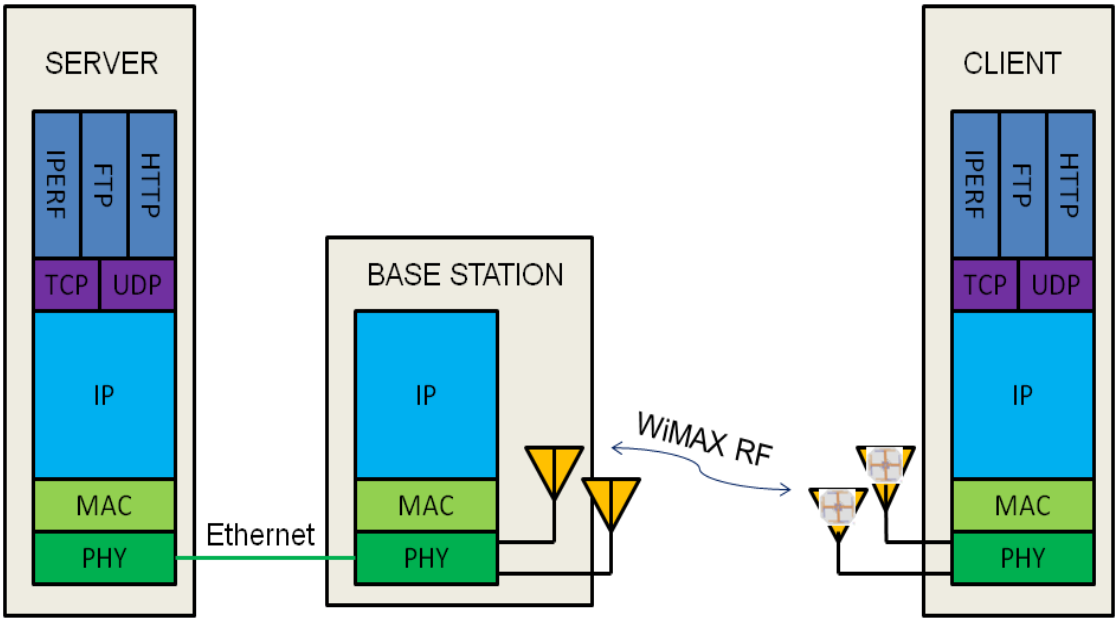

Figure 8.7: WiMAX Setup Architecture

describes the throughput without protocol overheads from other layers such as the transport or network layers. However, as demonstrated in [150] the upper bounds for the expected throughput rates measured at the application layer yields the same performance as measurements based on PHYsical or transport layer methodology. The works in [150] and [151] provides benchmarks for throughput measurements obtained at various OSI-model layers. Fig. 8.7 illustrates the overall network architecture and the main components of the setup based on the OSI-model layers.

In this experimental setup we used the IPERF application for streaming traffic UDP/TCP traffic to measure maximum DL/UL throughput. In order to test the different PHYlayer algorithms, we leveraged the programmability of the base station to configure the settings as described the above. First, we test the multimode PHY layer algorithm that enables the system to dynamically switch between three multi-antenna architectures: beamforming, Spatial multiplexing and spatial diversity. For operation in the multimode state, we configure the base station downlink subframe

property, MIMO matrix, to "dynamic". Similarly, to benchmark performance in this state against the proposed algorithm that uses spatial multiplexing, we also make measurements when the BS downlink property, MIMO Matrix is set to "Matrix B".

We note, that the same antenna array is used in the two measurement scenarios: in the multimode scenario, all the antenna elements of the array are set to operate in the omnidirectional state; while in the reconfigurable scenario, antenna mode switching is allowed. In order to avoid synchronization issues in the switching of the antenna states, we take measurements using each of the antenna array states in a round-robin fashion and process the results offline. Thus, one packet per antenna state is transmitted during each transmission period. We assume that the channel environment is semi-static during the period of transmission that spans all the antenna states. Also, since the reconfigurable Alford is a directional microstrip antenna and the client node is fixed, the number of antenna array states can be minimized.

8.4.2 System Performance

In this section, we present the throughput and PER measurement results and provide explanations for the observed performances. We benchmark the throughput performance against the value of achievable throughput on the derivations in [152]. The achievable throughput is derived from the mutual information or capacity of the channel and accounts for inherent system losses and is given by equation (7) in [152]:

$$D_{achievable} = \frac{1}{1+GI}\frac{1/T_s}{N_{FFT}}\frac{N_{data}}{N_{OFDM}} * C_{Shannon} \tag{8.1}$$

where GI corresponds to the ratio of cyclic prefix time and the useful OFDM symbol time, N_{FFT} is the OFDM size, N_{data} is the number of OFDM data symbols, N_{OFDM} is the total number of OFDM symbols in one transmission frame, and T_s is the sampling rate of the transmit signal. $C_{Shannon}$ is the theoretical Shannon capacity

given by $log_2(1 + SNR)$.

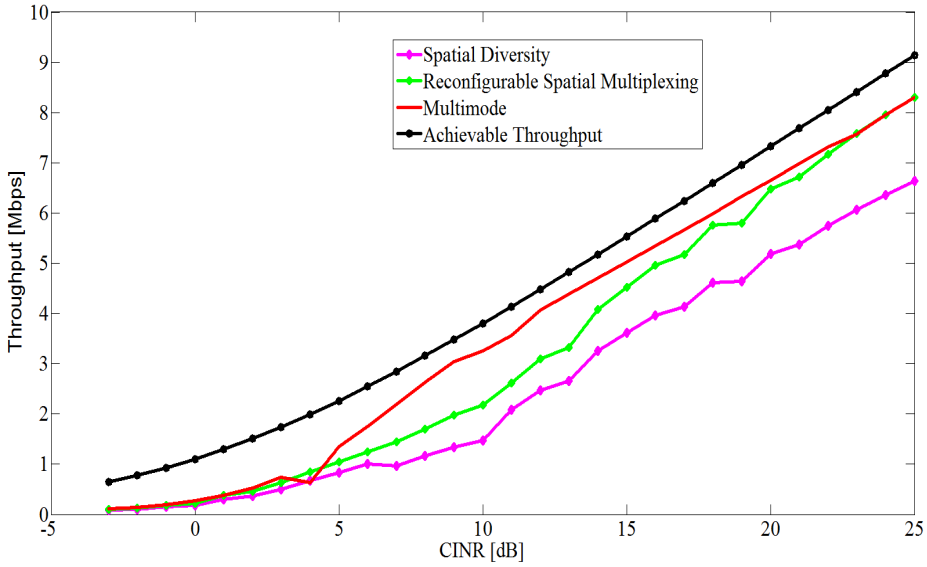

Figure 8.8: Downlink Throughput Performance against CINR

Fig. 8.8 depicts the achieved throughput and the measured throughput for the two measurement scenarios. It can be observed that the throughput achieved from the multimode state outperforms the throughput in the reconfigurable state. This can be attributed to the usage of higher modulation orders in the multimode state as can be observed in Fig. 8.9. The lack of seamless antenna state switching in the client receiving array and other imperfections or constraints of the proposed system might also affect the overall throughput performance. Fig. 8.10 depicts the throughput depending on packet error rate PER for the proposed and benchmark technique.

In the uplink channel, the throughput performance as observed in Fig. 8.11 is relatively the same for both scenarios. This may be explained by the frequent usage of the omnidirectional state of the antenna array in the reconfigurable scenario. Fig.

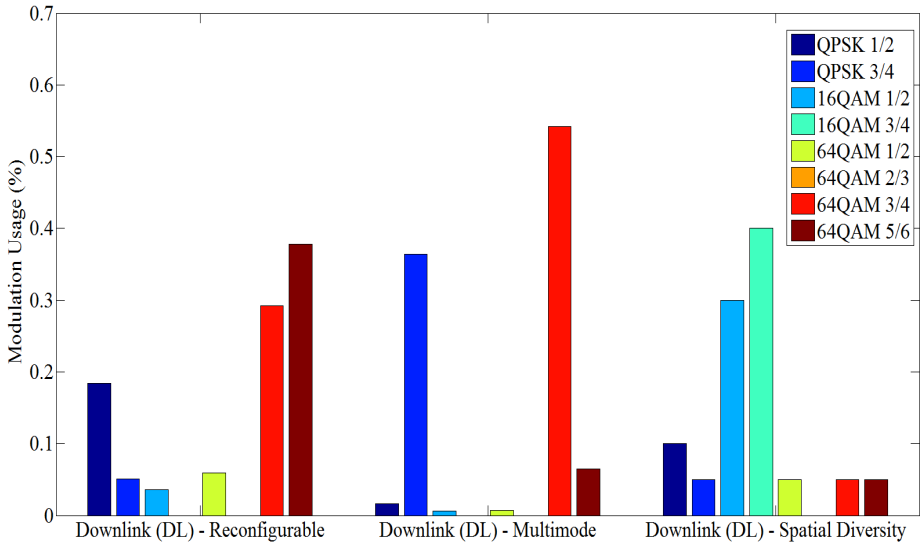

Figure 8.9: Downlink Modulation Usage Performance

?? shows the CDF of the uplink PER. It can be observed that over 90% of coverage is achieved at PER operating less than 2%,in all scenarios.

8.5 Summary

In this Chapter, we presented an overview of software defined radio platforms and the relevant next generation technologies that are often used for testing multi-antenna systems. We then focused on developing a platform for integrating pattern reconfigurable antennas in a 4G systems. Specifically, we discussed the proposed solution and experimental testbed and discussed the system performance testing methodology. And, finally, presented some performance results from an experimental test campaign based on the discussed methodology. These results effectively demonstrate the functionality of the pattern reconfigurable antennas as part of the holistic 4G system. Future work, will focus on improving the efficiency of antenna state switching in a multi-antenna system that uses these pattern reconfigurable antennas.

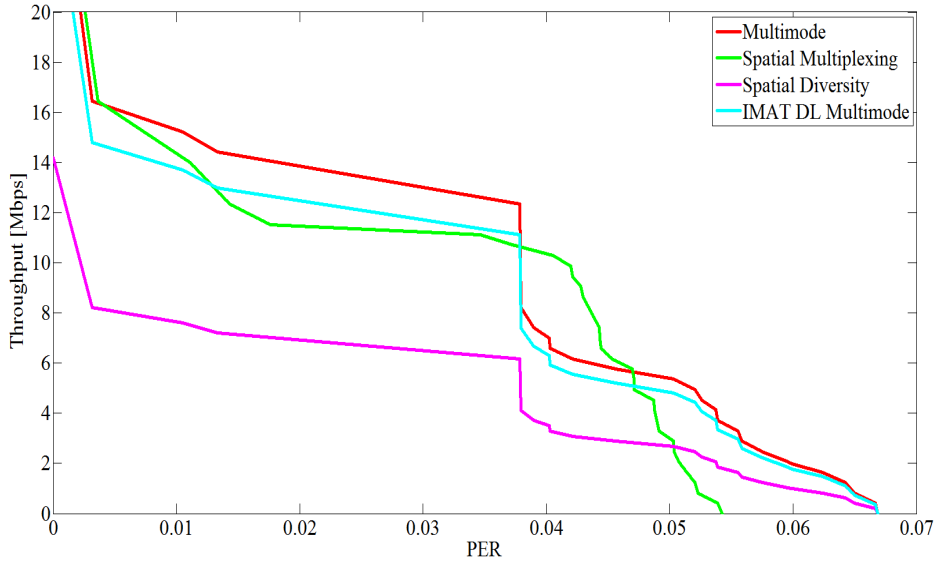

Figure 8.10: Downlink Performance of Throughput versus PER

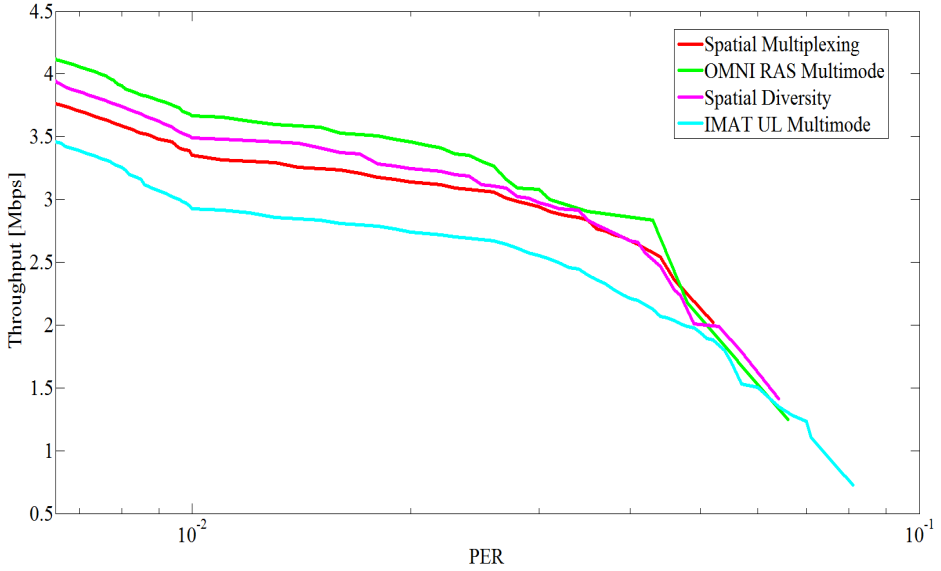

Figure 8.11: Uplink Throughput versus PER Performance

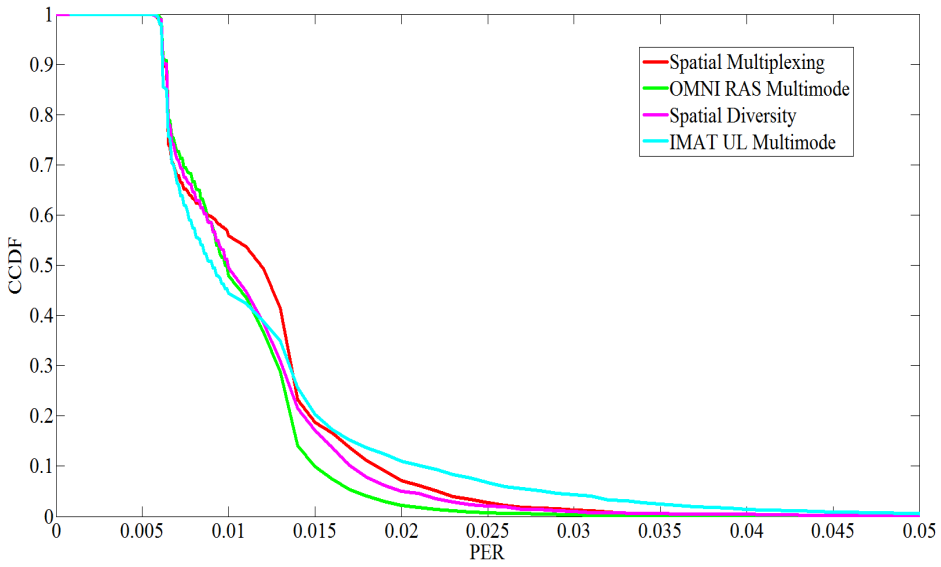

Figure 8.12: Uplink PER Performance

CHAPTER 9: CONCLUDING REMARKS

In this thesis, we investigated the benefits of a new class of smart wireless antenna systems known as reconfigurable antennas. Specifically, we focused on investigating the benefits of integrating these antennas in a holistic 4G wireless system. Through a range of research projects and tasks, we have studied, designed, characterized and analyzed the application of these reconfigurable antenna arrays in small mobile devices that operate at 4G frequencies. These study was carried out in three main phases:

i) In the first phase, we used commercially available antenna design modeling tools and software to study their characteristics in a simulation environment. The prototype of the optimized antenna design obtained from simulation was then fabricated through the use of laboratory rapid prototyping tools and tested in an isolated antenna testing facility –Anechoic chamber. During the characterization process, the scattering parameters and radiation characteristics of the antenna prototypes were also measured in order to understand their performance.

ii) In the second phase, the capabilities of the antennas were tested using a software-defined radio platform. The use of an SDR platform provided a cost-effective laboratory testing solution that was readily available. The SDR solution provided the flexibility to implement most of the radio operating functions in modifiable software or firmware operating on programmable processing technologies. In the SDR framework, we implemented a system-level physical layer model for a MIMO system that leverages the capabilities of these reconfigurable antennas along with wireless transmission architectures and algorithms. First, we proposed and experimentally tested a low complexity PHY model that leveraged the pattern diversity of these antennas in MIMO deployments. The preliminary work involved the design of a spatially adaptive antenna selection algorithm to optimize the pattern diversity gain. We then

subsequently, benchmarked the benefits of the pattern diversity realized from the use of reconfigurable antennas against other models that employ conventional antenna systems.

iii) The third phase of this thesis work was an effort to bridge the gap between laboratory testing of these reconfigurable antennas and real-world wireless system deployment. Their integration and deployment have been inhibited by prohibitively high costs of implementation and integration infrastructure. However, by leveraging a 4G platform that was part of a multi-disciplinary collaborative project, we were able to develop a MIMO testbed to integrate and test the performance of these antenna systems.

The burgeoning demand for high data rate wireless communication services such as multimedia, voice over IP, and ubiquitous data access, has become one of the main drivers of research in cognitive radios and multi-antenna communication systems. This thesis provides a framework that leverages the benefits of smart antenna systems to increase spectral efficiency and help alleviate the problem of limited spectrum.

Bibliography

[1] S. Haykin and M. Moher, Modern Wireless Communications, 4th Ed., *Pearson Prentice Hall*, 2000.

[2] M. A. Ingram,"Multipath Fading," Georgia Institute of Technology. [Online]. Available: http://www.ece.gatech.edu/research/labs/sarl/tutorials/ECE4606/21-MultipathFading.pdf [May, 2011].

[3] Wikipedia. [Online]. Available: http://en.wikipedia.org/wiki/Fading

[4] S. M. Alamouti, "A simple Transmit Diversity Technique for Wireless Communications," *IEEE Journal on Selected Areas in Communications,* Vol. 16, No. 8, pp. 1451–1458, Oct. 1998.

[5] G. J. Foschini, "Layered Space-Time Architecture for Wireless Communication in a Fading Environment When Using Multi-Element Antennas," *Bell Laboratories Technical Journal*, Vol. 1, No. 2, pp. 41–99, 1996.

[6] E. Telatar, "Capacity of Multi-Antenna Gaussian Channels," *European Transactions on Telecommunications,* Vol. 10, No. 6, pp. 585–595, Dec. 1999.

[7] G. J. Foschini, and M. J. Gans, "On the Limits of Wireless Communication in a Fading Environment when Using Multiple Antennas," *Wireless Personal Communications*, Vol. 6, pp. 131–335, 1998.

[8] D. Piazza, "Reconfigurable Antennas for Adaptive MIMO Communication Systems," Ph.D. Dissertation, Dept. Electrical and Computer Engineering, Drexel University, Philadelphia, PA, USA, 2009.

[9] A. Grau, H. Jafarkhani, and F. D. Flavis, "A Reconfigurable Multiple-Input Multiple-Output Communication System," *IEEE Transactions on Wireless Communication*, Vol. 7, No. 5, pp. 1719–1733, 2008.

[10] D. Piazza, N. J. Kirsch, A. Forenza, R. W. Heath, K. R. Dandekar, "Design and Evaluation of a Reconfigurable Antenna Array for MIMO Systems," *IEEE Transactions on Antennas and Propagation*, Vol. 56, No. 3, pp. 869–881, Mar. 2008.

[11] D. Piazza, M. D'Amico, and K. Dandekar, "Two Port Reconfigurable CRLH Leaky Wave Antenna with Improved Matching and Beam Tuning," *IEEE European Conference in Antennas and Propagation,* pp. 2046–2049, 2009.

[12] C. Sukumar, H. Eslami, A. Eltawil, and B. Cetiner, "Link Performance Improvement using Reconfigurable Multianenna Systems," *IEEE Antennas and Wireless Propagation Letters,* Vol. 8. pp. 873–876, 2009.

[13] J. Kountouriotis, D. Piazza, K. Dandekar, M. D'Amico, and C. Guardiani,"Performance Analysis of a Reconfigurable Antenna System for MIMO Communications," *IEEE European Conference on Antennas and Propagation,* Vol., No., pp. 543–547, 2011.

[14] R. Bahl, N. Gulati, K. Dandekar, and D. Jaggard, "Impact of Reconfigurable Antennas on Interference Alignment over Measured Channels," *IEEE GLOBECOM Workshops,* 2012.

[15] D. Qiao, S. Choi, and K. G. Shin, "Goodput Analysis and Link Adaptation for IEEE 802.11a Wireless LANs," *IEEE Transactions on Mobile Computing*, Vol. 1, No. 4, pp. 278–292, Oct. 2002.

[16] A. M. Wyglinski, F. Labeau, P. Kabal, "An Efficient Bit Allocation Algorithm for Multicarrier Modulation," *Wireless Communications and Networking Conference,* Vol.2, No., pp. 1194–1199, Mar. 2004.

[17] K. Song, A. Ekbal, J. M Cioffi, and S. T. Chung, "Adaptive Modulation and Coding (AMC) for Bit-interleaved Coded OFDM (BIC-OFDM)," *IEEE Transactions on Wireless Communications*, Vol. 5, No. 7, pp.3197–3201, Jul. 2006.

[18] C. K. Sung, S. Chung, J. Heo, and I. Lee, "Adaptive Bit-Interleaved Coded OFDM with Reduced Feedback Information," *IEEE Transactions on Wireless Communications*, Vol. 55, No. 9, pp. 1649–1655, Sept. 2007.

[19] A. Goldsmith, and S. Chua, "Variable-Rate Variable-Power MQAM for Fading Channels," *IEEE Transactions on Communications*, Vol. 45, No. 10, pp. 1218–1230, Oct. 1997.

[20] J. T. Bernhard and C. Balanis, "Reconfigurable Antennas (Synthesis Lectures on Antennas and Propagation)," Morgan and Claypool, San Rafael, CA, USA, 2006.

[21] R. Heath Jr, and D. Love, "Multimode Antenna Selection for Spatially Multiplexing Systems with Linear Receivers," *IEEE Transactions on Signal Processing*, Vol. 53, No. 8, pp. 3042–3056, 2005.

[22] M. Kang,and M. Alouini, "Water-Filling Capacity and Beamforming Performance of MIMO Systems with Covariance Feedback," *IEEE Workshop on Signal Processing Advances in Wireless Communications,* 2003.

[23] A. Forenza, M. R. McKay, A. Pandharipande, and R. W. Heath, "Adaptive MIMO Transmission for Exploiting the Capacity of Spatially Correlated Channels," *IEEE Transactions on Vehicular Technology*, Vol. 56, No. 2, pp. , 2007.

[24] B. A. Cetiner, H. Jafarkhani, J. Qian, H. J. Yoo, and A. Grau, "Multifunctional Reconfigurable MEMS Integrated Antennas for Adaptive MIMO Systems," *IEEE Communications Magazine,* Vol. 42, No., pp. 62–70, Dec. 2004.

[25] M. I. Lai, T. Y. Wu, J. C. Hsieh, C. H. Hsieh, and S. K. Jeng, "Design of Reconfigurable Antennas based on an L-shaped slot and PIN diodes for Compact Wireless Devices," *Microwaves, Antennas & Propagation, IET*, Vol.3, No.1, pp. 47–54, Feb. 2009.

[26] H. Li, J. Xiong, Y. Yu, and S. He, "A Simple Compact Reconfigurable Slot Antenna With a Very Wide Tuning Range,"*IEEE Transaction on Antennas and Propagation*, Vol.58, No.11, pp.3725–3728, Nov. 2010.

[27] G. D. Sworo, M. Kam,and K. Dandekar, "Design and Analysis of Reconfigurable Antennas for WiMAX Applications," In Proceedings of *IEEE 14th Annual Wireless and Microwave Technology Conference*, Apr. 2013.

[28] G. D. Sworo, M. Kam, K. Dandekar, "Performance of Link Adaptation Algorithms and Reconfigurable Antennas for MIMO-OFDM Wireless Systems," In Proceedings of *the 46th Annual Conference on Information Science and Systems (CISS)*, Mar. 2012.

[29] G. D. Sworo, R. Measel, M. Kam, K. Dandekar, "Optimization of Adaptive Modulation and Coding techniques for wireless OFDM Systems," In Proceedings of *IEEE International Conference on Signal Processing and Communication Systems (ICSPCS)*, Dec. 2011.

[30] G. Anderson, G. D. Sworo, M. Kam, "Adaptive Control for Networked Multimedia Applications," In Proceedings of *the 47th Annual Conference on Information Science and Systems (CISS)*, Mar. 2013.

[31] J. Kermoal, L. Schumacher, K. I. Pedersen, P. Mogensen, F. Frederiksen, "A Stochastic MIMO Radio Channel Model With Experimental Validation," *IEEE Journal on Selected Areas Communications*, Vol 20, No., pp. 1211–1226, 2002.

[32] K. Yu, M. Bengtsson, B. Ottersten, D. McNamara, P. Karlsson, M. Beach, "Modeling of Wide-Band MIMO Radio Channels Based on NLoS Indoor Measurements," *IEEE Transactions on Vehicular Technology*, Vol 53, No., pp. 655–665, 2004.

[33] E. A. Jorswieck, H. Boche, "Optimal Transmission Strategies and Impact of Correlation in Multi-antenna Systems with different types of Channel State Information", *IEEE Transactions on Signal Processing,* Vol 52, No., pp. 3440–3453, 2004.

[34] A. Tulino, A. Lozano, S. Verd, "Impact of Antenna Correlation on the Capacity of Multiantenna Channels," *IEEE Transactions on Information Theory,* Vol 51, No., pp. 2491–2509, 2005.

[35] D. Shiu, G. J. Foschini, M. J. Gans, J.M. Kahn, "Fading Correlation and Its Effect on the Capacity of Multielement Antenna Systems," *IEEE Transactions on Communications,* Vol 48, No., pp. 502–513, 2000.

[36] B. Widrow, P. E. Mantey, L. J. Griffiths, and B. B. Goode, "Adaptive Antenna Systems," *Proceedings of IEEE,* Vol. 55, No. 12, pp. 2143–2159, Dec. 1967.

[37] F. B. Gross, "Smart Antennas for Wireless Communications with Matlab", McGraw-Hill, 2005.

[38] Array Processing Tutorial, The University of Texas at Austin. [Online] Available: http://users.ece.utexas.edu/~bevans/courses/ee381k/lectures/13_Array_Processing/lecture13/lec

[39] C. A. Balanis, *Antenna Theory: Analysis and Design.* New York: John Wiley & Sons, 2005.

[40] D. Piazza, P. Mookiah, M. D'Amico, and K. R. Dandekar, "Two port Reconfigurable Circular Patch Antenna for MIMO Systems," *Proceedings of the European Conference on Antennas and Propagation,* Vol., No., pp. 1-4, Jul. 2007.

[41] P. Mookiah, D. Piazza, and K. R. Dandekar, "Reconfigurable Spiral Antenna Array for Pattern Diversity in WideBand MIMO Communications Systems," *IEEE International Symposium on Antennas and Propagation Society,* Vol., No., pp., 2008.

[42] D. Piazza, M. D'Amico, and K. R. Dandekar, "Two port Reconfigurable CRLH Leaky Wave Antenna with Improved Impedance Matching and Beam Tuning," *Proceedings of the European Conference on Antennas and Propagation,* Vol., No., pp., 2009.

[43] S. Zhang, G. H. Huff, J. Feng, and J. T. Bernhard, "A Pattern Reconfigurable Microstrip Parasitic Array," *IEEE Transactions on Antennas and Propagation,*

[44] Y. Cai and Z. Du, "A Novel Pattern Reconfigurable Antenna Array for Diversity," *IEEE Antennas and Wireless Propagation Letters*, Vol. 8, No., pp. 1227–1230, 2009

[45] M. Donelli, R. Azaro, L. Fimognari, and A. Massa, "A Planar Electronically Reconfigurable Wi-Fi band Antenna based on a Parasitic Microstrip Structure," *IEEE Antennas and Wireless Propagation Letters*, Vol. 6, No., pp. 623–626, 2007.

[46] A. Forenza and R. W. Heath, "Benefit of Pattern Diversity via two-element Array of Circular Patch Antennas in indoor Clustered MIMO Channels," *IEEE Transactions on Communications*, Vol. 54, No. 5, pp. 943–954, 2006.

[47] W. C. Jakes, Microwave Mobile Communications. *Wiley*, New York, 1974.

[48] D. Liang, C. Hosung, R. W. Heath, and L. Hao, "Simulation of MIMO Channel Capacity with Antenna Polarization Diversity," *IEEE Transactions on Wireless Communications,* Vol. 4, No. 4, pp. 1869–73, 2005.

[49] G. J. Foschini, G. D. Golden, R. A. Valenzuela, P. W. Wolniansky, "Simplified Processing for High Spectral Efficiency Wireless Communication Employing Multi-Element Arrays," *IEEE Journal on Selected Areas in Communications,* Vol. 17, No. 11, pp. 1841–1852, 1999.

[50] J. Winters, "On the Capacity of Radio Communication Systems with Diversity in a Rayleigh Fading Environment," *IEEE Journal on Selected Areas in Communications,* Vol. 5, No. 5, pp. 871–878, 1987.

[51] P. W. Wolniansky, G. J. Foschini, G. D. Golden, and R. A. Valenzuela, "V-BLAST: An Architecture for Realizing Very High Data Rates Over the Rich-Scattering Wireless Channel," *Proceedings IEEE International Symposium on Signals, Systems, and Electronics*, Vol., No., pp. 295–300, Oct. 1998.

[52] C. E. Shannon, "A Mathematical Theory of Communication," *Bell System Technical Journal*, Vol. 27, No., pp. 379-423 and 623-656, Oct. 1948.

[53] M. Jankiraman, Space-Time Codes and MIMO Systems. *Artech House, Inc*, 2004.

[54] E. Biglieri, R. Calderbank, A. Constantinides, A. Goldsmith, A. Paulraj, and V. H. Poor, MIMO Wireless Communications. *Cambridge University Press,* 2007.

[55] E. Biglieri, J. Proakis, and S. Shamai, "Fading Channels: Information-theoretic and Communications aspects," *IEEE Transaction on Information Theory,* Vol. 44, No. 6, pp. 2619–2692, Oct. 1998.

[56] R. L. Cupo, G. D. Golden, C. C. Martin, K. L. Sherman, N. R. Sollenberger, J. H. Winters, and P. W. Wolniansky, "A Four-Element Adaptive Antenna Array for IS-136 PCS Base Stations," *IEEE Transactions on Vehicular Technology,* Vol. 3, No., pp. 1577–1581, May. 1997.

[57] G. H. Golub and C. F. Van Loan, *Matrix Computation*," John Hopkins University Press, USA, 1983.

[58] B. G. Lee and S. Choi, Broadband Wireless Access and Local Networks : Mobile WiMAX and WiFi, Ed., *Artech House*, 2008.

[59] G. G. Raleigh, and J. M. Cioffi, "Spatio-Temporal Coding for Wireless Communication," *IEEE Transactions on Communications,* Vol. 46, No. 3, pp. 357–366, Mar. 1998.

[60] H, Bölcskei, D. Gesbert, and A. J. Paulraj, "On the Capacity of OFDM-based Spatial Multiplexing Systems," *IEEE Transactions on Communications,* Vol. 50, No. 2, pp. 225–234, Feb. 2002.

[61] H, Bölcskei,"MIMO-OFDM Wireless Systems: Basics, Perspectives, and Challenges," *IEEE Transactions on Communications,* Vol. 13, No. 4, pp. 31–37, Feb. 2006.

[62] H. Sampath, S. Talwar, J. Tellado, V. Erceg, and A. Paulraj, "A Fourth Generation MIMO-OFDM broadband Wireless System: Design, Performance, and Field Trial Results," *IEEE Communications Magazine,* Vol. 40, No. 9, pp. 143–149, 2002.

[63] IEEE 802.16 Working Group, "IEEE Standard for Local and Metropolitan Area Networks part 16: Air Interface for Fixed Broadband Wireless Access Systems," Nov. 2004.

[64] 3rd Generation Partnership Project (3GPP), "Physical Layer Aspect for Evolved Universal Terrestrial Radio Access (UTRA): Technical Report", 2006.

[65] 3rd Generation Partnership Project (3GPP) Technical Specification Group Radio Access Network (Release 9), "Further Advancements for E-UTRA Physical Layer Aspects: Technical Report, 2009.

[66] R. W. Chang,"Synthesis of Band-limited Orthogonal Signals for Multichannel data Transmission," *Bell Systems Technical Journal,* Vol. 45, No., pp. 1775–1796, 1966.

[67] S. Redl, M. Weber, and M. Oliphant, GSM and Personal Communications Handbook. Artech House Mobile Communications Library, 1998.

[68] J. Cioffi. (2008). EE379C-Digital Communication: Signal Processing. Stanford University, Stanford, CA. [online] Available: http:// www.stanford.edu/class/ee379c

[69] Z. Wang, and G. B. Giannakis, "Wireless Multicarrier Communications," *IEEE Signal Processing Magazine,* Vol. 17, No. 3, pp. 29–48, 2000.

[70] T. Hwang, C. Yang, G. Wu, and G. Li, "OFDM and its Wireless Applications: A Survey," *Transactions on Vehicular Technology,* Vol. 58, No. 4, pp. 1673–1694, 2009.

[71] D. Tse, and P. Vishwanath, Fundamentals of Wireless Communications. *Cambridge University Press*, Cambridge, UK, 2005.

[72] J. G. Proakis, Digital Communications, 4th Ed., *McGraw-Hill*, 2000.

[73] National Instruments: White Paper. [Online] Available: http://www.ni.com/white-paper/3740/en

[74] D. Agrawal, V. Tarokh, A. Naguib, and N. Seshadri, "Space-Time Coded OFDM for High Data-rate Wireless Communication over Wideband Channels," *IEEE Vehicular Technology Conference,* Vol. 3, No., pp. 2232–2236, 1998.

[75] J. Uddin, E. A. Oyekanlu, G. D. Sworo, and J. Kim, "Next Generation Internet Services: Bellman Ford Distance Vector Algorithm on GPU using CUDA," *To be submitted to an IEEE conference*, Jan. 2013.

[76] NXP Semiconductors. "PIN Diodes for Mobile Communications and RF Applications," Internet: http://www.nxp.com/products/rf/diodes/pin_diodes/BAP63-03.html , 2012, [Nov. 30, 2012].

[77] Digi-Key. "RF small signal products part 2: PIN diodes." Internet: http://dkc1.digikey.com/us/en/tod/NXP/RFSmallSignal ProductsPart2_NoAudio/RF_Small_Signal_Part2_NoAudio.swf , 2012 [Nov. 30, 2012].

[78] S. Blanch, J. Romeu, and I. Corbella, "Exact Representation of Antenna System Diversity Performance from Input Parameter Description," *IEEE Electronic Letters*, Vol. 39, No. 9, pp. 705 –707, May, 2003.

[79] R. G. Vaughan, J. B. Andersen, "Antenna Diversity in Mobile Communications," *IEEE Transactions on Vehicular Technology,* Vol. 36, No., pp. 149–172, 1987.

[80] V. Plicanic, Z. Yang, T. Bolin, G. Kristensson, and A. Derneryd, "Antenna Diversity Evaluation for Mobile Terminals," *European Conference on Antennas and Propagation*, Vol., No., pp. 1–3, Nov. 2006.

[81] D. Patron, A. Daryoush, and K. R. Dandekar, "Optical Control of Reconfigurable Antennas and Application to a Novel Pattern-Reconfigurable Planar Design," *IEEE Journal of Lightwave Technology,* Vol. 32, No. 20, pp., 2014.

[82] M. Facco, and D. Piazza, "Reconfigurable Zero-Order Loop Antenna," *IEEE International Symposium on Antennas and Propagation,* Vol., No., pp. 1 – 2, 2012.

[83] WARP Research Platform. *Rice University.* [Online]. Available: http://warp.rice.edu/

[84] D. Piazza, K. Dandekar, "Reconfigurable Antenna Solution for MIMO-OFDM systems," *Electronic Letters*, Vol. 42, No. 8, pp. 446–447, 2006.

[85] J. Boerman and J. Bernhard, "Performance study of Pattern Reconfigurable Antennas in MIMO Communications Systems," *IEEE Transactions on Antennas and Propagation*, Vol. 56, No. 1, pp. 231–236, 2008.

[86] I. F. Akyildiz, D. M. Gutierrez-Estevez, and E. C. Reyes, "The Evolution to 4G Cellular Systems: LTE-Advanced," *Elsevier Journal of Physical Communication*, Vol. 3, No., pp. 217-244, 2010.

[87] R. T. Becker, "Precoding and Spatially Multiplexed MIMO in 3GPP Long-Term Evolution," *High Frequency Electronics*, Oct. 2009.

[88] W. Utschick and J. Brehmer, "Monotonic Optimization Framework for Coordinated Beamforming in Multicell Networks", *IEEE Transactions on Signal Processing*, Vol. 60, No. 4, pp. 1899–1909, 2012.

[89] D. Gonzalez, J. Kountouriotis, D. Lach, R. Bertolazzi, P. Das, K. Dandekar, "Performance of a Reconfigurable Antenna Configuration Selection Scheme in a MIMO-OFDM System with Modulation Rate Adaptation," *International Symposium on Modeling and Optimization in Mobile, Ad Hoc, and Wireless Networks*, Vol., No., pp. 307-313, May. 2011.

[90] IEEE 802.16 Working Group, "IEEE Standard for Local and Metropolitan Area Networks," Nov. 2004.

[91] J. Medbo, J., and P. Schramm, "Channel models for HIPERLAN/2," ETSI/BRAN, No. 3ERI085B, Mar. 1998.

[92] A. Molisch, Wireless Communications, 2nd Ed. *John Wiley & Sons*, Aug. 2011.

[93] A. Goldsmith, Wireless Communications. *Cambridge University Press*, Aug. 2005.

[94] P. Frenger, P. O. Tony, and A. Svensson, "Multi-rate Convolutional Codes," *Chalmers University Technology*, Gotenberg, Sweden, Technology Republic 21, 1998.

[95] J. M. Cioffi, "A Multicarrier Primer," *Standford University*. last accessed Sept. 2010. [online] Available: http://www.stanford.edu/group/cioffi/documents/multicarrier.pdf

[96] X. Vu, D. Nguyen, and T. A. Vu, "An Finite-State Markov Channel Model for ACM Scheme in WiMAX," *IEEE Emerging Technologies for Sustainable Development*, Vol., No., pp.1-6, Jan. 2009.

[97] H. S. Wang and N. Moayeri, "Finite-State Markov Channel - A useful model for radio communication channels," *IEEE Transactions on Vehicular Technology*, Vol. 44, No. 1, pp. 825-830, Sept. 1995.

[98] C. C. Tan and N. C. Beaulieu, "On First-Order Markov Modeling for the Rayleigh Fading Channels," *IEEE Transactions Communications*, Vol.48, No. 12, pp. 2032-2040, Dec. 2000.

[99] M. Chu and W. Stark, "Effect of Mobile Velocity on Communications in Fading Channels," *IEEE Transanctions Vehicular Technology*, Vol. 49, No. 1, pp. 202-210, Jan. 2000.

[100] L. Kleinrock and R. Gail, Queuing systems: Theory. *Wiley*, Vol. 1, New York, 1996.

[101] I. Parberry (2001). Algorithm Analysis and Computational Complexity, *University of North Texas, TX.* [online] Available: http://larc.unt.edu/ian/books/free/lnoa.pdf

[102] A. Quarteroni and F. Saleri, Scientific Computing with Matlab. *Springer*, Aug. 2003.

[103] D. Qiao and S. Choi, "Goodput Enhancement of IEEE 802.11a Wireless LAN via Link Adaptation," *IEEE International Conference on Communications*, Vol. 7, pp. 1995–2000, Jun. 2001.

[104] K. Kim, K. Ko, and J. Lee, "Adaptive Selection of Antenna Grouping and Beamforming for MIMO Systems," *EURASIP Journal on Wireless Communications and Networking,* Vol., No., pp., 2011.

[105] R. Heath Jr, and A. Paulraj, "Switching Between Diversity and Multiplexing in MIMO Systems," *IEEE Transactions on Communications*, Vol. 53, No. 6, pp. 962 – 968, 2005.

[106] C-n. Chuah, G. J. Foschini, R. A. Valenzuela, D. Chizhik, J. Ling, and J. M. Kahn, "Capacity Growth of Multi-Element Arrays in Indoor and Outdoor Wireless Channels," *IEEE Wireless Communications and Networking Conference,* Vol. 3, No., pp. 1340–1344, 2000.

[107] D. Shiu, G. J. Foschini, M. J. Gans, and J. M. Kahn, "Fading Correlation and Its Effect on the Capacity of Multielement Antenna Systems," *IEEE Transactions on Communications*, Vol. 48, No. 3, pp. , 2000.

[108] A. M. Tulino, A. Lozano, and S. Verdu, "Impact of Antenna Correlation on the Capacity of Multiantenna Channels," *IEEE Transactions on Information Theory*, Vol. 51, No. 7, pp. 2491–2509, Jul. 2005.

[109] M. Chiani, M. Z. Win, and A. Zanella, "On the Capacity of Spatially Correlated MIMO Rayleigh-Fading Channels," *IEEE Transactions on Information Theory,* Vol 49, No. 10, pp., 2003.

[110] V. Veeravalli, Y. Liang, A. M. Sayeed, "Correlated MIMO Wireless Channels: Capacity, Optimal Signaling, and Asymptotics," *IEEE Transactions on Information Theory,* Vol. 51, No. 6, Jun. 2005.

[111] M. Paetzold. Mobile Radio Channels (2nd Edition). Hoboken, NJ, USA: John Wiley & Sons, 2011.

[112] C. Sukumar, H. Eslami, A. Eltawil, and B. Cetiner, "Link Performance Improvement using Reconfigurable Multianenna Systems," *IEEE Antennas and Wireless Propagation Letters,* Vol. 8. pp. 873–876, 2009.

[113] N. Gulati and K.R. Dandekar, "Learning State Selection for Reconfigurable Antennas: A Multi-Armed Bandit Approach", *IEEE Transactions on Antennas and Propagation (Special Issue: Antenna Systems and Propagation for Cognitive Radio)*, Vol., No., pp., 2013.

[114] J. Kountouriotis, D. Piazza, P. Mookiah, and K. R. Dandekar, "Reconfigurable Antennas and Configuration Selection Methods for MIMO Ad-Hoc Networks", *EURASIP Journal on Wireless Communications and Networking (Special Issue on Recent Advances in Multiuser MIMO Systems)*, Vol., No., pp., 2011.

[115] P. Mookiah, and K. R. Dandekar, "A Reconfigurable Antenna Based Solution for Stationary Device Authentication in Wireless Networks",*International Journal on Antennas and Propagation (Special Issue on Reconfigurable Antennas and Their Applications in Wireless Communications)*, Vol., No., pp., 2012.

[116] A. Forenza and J. R. W. Heath, "Benefit of pattern diversity via two-element array of circular patch antennas in indoor clustered MIMO Channels," *IEEE Transactions on Communications*, Vol. 54, No. 5, pp. 943–954, 2006.

[117] M. Kang,and M. Alouini, "Water-Filling Capacity and Beamforming Performance of MIMO Systems with Covariance Feedback," *IEEE Workshop on Signal Processing Advances in Wireless Communications,* 2003.

[118] G. D. Sworo, M. Kam, K. Dandekar, "Performance of Link Adaptation Algorithms and Reconfigurable Antennas for MIMO-OFDM Wireless Systems," In Proceedings of *the 46th Annual Conference on Information Science and Systems (CISS)*, Mar. 2012.

[119] A. A. M. Saleh, and R. A. Valenzuela, "A Statistical Model for Indoor Multipath Propagation," *IEEE Journal of Selected Areas in Communications,* Vol. 5, No. 2, pp. 128–137, Feb. 1987.

[120] IST WINNER II Deliverable 1.1.2 v.1.2, "WINNER II Channel Models," *WINNER II, Technical Report,* 2008. [Online]. Available: https://www.ist-winner.org

[121] Elektrobit, Nokia, Siemens, Philips, Alcatel, Telefonica, Lucent, Ericsson, "Spatial Radio Channel Models for Systems Beyond 3G," *Contribution to 3GPP RAN4, R4-050854*, London, Sept. 2005.

[122] M. Narandzic, C. Schneider, R. Thoma, T. Jamsa, P. Kyosti, and X. Zhao, "Comparison of SCM, SCME, and WINNER Channel Models," *IEEE Vehicular Technology Conference*, Vol., No., pp. 413–417, Apr. 2007.

[123] M. Narandzic, C. Schneider, W. Kotterman, and R. S. Thoma, "Quantification of Scenario Distance within Generic WINNER Channel Model," *International Journal of Antennas and Propagation,* Vol. 2013, No. 176704, pp., 2013.

[124] M. Narandzic, M. Kaske, C. Schneider, M. Milojevic, M. Landmann, G. Sommerkorn, and R. S. Thoma, "3D-Antenna Array Model for IST-WINNER Channel Simulations," *IEEE Vehicular Technology Conference*, Vol., No., pp. 319–323, Apr. 2007.

[125] G. D. Galdo, "Geometry-based Channel Modeling for Multi-User MIMO Systems and Applications," Ph.D Thesis, Fakultat fur Elektrotechnik und Informationstechnik, Universitat Ilmenau, Germany, 2007.

[126] L. Schumacher, and B. Raghothaman, "Closed-Form Expressions for the Correlation Coefficient of Directive Antennas Impinged by a Multimodal trancated Laplacian PAS," *IEEE Transactions on Wireless Communications,* Vol. 4, No. 4, pp., Jul. 2005.

[127] Y. A. Dama, R. A. Abd-Alhameed, S. M. R. Jones, D. Zhou, N. J. McEwan, M. B. Child, and P. S. Excell, "An Envelop Correlation Formula for (N,N) MIMO Antenna Arrays Using Scattering Parameters, and Including Power Losses," *International Journal of Antennas and Propagation,* Vol. 2011, No. 421691, pp., 2011.

[128] D. Patron, K. R. Dandekar, "Planar Reconfigurable Antenna with Integrated Switching Control Circuitry," *European Conference on Antennas and Propagation,*, Vol., No., pp., 2014.

[129] Q. H. Spencer, et al., "Modeling the statistical time and angle of arrival characteristics of an indoor multipath channel," *IEEE Journal of Selected Areas in Communications,* Vol. 18, No., pp. 347–360, Mar. 2000.

[130] A. S. Y. Poon, and M. Ho, "Indoor Multiple-Antenna Channel Characterization from 2–8 GHz," *IEEE International Conference on Communications,* Vol. 2, No., pp. 3519–3523, May. 2003.

[131] P. Mattheijssen, M. H. Herben, G. Dolmans, and L. Leyten,"Antenna-Pattern Diversity Versus Space Diversity for Use at Handhelds," IEEE Transactions on Vehicular Technology, Vol. 53, No. 4, pp., 2002.

[132] S. Choi, D. E. Perry, and S. M. Nettles, "A Software Architecture for Cross-Layer Wireless Network Adaptations," *IEEE Conference on Software Architecture,* Vol., No., pp. 281–284, 2008.

[133] K. Mandke, S. Choi, G. Kim, R. Grant, R. C. Daniels, W. Kim, R. W. Heath, and S. M. Nettles, "Early Results on Hydra: A Flexible MAC/PHY Multihop Testbed," *IEEE Conference on Vehicular Technology,* Vol., No., pp. 1896–1900, 2007.

[134] R. Dhar, G. George, A. Malani, and P. Steenkiste, "Supporting Integrated MAC and PHY Software Development for the USRP SDR," Vol., No., pp. 68–77, 2006.

[135] M. Dillinger, K. Madani, and N. Alonistioti, Software Defined Radio: Architectures, Systems and Functions. *John Wiley & Sons*, 2003.

[136] "Software Defined Radio," [Online] Available: http://www.wirelessinnovation.org/introduction_to_sdr , [April, 2014].

[137] V. Gardellin, K. Mammasis, F. Martelli, and P. Santi, "The MIMONet Software Defined Radio Testbed", *Proc. InfQ,* Vol., No., pp., 2012.

[138] C. Dubuc, D. Starks, T. Creasy, and Y. Hou, "A MIMO-OFDM Prototype for Next-generation Wireless WANs, *IEEE Communications Magazine,* vol. 42, No. 12, pp. 82-87, 2004.

[139] M. Takai, R. Bagrodia, M. Gerla, B. Daneshrad, M. Fitz, M. Srivastava, E. Belding-Royer, S. Krishnamurthy, M. Molle, P. Mohapatra, U. Mitra, and J. Evans, "Scalable Testbed for Next-Generation Wireless Networking Technologies," *IEEE International Conference on Testbeds and Research Infrastructures for the Development of Networks and Communities,* Vol., No., pp. 162–171, 2005.

[140] W. Kim, O. Khan, K. T. Troung, S. H. Choi, R. Grant, H. K. Wright, K. Mandke, R. C. Daniels, R. W. Heath, and S. M Nettles, "An Experimental Evaluation of Rate Adaptation for Multi-antenna Systems," *IEEE Conference on Computer Communications,* Vol., No., pp. 2313–2321, 2009.

[141] J. Yoon, H. Zhang, S. Banerjee, and S. Rangarajan, "MuVi: a Multicast Video Delivery Scheme for 4G Cellular Networks," *International Conference on Mobile Computing Networking,* Vol., No., pp. 209–220, 2012.

[142] Ettus Research. [Online] Available: http://www.ettus.com , [April, 2014].

[143] PicoChip Femtocell Solutions. [Online] Available: http://www.mindspeed.com, [April, 2014].

[144] IEEE 802.16e-2005 Part 16: Air Interface for Fixed and Mobile Broadband Wireless Access Systems , IEEE 802.16e standard. [Online] Available: http://standards.ieee.org/about/get/802/802.16.html , [April, 2014].

[145] Gnu Radio. [Online] Available: http://gnuradio.org/redmine/projects/gnuradio/wiki , [April, 2014].

[146] E. Kohler, R. Morris, B. Chen, J. Jannotti, and M. F. Kaashoek. The Click Modular Router. Massachusetts Intitute of Technology. [Online] Available: http://pdos.csail.mit.edu/papers/click:tocs00/paper.pdf , [April, 2014].

[147] E. Kohler, R. Morris, B. Chen, J. Jannotti, and M. F. Kaashoek, "The Click Modular Router," *ACM Transactions on Computer Systems,* Vol. 18, No. 3, pp. 263–297, 2000.

[148] GENI WIMAX. [Online] Available: http://www.geni.net/?p=2001 , [April, 2014].

[149] Tecom WiMAX USB Dongle. [Online] Available: http://www.tecom.com.tw/en/uploads/upload-documents/WU217-WU314.pdf , [April, 2014].

[150] Rohde-Schwarz. Mobile WiMAX Throughput Measurements. [Online]. Available: http://cdn.rohde-schwarz.com/dl_downloads/dl_application/application_notes/1sc10/1SP10_2e.pdf , [April, 2014].

[151] WiMAX Forum. [Online] Available: http://www.wimaxforum.org/news/downloads/Mobile_W , [April, 2014].

[152] C. Mehlfuhrer, S. Caban, and M. Rupp, "Experimental Evaluation of Adaptive Modulation and Coding in MIMO WiMAX with Limited Feedback," *EURASIP Journal of Advances in Signal Processing,* Vol., No., pp., 2008.

[153] M. Paetzold. Mobile Radio Channels (2nd Edition). Hoboken, NJ, USA: John Wiley & Sons, 2011.

[154] C-n. Chuah, G. J. Foschini, R. A. Valenzuela, D. Chizhik, J. Ling, and J. M. Kahn, "Capacity Growth of Multi-Element Arrays in Indoor and Outdoor Wireless Channels," *IEEE Wireless Communications and Networking Conference,* Vol. 3, No., pp. 1340–1344, 2000.

[155] D. Shiu, G. J. Foschini, M. J. Gans, and J. M. Kahn, "Fading Correlation and Its Effect on the Capacity of Multielement Antenna Systems," *IEEE Transactions on Communications*, Vol. 48, No. 3, pp. , 2000.

[156] A. M. Tulino, A. Lozano, and S. Verdu, "Impact of Antenna Correlation on the Capacity of Multiantenna Channels," *IEEE Transactions on Information Theory*, Vol. 51, No. 7, pp. 2491–2509, Jul. 2005.

[157] V. Veeravalli, Y. Liang, A. M. Sayeed, "Correlated MIMO Wireless Channels: Capacity, Optimal Signaling, and Asymptotics," *IEEE Transactions on Information Theory,* Vol. 51, No. 6, Jun. 2005.

[158] M. Chiani, M. Z. Win, and A. Zanella, "On the Capacity of Spatially Correlated MIMO Rayleigh-Fading Channels," *IEEE Transactions on Information Theory,* Vol 49, No. 10, pp., 2003.

[159] C. Waldschmidt, C. Kuhnert, S. Schulteis, and W. Wiesbeck, "Compact MIMO-arrays based on polarisation-diversity," *IEEE Antennas and Propagation Symposium*, Vol. 2, No., pp. 499–502, Jun. 2003.

[160] C. B. Dietrich Jr, K. Dietze, J. R. Nealy, and W. L. Stutzman, "Spatial, Polarization, and Pattern diversity for Wireless Handheld Terminals,"*IEEE Antennas and Propagation Symposium*, Vol. 49, No., pp. 1271-1281, Sep. 2001.

[161] P. Mattheijssen, M. H. Herben, G. Dolmans, and L. Leyten, "Antenna-Pattern Diversity Versus Space Diversity for Use at Handhelds," *IEEE Transactions on Vehicular Technology*, Vol. 53, No. 4, pp., 2002.

[162] R. B. Ertel, P. Cardieri, K. W. Sowerby, T. S. Rappaport, and J. H. Reed, "Overview of Spatial Channel Models for Antenna Array Communication Systems," *IEEE Personal Communications*, Vol. No., pp., 1998.

[163] A. M. Tulino, S. Verdu, and A. Lozano, "Capacity of Antenna Arrays with Space, Polarization and Pattern Diversity," *IEEE Information Theory Workshop*, Vol., No., pp. 324-327, Mar. 2003.

[164] T. Svantesson, "Correlation and Channel Capacity of MIMO Systems employing Multimode Antennas," *IEEE Transactions on Vehicular Technology*, Vol. 51, No., pp. 1304–1312, Nov. 2002.

[165] A. Abdi, and M. Kaveh, "A Space-Time Correlation Model for Multielement Antenna Systems in Mobile Fading Channels", *IEEE Journal on Selected Areas in Communications*, Vol. 20, No. 3, pp., Apr. 2002.

[166] A. Zohur, H. Mopidevi, D. Rodrigo, M. Unlu, L. Jofre, B. A. Cetiner, "RF MEMS Reconfigurable Two-Band Antenna," *IEEE Antennas and Wireless Propagation Letters,* Vol. 12, No., pp., 2013.

[167] J.-S. Chen,"Multi-frequency Characteristics of Annular-ring Slot antennas," *Microwave and Optical Technology Letter,* Vol. 38, No. 6, pp., Sep. 2003.

[168] B. A. Cetiner, G. R. Crusats, L. Jofre,and N. Biyikli, "RF MEMS Integrated Frequency Reconfigurable Annular Slot Antenna," *IEEE Transactions on Antenna Propagation,* Vol. 58, No. 3, pp. 626–632, Mar. 2010.

[169] H. Mopidevi, D. Rodrigo, O. Kaynar, L. Jofre, and B. A. Cetiner, "Compact and Broadband Antenna for LTE and Public Safety Applications," *IEEE Antennas Wireless Propagation Letters*, Vol. 10, No., pp. 1224–1227, 2011.

[170] Y. Damgaci, and B. A. Cetiner, "A Frequency Reconfigurable Antenna based on Digital Microfluidic," *Lab on Chip*, Vol., No. 15, pp. 2883–2887, Aug. 2013.

[171] A. J. King, J. F. Patrick, N. R. Sottos, S. R. White, G. H. Huff, and J. T. Bernhard, "Microfluidically Switched FrequencyReconfigurable Slot Antennas," *IEEE Antennas Wireless Propagagation Letter*, Vol. 12, No., pp. 828-831, Jun. 2013.

List of Notations and Acronyms

$(.)^{\dagger}$ *pseudo-inverse*

$(.)^{-1}$ denotes the inverse

$(\mathbf{H})_q$ denotes $q-th$ column of $\mathbf{H}$

$\bar{\gamma}$ average SNR

$\bar{\tau_{\chi}}$ average fade region duration

χ modulation mode or index

χ^{th} steady-state distribution corresponding to the χ^{th} region

η_{χ} level-crossing rate at boundary ξ_{χ}

γ SNR

$\hat{x}$ estimated decision statistic of $\mathbf{x}$

Ψ_0 target data rate

$\rho = E_x/N_o$ Signal-to-Noise Ratio per receive antenna

σ^2 noise variance

$(.)^H$ denotes the hermitian transpose

$(.)^T$ denotes the transpose

$(.)^+$ *Moore-Penrose psuedoinverse*

$(.)^-$ zeroing columns

AAA Adaptive Antenna Arrays

AAS Adaptive Antenna System

AMC Adaptive Modulation and Coding

AWGN Additive White Complex Gaussian Noise

BER Bit Error Rate

BL-AMC Block Adaptive Modulation and Coding

BLAST Bell Laboratories Layered Space-Time

CINR Carrier to Interference–plus–Noise Ratio

CRLH Composite Right Left Handed

CSI Channel State Information

D-BLAST Diagonal Bell Laboratories Layered Space-Time

Demux Demultiplexer

$\mathbf{E}_x$ total average energy

FDM Frequency Division Multiplexing

FEC Forward Error Correction

$\mathbf{H}$ channel matrix

$\mathbf{H}_{p,q}$ channel gain between the pth receive and qth transmit antenna pair

i.i.d independent and identically distributed

IFFT Inverse Fast Fourier Transform

ISI Inter-Symbol Interference

$\mathbf{I}_P$ PxP identity matrix

LTE Long-Term Evolution

M-QAM Multi-level Quadrature Amplitude Modulation

MIMO Multiple Input and Multiple Output

OFDM Orthogonal Frequency Division Multiplexing

ppSNR post processing Signal-to-Noise Ratio

QAM Quadrature Amplitude Modulation

RAS Reconfigurable Antenna Systems

RPDA Reconfigurable Printed Dipole Array

$\mathbf{R}_{xx}$ covariance matrix of

SAMC Spatially Adaptive Modulation and Coding

SIC Successive Interference Cancellation

SISO Single Input Single Output

SNR Signal-to-Noise Ratio

V-BLAST Vertical Bell Laboratories Layered Space-Time

WARP Wireless open-Access Radio Platform

WF-AMC Water-Filling Adaptive Modulation and Coding

Wi-Fi Wireless Fidelity

WiMAX Worldwide Interoperability for Microwave Access

$\mathbf{W}$ denotes nulling matrix

$\mathbf{w}_i$ denotes ith column of the nulling vector $\mathbf{w}$

$\mathbf{x}$ transmitted signal vector

$\mathbf{x}_{est}$ estimate of the transmit signal vector

$\mathbf{y}$ received signal vector

ZF Zero Forcing

$\mathbf{z}$ noise

ς_{max} number of coding rates

$||(.)||$ norm operator

ξ_χ SNR threshold

ζ ordered set

ζ_i permutations of ordered set

f_D doppler frequency

J total number of antenna configurations

J^* optimal antenna configurations

K total number of subcarriers or subchannels

L block of symbols

M	constellation size
N_o	noise power
P	number of receive antennas
P_e	bit error rate constraint
Q	number of transmit antennas
r	coding rate
R_χ	SNR region
r_i	denotes the decision statistic for the $i-th$ substream
$sgn(.)$	sign function
T	Symbol period
$Tr(.)$	trace of a matrix

Vita

George D. Sworo received the B.S. degree in Electrical and Systems Engineering and the M.S. degree in Telecommunication and Networking Engineering from the University of Pennsylvania, Philadelphia in 2009, respectively.

He joined Drexel University in the fall of 2009 to pursue his Ph.D. degree in Electrical and Telecommunication Engineering and was a member of the Data Fusion Laboratory and its sister lab, Drexel Wireless Systems laboratory. His research interests include adaptive antenna system design, MIMO communications, MAC/PHYsical layer algorithms and networking protocols for 4G standards including mobile WiMAX and LTE, and Ad-Hoc networking.